UAB
Universitat Autònoma de Barcelona

Functional Analyses of Tissue and Organ Specificity at the Core of the Arabidopsis Circadian Clock

Nozomu Takahashi

ADVERTIMENT. L'accés als continguts d'aquesta tesi queda condicionat a l'acceptació de les condicions d'ús establertes per la següent llicència Creative Commons: http://cat.creativecommons.org/?page_id=184

ADVERTENCIA. El acceso a los contenidos de esta tesis queda condicionado a la aceptación de las condiciones de uso establecidas por la siguiente licencia Creative Commons: http://es.creativecommons.org/blog/licencias/

WARNING. The access to the contents of this doctoral thesis it is limited to the acceptance of the use conditions set by the following Creative Commons license: https://creativecommons.org/licenses/?lang=en

Universitat Autònoma de Barcelona

crag CENTRE FOR RESEARCH IN AGRICULTURAL GENOMICS
CSIC IRTA UAB

Functional Analyses of Tissue and Organ Specificity at the Core of the Arabidopsis Circadian Clock

PhD Thesis
Nozomu Takahashi
Barcelona, 2017

Universitat Autònoma
de Barcelona

CRAG CENTRE FOR RESEARCH IN AGRICULTURAL GENOMICS
CSIC IRTA UAB

Faculty of Bioscience
Department of the Animal Biology, Plant Biology and Ecology

Functional Analyses of Tissue and Organ Specificity at the Core of the Arabidopsis Circadian Clock

Submitted to the Universitat Autònoma de Barcelona for the degree of
Doctor of Philosophy in Plant Biology and Biotechnology

Thesis Director

Dr. Paloma Más Martínez

PhD Candidate

Nozomu Takahashi

Thesis Tutor

Dr. Soledad Martos Arias

Barcelona, 2017

"D'où Venons Nous? Que Sommes Nous? Où Allons Nous?"
"我々はどこから来たのか? 我々は何者か? 我々はどこへ行くのか?"

Paul Gauguin, 1897
ポール・ゴーギャン, 1897

Contents

INTRODUCTION 9

1. Plant circadian rhythms 11

2. Parameters of circadian rhythms 12

3. Architecture of the plant circadian clock 13

3.1 Central oscillator 14

3.2 Input pathways 17

3.3 Output pathways 20

4. Organization of the circadian system: from single cells to whole organisms 22

4.1. Cell-type specific clock function and circadian coupling in plants 22

4.2. Cell-type specific clock function and circadian coupling in mammals 26

OBJECTIVES 29

RESULTS 33

1. Differences in robustness and precision of circadian rhythms in different dissected organs 35

2. Specific properties for synchronization and phase readjustments of shoot apex clocks 38

3. Conserved molecular architecture of the circadian network at the shoot apex clocks 43

4. Differences in synchrony of clock cells in various organs and tissues 49

5. Intercellular circadian coupling among clock cells of the shoot apex 53

6. Relevance of the shoot apex clocks in the modulation of circadian oscillations in roots 58

7. A hierarchical structure at the core of the Arabidopsis clock 64

DISCUSSION 69

CONCLUSIONS 81

RESUMEN EN CASTELLANO 87

MATERIALS AND METHODS 91

1. Plant material, seed sterilization and growing conditions 93

2. Plant dissection 93

3. *In vivo* luminescence assays 94

4. Micrografting 95

5. RNA extraction, RNA sequencing and analysis of circadian oscillations 96

6. Gene expression analysis by RT-qPCR 98

7. Single cell confocal microscopy imaging 99

8. Protoplast preparation 100

9. Mathematical analysis 101

ANNEXES 103

ACKNOWLEDGEMENTS 159

REFERENCES 163

INTRODUCTION

Introduction

1. Plant circadian rhythms

The rotation of the Earth around its axis results in periodic environmental changes such as the light/dark and temperature cycles. A wide range of organisms, including plants, have evolved an endogenous mechanism or circadian clock able to integrate the environmental information to generate and sustain biological rhythms with a period of 24 hours (Young and Kay, 2001). The circadian clock function has been proposed to provide an adaptive advantage to organisms as it allows the anticipation of the predictable environmental transitions, coordinating essential biological processes to occur at the most appropriate time (Johnson and Kyriacou, 2007).

Plants have played a pivotal role in the history of circadian biology, as the very first known documentation of the circadian rhythms goes back to 325 BC, when the admiral Androsthenes of Thasos in the record of marches of Alexander the Great described the diurnal movement of *Tamarindus indicus* (Tamarind tree) leaves (Bretzl, 1903). It took about 2000 years for a more scientific evaluation of such rhythmic movements when the French astronomer de Mairan (1729) demonstrated that leaf movement persisted even under constant darkness. Following his study, three botanists, Hill (1757), Duhamel du Monceau (1758) and Zinn (1759) independently reported that daily rhythms in leaves were not significantly affected by temperature variations. In 1832, de Candolle observed that rhythms of leaf movement under constant dark conditions were not exactly

24 hours but approximately 22 to 23 hours, and further showed that rhythms could be synchronized to inverted light/dark cycles (McClung, 2006). All these findings conclusively confirmed the existence of a biological clock (McClung, 2006; Más, 2008) and provided the basis for defining three main features of the clockwork: 1) Circadian rhythms are driven by endogenous mechanisms, which persist in the absence of external timing cues; 2) the rhythms exhibit temperature compensation, i.e. the pace of the oscillations is maintained over a range of physiological temperatures; and 3) the rhythms can be entrained or synchronized to environmental conditions by exposure to the external cues.

2. Parameters of circadian rhythms

As circadian rhythms often exhibit sinusoidal waveforms when plotted over time, several mathematical terms are used to describe their properties (Más, 2008) (Figure 1). The period refers to the amount of time required to complete one cycle and therefore represents the pace of the circadian oscillation. The phase is a particular time point of a rhythmic oscillation relative to an external oscillating synchronizing phase. This term is frequently used to indicate the time of the day where the peak of the event is observed. The amplitude is calculated as half the difference between the peak and trough of an oscillation. In circadian biology, the time is often represented in hours, either under constant free-running conditions, the so-called Circadian Time (CT), or under resetting external cues (Zeitgeber signals), which define the Zeitgeber Time (ZT) (Golombek and Rosenstein, 2010). By convention, the time of onset of a Zeitgeber is usually defined as ZT0.

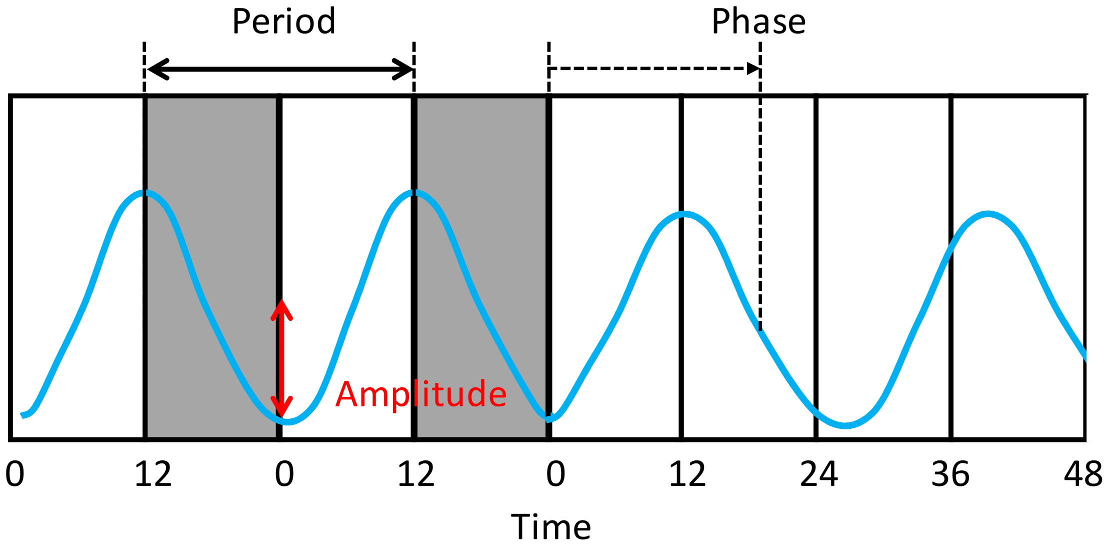

Figure 1. Mathematical terms used to describe the circadian rhythms. The period is defined as the amount of time required to complete one cycle. The phase is a particular time point of a physiological event within a cycle relative to an external synchronizing cycle. The amplitude is calculated as half the difference between the peak and trough of an oscillation. White boxes: day; Shaded boxes: night. Modified from (Harmer, 2009).

3. Architecture of the plant circadian clock

Classically, the circadian clock system has been proposed to consist of three different components: input pathways, central oscillator and output pathways (Figure 2). The input pathways perceive the environmental cues such as changes in light or temperature and feed this information to reset every day the central oscillator. This central oscillator is composed of a network of regulatory components that regulate each other and generate self-sustaining rhythms. The output pathways consist of all of the rhythmic biological processes under the control of the circadian clock. When correctly tuned with the environment, the circadian system is shown to confer improved fitness to plants (Green et al., 2002; Dodd et al., 2005). Currently, it is clear that the functioning of the clock is much more complicated, but this conceptual model is still a simple and convenient way to understand how the clock might be working. In the following sub-sections (3.1, 3.2 and 3.3), these three main components of the circadian system are briefly described.

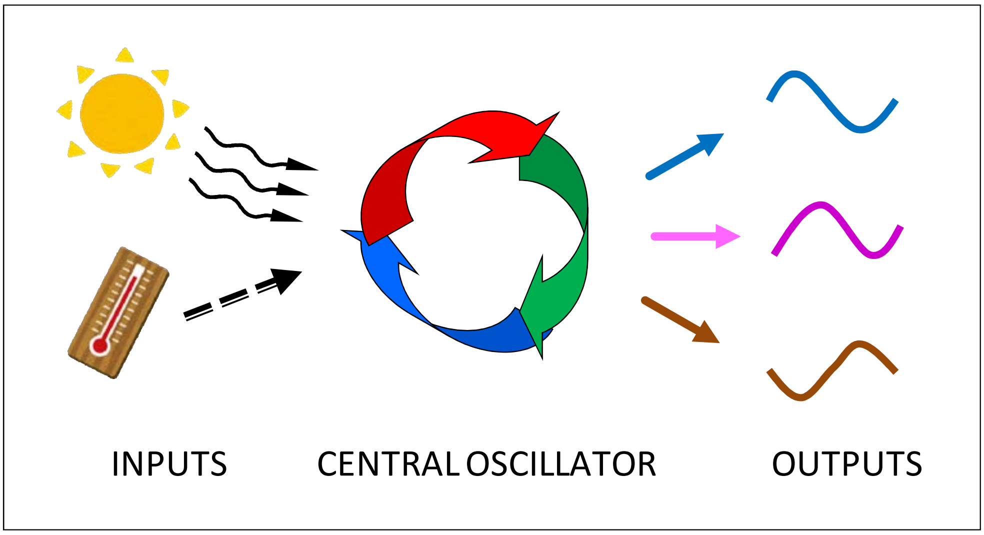

Figure 2. Scheme depicting the different compartments of the circadian clock. This simplified model consists of input pathways that perceive environmental cues such as light or temperature, the central oscillator that generate ～24 hour rhythms, and output pathways that are the rhythmic processes controlled by the clock. Arrows with different colors and shapes denote different pathways. Modified from (Más, 2008).

3.1 Central oscillator

In plants, the molecular network at the core of the clock has been particularly well studied in the model system *Arabidopsis thaliana*. Recent experimental and computational studies have suggested that the central oscillator consists of various components that temporally regulate each other in a complex network (Hsu and Harmer, 2014) (Figure 3). The very first described components of the oscillator included two morning-phased Myb-like transcription factors known as CIRCADIAN AND CLOCK ASSOCIATED 1 (CCA1) and LATE ELONGATE HYPOCOTYL (LHY) (Schaffer et al., 1998; Wang and Tobin, 1998). The relevance of these repressors for proper clock function was evidenced by the circadian phenotype of the respective mutants: single loss of either *CCA1* or *LHY* caused a shortening of the circadian period under constant conditions (Green and Tobin, 1999; Mizoguchi et al., 2002) while the *cca1/lhy* double mutant was arrhythmic (Alabadí et al., 2002; Mizoguchi et al., 2002). CCA1 and LHY share sequence homology and consequently they are partially redundant in their function as negative regulators of evening-expressed gene *TIMING OF CAB EXPRESSION 1* (*TOC1*), another important component of the central oscillator (Strayer et al., 2000; Makino et al., 2002). CCA1 and LHY repress *TOC1* expression by directly binding to the Evening Element (EE) motif present in the *TOC1* promoter (Alabadí et al., 2002). In turn, TOC1 protein binds to the promoters of *CCA1* and *LHY,* and represses their expression in the evening (Gendron et al., 2012; Huang et al., 2012). Loss of *TOC1* functions results in a short period phenotype (Strayer et al., 2000) while over-expression of TOC1 leads to arrhythmia (Más et al., 2003a). Together with TOC1, other members of the PSEUDO-RESPONSE REGULATOR (PRR) family including PRR5, PRR7, PRR9 also negatively regulate the expression of *CCA1* and *LHY* (Nakamichi et al., 2010). In turn, *PRR5* expression is negatively regulated by CCA1 and LHY, whereas *PRR7* and *PRR9* seem to be positively regulated by them (Farré et al., 2005; Kamioka et al., 2016).

Other clock components expressed during the evening include EARLY FLOWERING 3 (ELF3), ELF4, and LUX ARRYTHMO (LUX), which form the Evening Complex (EC) and repress *PRR9* expression (Nusinow et al., 2011; Herrero et al., 2012). Every member of the EC is required for sustaining circadian rhythms, as mutation in any of these genes results in arrhythmia (Hicks et al., 2001; Doyle et al., 2002; Hazen et al., 2005). As these key regulators mainly act as repressors, it was proposed that activation of clock genes is achieved rather indirectly through a repression-based transcriptional interaction (the so-called repressilator) (Pokhilko et al., 2012). The real structure of the core clock network is more complicated than a simplified repressilator as it also involves transcriptional regulation of many other clock genes, post-translational modification of clock proteins and epigenetic regulation through chromatin modifications (Nohales and Kay, 2016).

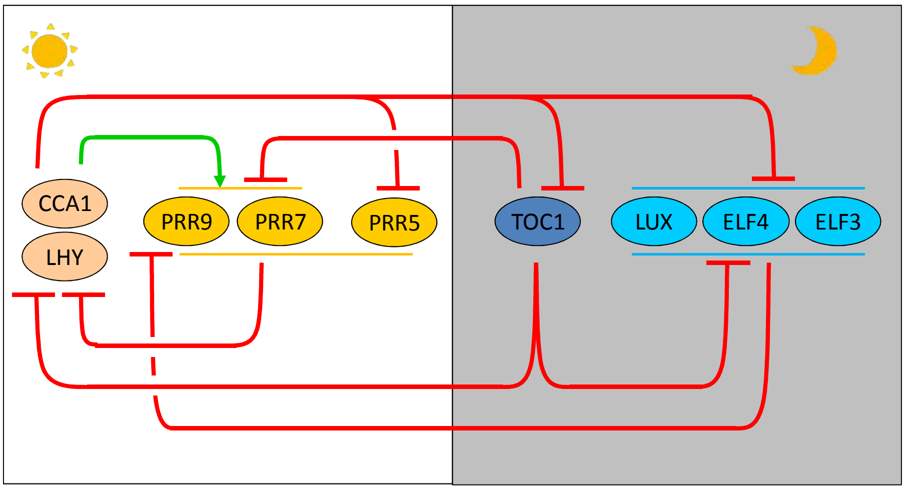

Figure 3. Scheme depicting a simplified view of the main components and the regulatory network at the core of the Arabidopsis oscillator. Green lines ending with an arrow denote gene activation while red lines ending with perpendicular dashes denote gene repression. Please see the main text (section 3.1) for details.

3.2 Input pathways

In Arabidopsis, the clock period under constant conditions (i.e. the endogenous pace of the clock) varies from 22 to 28.5 hours, depending on the accessions and growth conditions (Michael et al., 2003). Thus, for the circadian clock to be effective, it is essential to adjust the endogenous pace with the external synchronizing signals from the day/night cycles. Light, which is sensed by multiple photoreceptors in plants, acts as a strong entrainment signal that resets the clock every day. In higher plants, a number of different photoreceptors are involved in the modulation of the central oscillator (Chen et al., 2004). The mechanism for resetting is not fully understood in all cases but it seems to involve changes in the expression, protein accumulation and activity of key central oscillator components (Inoue et al., 2017). The five members of the PHYTOCHROME (PHY) family (PHYA to PHYE) are red and far-red light receptors found in Arabidopsis. PHYA regulates the light input to the clock mainly under low intensity of red light while PHYB is more important under higher intensities of red light (Somers et al., 1998a). A couple of studies have provided some insights into the regulation of core clock components by PHYTOCHROMES. Downstream intermediates of *PHYA* signaling such as FAR RED ELONGATED HYPOCOTYL3 (FHY3), FAR-RED IMPAIRED RESPONSE 1 (FAR1), and ELONGATED HYPOCOTYL 5 (HY5) are shown to act as positive transcriptional regulators of *ELF4* by directly binding to its promoter region (Li et al., 2011). PHYB also appears to directly interact with several clock components including CCA1, LHY, TOC1, and LUX in a light-quality dependent manner (red and far-red light), possibly transferring the environmental light information to the central oscillator (Yeom et al., 2014). The blue light receptors CRYPTOCROME 1 and CRYPTOCROME 2 (CRY1 and CRY2) also act as photoreceptors resetting the clock with a certain degree of redundancy (Devlin and Kay, 2000; Gardner et al., 2006). The members of the ZEITLUPE family are another set of blue light receptors, which include *ZTL, FLAVIN BINDING, KELCH REPEAT, F-BOX* (*FKF1*), and *LOV KELCH PROTEIN 2* (*LKP2*). *ZTL* is involved in the targeted degradation of TOC1 and PRR5 proteins (Más et al., 2003b; Kiba et al., 2007). *FKF1* and *LKP2* are thought play redundant role with *ZTL* (Baudry et al., 2010).

For proper entrainment, the circadian clock responds to light signals differently at various times of the day (Johnson, 1999). In many organisms, including plants, light pulses around dawn typically advance the phase of the circadian oscillator whereas the same pulses at dusk generally delay the phase (Devlin and Kay, 2001). This property is often studied by Phase Response Curves (PRC) in which phase shifts of a circadian rhythm are plotted as a function of the circadian phase (Johnson, 1999).

Temperature is also capable of entraining the plant clock. Circadian rhythms are synchronized by warm/cold cycles with differences as small as 4^{o}C (12 hour 24 ^{o}C:12 hour 20 ^{o}C) under constant light conditions (Somers et al., 1998b). The molecular mechanisms responsible for temperature-dependent synchronization, however, are not well understood (Jones, 2009). Several studies suggest that ambient temperature signals might feed into the circadian clock through the EC. When Arabidopsis seedlings are exposed to temperature upshifts (22^{o}C to 28^{o}C or 16^{o}C to 22^{o}C), several clock genes including *PRR7*, *PRR9,* and *LUX* are up-regulated and this thermoresponsiveness is abolished in *elf4*, *elf3* or *lux* mutant (Mizuno et al., 2014). Furthermore, it has been reported that dark-grown *elf3* mutant seedlings cannot be entrained by temperature cycles (Thines and Harmon, 2010).

Despite the ability to be reset by temperature, and as mentioned above, the clock also displays a very interesting property known as temperature compensation: the pace of the circadian oscillation is maintained with a $Q_{10} \fallingdotseq 1$ ($Q_{10:}$ rate of change in a chemical / biological reaction due to a temperature shift of 10 ^{o}C). The clock temperature compensation is crucial for organisms to maintain stable endogenous rhythms regardless the temperature variation in the environment. In Arabidopsis, temperature compensation is disrupted in mutants of several clock genes. Particularly, *PRR7* and *PRR9* seem to play a important role as the effects of temperature are overcompensated in *prr7/prr9* double mutant, and this defect is fully suppressed when *CCA1* and *LHY* expressions are knocked-down by the use of artificial microRNAs (Salome et al., 2010). This suggests that PRR7 and PRR9 regulate CCA1 and LHY activities in response to ambient temperature (Salome et al., 2010). Furthermore, CCA1 and the protein kinase CK2 (formerly casein kinase 2) are essential for clock temperate compensation (Portolés and Más, 2010). Indeed, high temperatures enhance the CCA1 promoter-binding activity, leading to increased repression of its target genes. In turn, high temperatures also stimulate CK2-dependent phosphorylation of CCA1, and the phosphorylated isoforms display a reduced affinity for the promoters of clock genes. Therefore, two activities (CCA1 promoter-binding and repression, and CK2-dependent CCA1 phosphorylation) are precisely balanced and control temperature compensation in Arabidopsis (Portolés and Más, 2010).

Alternative splicing events of some clock components are also regulated by temperature (James et al., 2012; Seo et al., 2012). Indeed, a recent study has illustrated the link between alternative splicing and the proper temperature response of the clock. The study showed that mutants of *SICKLE* (*SIC*), a putative regulator of spliceosomal activity, exhibited defects in temperature compensation, accompanied with aberrant splice variant accumulation (Marshall et al., 2016). *sic* mutants also displayed low-amplitude or arrhythmic expression of core circadian clock genes and under cool temperature cycles (12 hour 22 ^{o}C: 12 hour 18 ^{o}C). The results suggest the importance of alternative splicing for both temperature compensation and entrainment of the clock (Marshall et al., 2016).

3.3 Output pathways

In Arabidopsis, approximately 30%-40% of the genes are considered to be under the regulation of the circadian clock and therefore the clockwork plays a crucial role in coordinating a number of biological processes (Covington et al., 2008). These processes or clock outputs are numerous and include among others the rhythmic movement of leaves (Millar et al., 1995), stomatal opening (Somers et al., 1998b), elongation of hypocotyl, stem and root (Dowson-Day and Millar, 1999; Ruts et al., 2012), seed dormancy (Penfield and Hall, 2009), drought responses (Legnaioli et al., 2009) and immune defense against pathogens (Wang et al., 2011).

One well-defined clock output in plants is the photoperiodic control of the transition from the vegetative state to its reproductive state (Más, 2008). Several pathways regulate the initiation of flowering (Amasino and Michaels, 2010). Regarding the photoperiodic pathway, plants are able to measure the duration of the day and determine whether to flower or not. The mechanism responsible for measuring the duration of the day is the circadian clock (Kobayashi and Weigel, 2007). In Arabidopsis, flowering is controlled by the tight regulation on the florigen gene, *FLOWERING LOCUS T* (*FT*), which is activated by CONSTANS (CO) (Kobayashi, 1999). CO is a clock regulated zinc-finger protein which is unstable in the dark (Putterill et al., 1995; Valverde, 2004). Under short days, the peak of *CO* expression occurs at night, and therefore the protein does not accumulate. However, under long day conditions, *CO* expression peaks during the light period, thus CO protein accumulates and induces the expression of *FT*. *FT* is predominantly expressed in leaves, but the protein eventually travels to the shoot apex to initiate flowering (Corbesier et al., 2007). This mechanism controlled by the clock ensures that flowering occurs at the appropriate seasonal time.

4. Organization of the circadian system: from single cells to whole organisms

Despite the recognized importance of the circadian system and the details about the molecular components and mechanisms of clock regulation and function, one essential aspect of the circadian system is how rhythms are organized within the organism and whether there is communication among the different cells to synchronize the overall rhythmicity at the level of the whole organism. Prevalent studies in animal circadian systems have provided evidence for a hierarchical organization. Our studies have shown a similar organization in plants. The following subsections briefly describe the main knowledge of the cellular specificity and communication of the circadian information in plants (section 4.1) and in mammals (section 4.2).

4.1. Cell-type specific clock function and circadian coupling in plants

Identification of the circadian components and mechanisms of circadian regulation have been traditionally conducted using whole seedlings. This approach has rendered useful information, but outputs represent blended signals from different tissues, which limit the cellular resolution of the studies. Several recent reports have focused on the cellular specificity of the clock function showing that the circadian clock system might work differently in distinct tissues or organs. For instance, in Arabidopsis leaves, the stomatal guard cells were found to have a different free-running period from the surrounding epidermal and mesophyll cells (Yakir et al., 2011). Another example includes the clock gene *PRR3,* which is predominantly expressed in the vasculature and its function is associated with the tissue-specific regulation of TOC1 protein stability (Para et al., 2007).

Regarding the specific function of the oscillator, the circadian clock in roots was proposed to be a simplified version of the shoot clock (James et al., 2008). Gene expression analysis using plants transferred to constant light conditions following synchronization under light/dark cycles showed that transcripts of evening-phased genes such as *TOC1, LUX, ELF3* and *ELF4* from mature roots remained at a constant level throughout the circadian cycle. Contrarily, morning-phased genes such as *CCA1, LHY, PRR7* and *PRR9* sustained their oscillations although their peak phases were delayed and the amplitudes were reduced compared to the oscillations in the aerial parts. Also, *toc1* null mutation was shown to shorten the period length of *CCA1* and *LHY* only in shoots. As mentioned above, CCA1 and LHY repress the expression of evening-phased genes by binding to the EE motif present in their promoters (Alabadí et al., 2002). However, gel shift assays showed that the EE-binding occurred in shoots but not in roots. Thus, the authors concluded that evening components of the clock are disengaged from the morning components in roots (James et al., 2008).

Despite these conclusions, recent results from the same group argue against this idea. Indeed, by using improved techniques, the authors now describe that the promoter activities of both morning-phased and evening-phased genes sustained rhythmicity under constant light conditions. Furthermore, the oscillation of the evening clock components was confirmed by gene expression analysis. Therefore, the authors now conclude that the evening components are fully functional and engaged with the morning components in roots (Bordage et al., 2016).

When rhythms were analyzed by bioluminescence assays specifically at the root tip, they showed that the promoter activity of *CCA1* was very weak under free-running conditions, suggesting that the circadian clock might be constantly reset (Fukuda et al., 2012). Additionally, the clock re-phasing seemed to be important in roots as it was observed at the site of lateral root emergence (Voß et al., 2015). Consistently, the disruption of the circadian clock function leads to strong defects in lateral root development (Voß et al., 2015).

Another key aspect of circadian function relates to the existence of circadian intercellular communication or coupling. Studies using an Arabidopsis cultured cell line (Nakamichi et al., 2003) or mesophyll protoplasts (Kim and Somers, 2010) showed that the clock is able to function autonomously within a single cell. Imaging assays in Arabidopsis leaves showed desynchronization of circadian rhythms from individual cells under constant light conditions (Yakir et al., 2011; Wenden et al., 2012). These findings suggest that coupling between cellular clocks in leaves is weak. However, other studies have suggested the presence of circadian cell-to-cell communication. For instance, bioluminescent analyses in Arabidopsis have identified phase-wave propagations in coupled circadian oscillators of leaves (Fukuda et al., 2007). Coupling of clocks between nearby cells was also reported in *Lemna gabba* (Muranaka et al., 2013) and in *Kalanchoe daigremontiana* (Rascher et al., 2001). Furthermore, photosynthetic signals from shoots are suggested to entrain the root clock, as rhythms in shoots and roots are synchronized under the light/dark cycles and this entrainment of the root clock was disrupted by addition of sucrose or an inhibitor of the photosynthetic electron transport, indicating that long-distance communication may modulate clocks in distal parts of plants (James et al., 2008; Bordage et al., 2016).

The issue of circadian coupling in Arabidopsis leaves has been also recently addressed in more detail (Endo et al., 2014). Expression analysis from isolated cotyledons showed that evening-phased clock genes such as *TOC1* tend to be preferentially expressed in the vasculature compared to mesophyll cells. The opposite was found for morning-phased clock genes such as *CCA1*. Genome-wide analyses of the transcriptome showed that clock output genes were also found to have similar trends, i.e. evening-phased output genes were particularly expressed in the vasculature whereas morning-phased outputs were preferentially expressed in mesophyll cells. As significantly enriched gene ontology terms were different between these two fractions of differentially expressed genes, the results indicate that the tissue-specific clock function regulates the expression of output components matching specialized cell functions. Moreover, over-expression of *CCA1* in the vasculature was found to inhibit not only the clock in the vasculature but also clocks of neighboring mesophyll cells, suggesting a local coupling with a dominant role of the vascular clock over the mesophyll clock (Endo et al., 2014).

Overall, full characterization of the expression and function of clock genes in specific plant tissues or cell types is essential to obtain both a global and a cell-specific view of the plant circadian function. The work described in the present Thesis precisely addresses this point, focusing on the organization, cell-to-cell coupling and long-distance communication of the circadian system in Arabidopsis.

4.2. Cell-type specific clock function and circadian coupling in mammals

The circadian organization has been extensively documented in mammals. The mammalian clock contains a "master clock" located at the superchiasmatic nucleus (SCN) in the hypothalamus regulates "slave clocks" in peripheral tissues via humoral factors and autonomic nervous system (Eckel-Mahan and Sassone-Corsi, 2013; Mohawk et al., 2013) (Figure 4). The SCN is a network composed of approximately 20,000 neurons in mice, each of which has a cell autonomous circadian oscillator. The different SCN neurons exhibit a wide range of circadian periods that vary from 22 to 30 hours when dispersed. However, intercellular coupling among neurons acts to mutually couple the entire population and confers the robustness and the precision necessary for the proper function as a master clock (Welsh et al., 1995; Abraham et al., 2010). Indeed, loss of the SCN results in desynchronization of peripheral circadian clocks, which ultimately abolishes rhythms in activity or rest, feeding, body temperature and hormones (Moore and Eichler, 1972; Stephan and Zucker, 1972; Yoo et al., 2004). The circadian coupling at the SCN also provides robustness against perturbations. For instance, mutation of key oscillator genes diminished the circadian oscillation in dissociated SCN neurons and fibroblast cells, but the clock maintained its rhythmicity in intact SCN (Liu et al., 2007).

Cells in both the SCN and the peripheral tissues share the same transcriptional-translational feedback loop mechanism at the core of the circadian oscillator. Two basic helix-loop-helix (bHLH) transcription factors, CLOCK and BRAIN AND MUSCLE ARNT-LIKE1 (BMAL1), heterodimerize and subsequently bind to conserved E-box sequences in promoters and drive the rhythmic expression of *PERIOD* (*PER1*, *PER2*, and *PER3*) and *CRYPTOCHROME* (*CRY1* and *CRY2*) (Eckel-Mahan and Sassone-Corsi, 2013). PER and CRY proteins form a complex that translocates back to the nucleus to inhibit CLOCK-BMAL1 mediated gene expression. However, while the mechanism itself is conserved, the robustness of the feedback loop and the control of downstream targets seem to be different (Oishi et al., 1998; Marcheva et al., 2013). In fact, the phase of the peripheral clock could be delayed by 6 to 8 hours compared to the SCN, and some potent Zeitgebers such as dexamethasone (glucocorticoid hormone analog) treatment or restricted feeding reset the clock of peripheral tissues but not the SCN clock (Balsalobre et al., 2000; Damiola et al., 2000; Stokkan et al., 2001). Furthermore, isolated peripheral tissues rapidly lose their circadian oscillations unlike the persistent clock activity in isolated SCN neurons (Yamazaki, 2000; Abe et al., 2002; Morse and Sassone-Corsi, 2002). Together, the studies reveal a hierarchical organization of the circadian system in mammals, with the presence of a master clock with very precise rhythms due to circadian coupling. The coupling and precision of the master clock is important for synchronizing the rhythms in peripheral clocks.

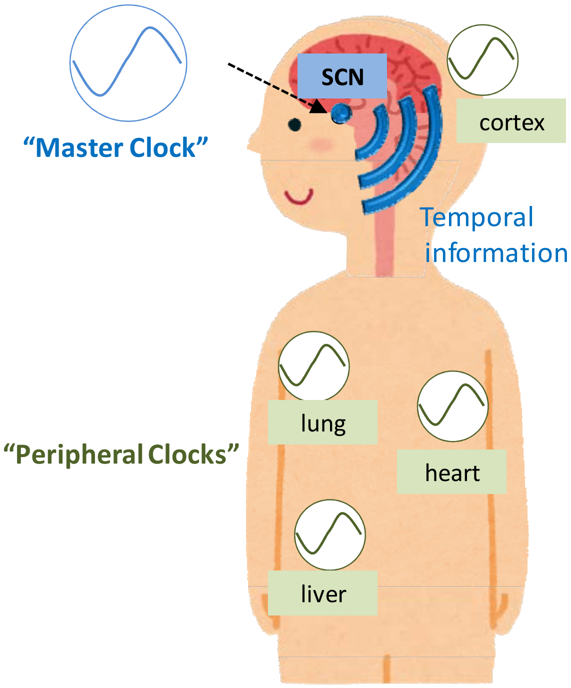
"Master Clock"
SCN
cortex
Temporal information
"Peripheral Clocks"
lung
heart
liver

Figure 4. Schematic drawing depicting the hierarchical organization of the mammalian circadian clock. The master clock at the suprachiasmatic nucleus (SCN) in the hypothalamus controls the clocks in peripheral tissues via humoral factors and autonomic nervous system. Modified from (Ishida et al., 1999)

OBJECTIVES

Objectives

The general aim of this Thesis is to understand the circadian clock organization in plants, specifically focusing on the circadian function in specific tissues and organs as well as in cell-to-cell coupling and long-distance circadian communication. This general goal was studied through the following specific objectives:

1. To develop a specific *in vivo* analysis by bioluminescent assays to examine the circadian function in dissected plant organs. We aimed to perform comparative analyses under different environmental conditions to discern the precision and robustness of rhythms in different dissected organs.

2. To elucidate the molecular architecture of the circadian network in different organs, examining similarities and differences among them. We aimed to examine rhythms in a battery of clock mutants and perform genome-wide transcriptional assays to obtain a global view of the circadian transcriptional landscape at the shoot apex clocks.

4. To identify the possible circadian coupling and define its strength in different organs. We aimed to develop single cell live-imaging assays, in-vivo bioluminescent assays with dispersed protoplasts and mathematical analysis using barycentric coordinates for high-dimensional space to identify the circadian coupling and define its strength in different organs.

5. To examine the role of circadian coupling controlling the precision and robustness of rhythms. We aimed to analyze the degree of rhythmic synchrony and the particular capabilities for phase readjustments during “jet-lag” experiments.

6. To identify and characterize the possible long-distance communication of circadian clocks between distal part of plants. We aimed to examine rhythms in shoots and roots from the same plant and determine the rhythmic robustness against genetic and pharmacological perturbations.

7. To develop micrografting assays in order to discern the hierarchical organization and the long-distance circadian communication in plants. We aimed to use a combination of Wild-Type and arrhythmic clock mutants to perform micrografting and examine whether rhythms are affected in a specific organ by changing the clock function in a different one.

RESULTS

Results

1. Differences in robustness and precision of circadian rhythms in different dissected organs

To examine the organ specificity of the circadian clock function, we analyzed circadian rhythms of several organs excised from 9-14 day-old Arabidopsis seedlings (Figure 5).

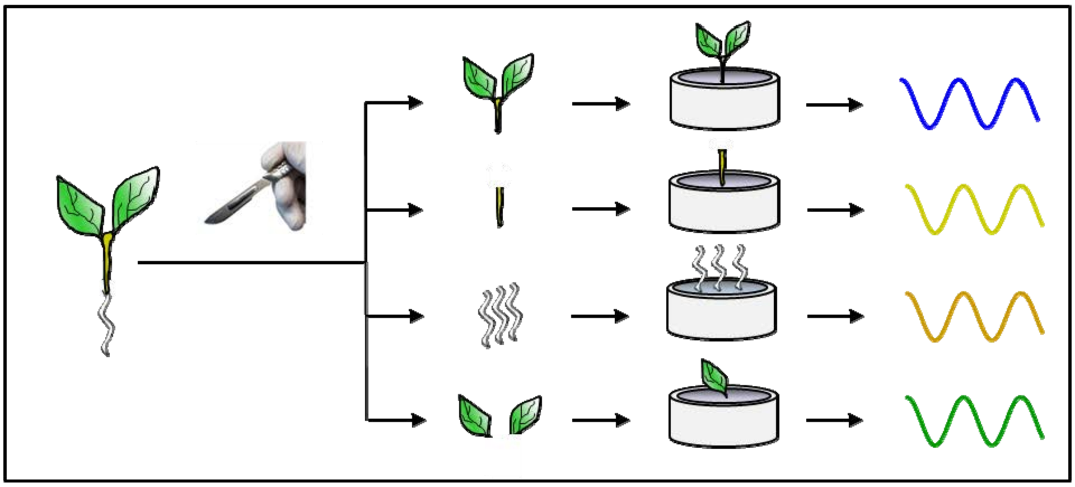

Figure 5. Schematic drawings depicting the dissection of the different parts of the plant and the subsequent analysis of circadian rhythms by luminescence assays. Seedlings of about 9-14 day old were dissected with a sterile surgical blade to separate shoots, hypocotyls, roots, and leaves.

Promoter activity was monitored by *in vivo* luminescence assays of transgenic plants expressing the morning- (*CCA1*) and evening-phased (*TOC1*) core clock component gene promoters fused to the *LUCIFERASE* (*LUC*). Under constant light conditions (LL), *CCA1::LUC* and *TOC1::LUC* expression in separated shoots robustly oscillated without evident dampening. Circadian waveforms closely matched those of whole plants (Figure 6 A and B), suggesting that under these experimental conditions, root excision did not manifestly affect the rhythmicity in shoots. Excised hypocotyls also sustained rhythms albeit with a long circadian period (27.02 ± 0.64 hours versus 24.61 ± 0.25 hours in entire plants) and a progressive decrease in amplitude over the days (Figure 6 C and D). Rhythms in excised roots were only sustained for about 2 days, dampening low afterward (Figure 6 E and F). The fact that oscillations in roots do not persist in the absence of sucrose could be due to energy limitation as excised roots are a sucrose sink, or it could be due to the loss of the communication with shoots, as previously reported (James et al., 2008). Analysis of root rhythms following excision with the same procedure but using medium with sucrose revealed that rhythms were sustained for more than 4 days (Figure 6 G and H) with a significantly longer period (26.21 ± 0.33 hours) than in shoots (24.63 ± 0.22 hours). The sustained oscillations suggest that the excision *per se* was not responsible for the dampened rhythms observed without sucrose. Adding sucrose to non-sucrose grown and arrhythmic excised roots did not restore the oscillatory pattern (Figure 7), suggesting that at least under these conditions, exogenous sugar cannot compensate for the severe arrhythmia.

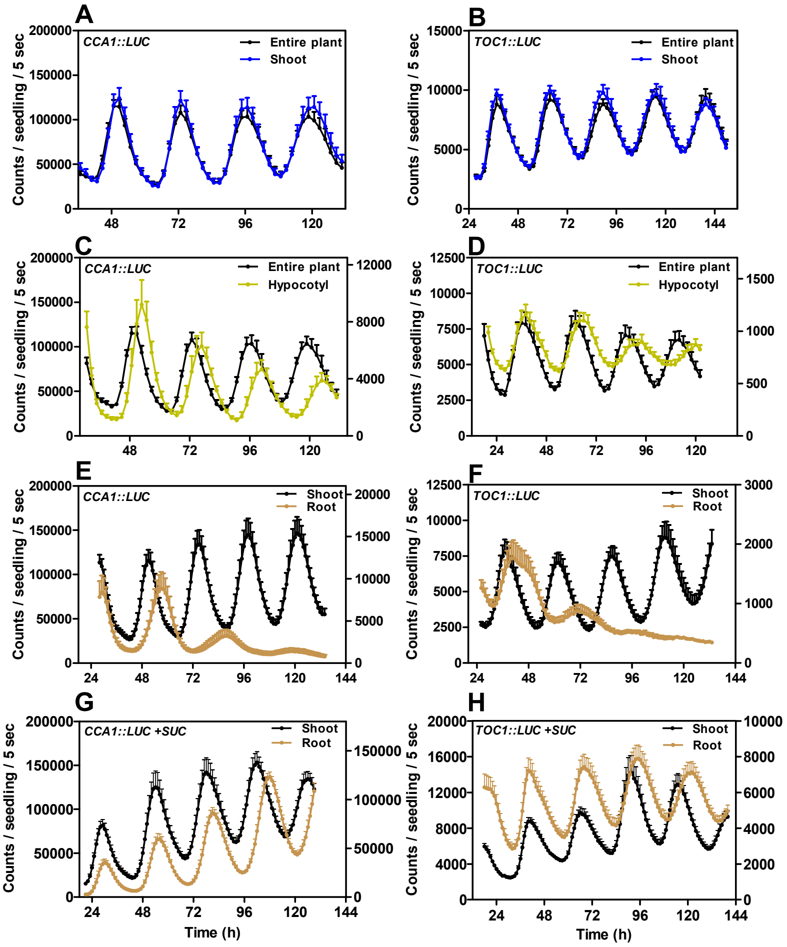

Figure 6. *In vivo* circadian analysis of luminescent rhythms under LL from *CCA1::LUC* (*A*, C, *E*, G) and *TOC1::LUC* (B, D, F, H) in shoots (A and B), hypocotyls (C and D), roots (E and F), roots with sucrose (G and H). Data are the means + SEM of the luminescence of 6–12 individual samples. Values of luminescence signals from hypocotyls, roots (C-H), are represented on the right Y axes.

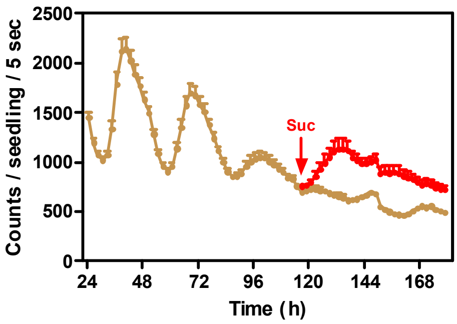

Figure 7. Circadian analysis of luminescent rhythms under LL from *TOC1::LUC* in roots without sucrose (brown waveform and after adding sucrose (red waveform). The red arrow indicates the time of sucrose addition. Data are the means + SEM of the luminescence of 12 individual samples.

When excised leaves were analyzed in the absence (Figure 8 A and B) or in the presence (Figure 8 C and D) of sucrose, we observed an averaged advanced phase compared to entire plants, suggesting that the rhythms were also not very precisely controlled.

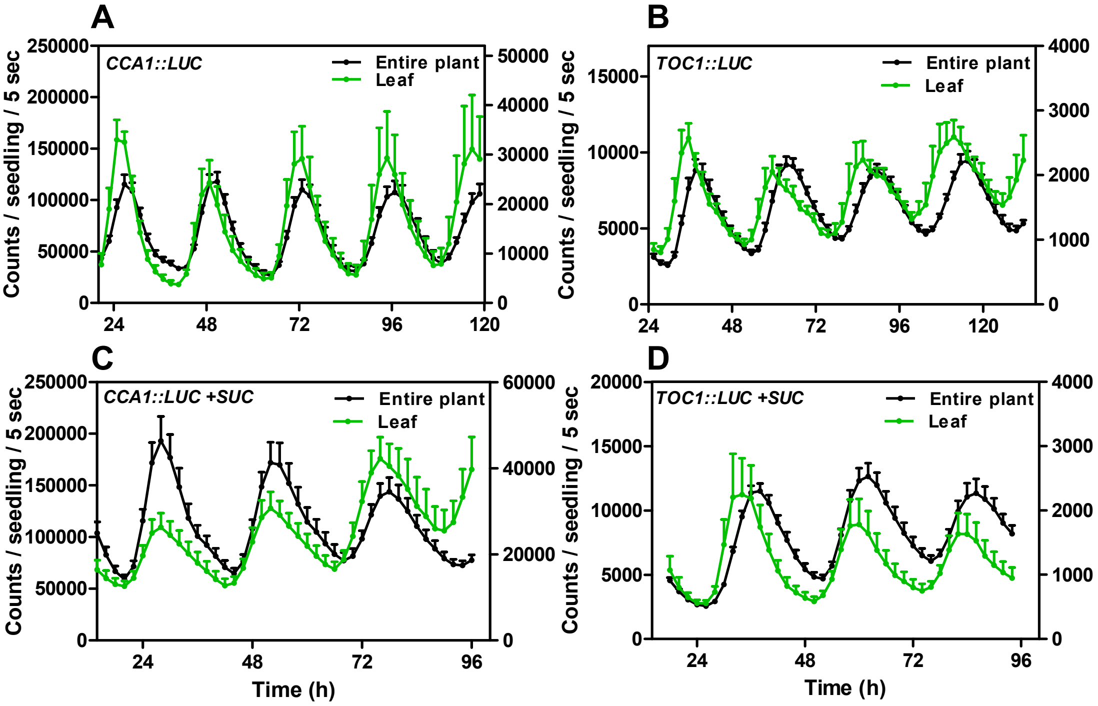

Figure 8. Average rhythms of *CCA1::LUC* (A and C) and *TOC1::LUC* (B and D) in leaves under LL. Luminescence rhythms in excised leaves from plants grown in medium without sucrose (A and B), and with sucrose (C and D). Data are the means + SEM of the luminescence of 8-12 individual samples. Values of luminescence signals from leaves are represented on the right Y axes.

2. Specific properties for synchronization and phase readjustments of shoot apex clocks

We next performed similar analysis with excised shoot apexes (Figure 9 A) and found that the phase, period, and amplitude remained synchronized showing rhythms very similar to those of the entire plants under the LL (Figure 9 B and C,

Figure 10 A-C). Time-course gene expression analysis by real-time quantitative polymerase chain reaction (RT-qPCR) further confirmed the similarity in the oscillation patterns of core clock components in shoot apexes and entire plants (Figure 11 A-C).

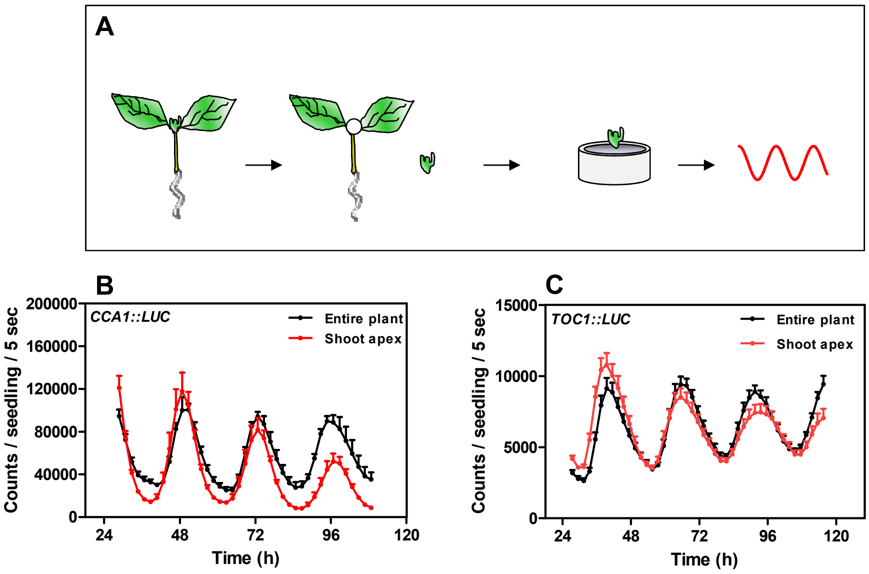

Figure 9. (A) Schematic drawing depicting the rhythmic analysis of excised shoot apexes. (B and C) *In vivo* circadian analysis of luminescent rhythms under LL from *CCA1::LUC* (B) and *TOC1::LUC* (C) in shoots apexes. Data are the means + SEM of the luminescence of 8-12 individual samples.

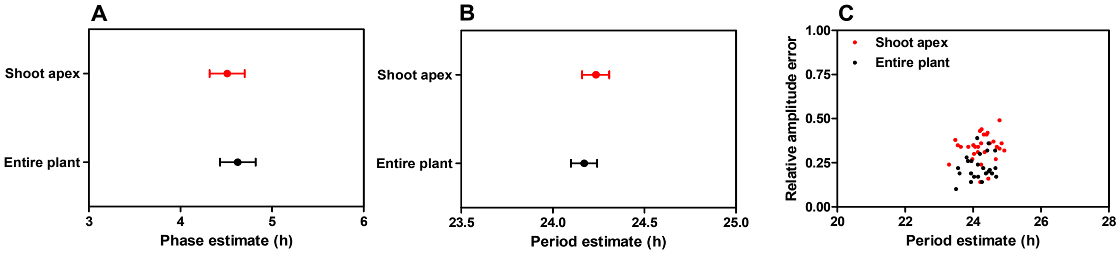

Figure 10. Phase (A), period (B and C), and relative amplitude (C) estimates of circadian rhythms in shoot apexes and entire plants of waveforms shown in Figure 9, using the Fast Fourier Transform–Non-Linear Least-squares (FFT-NLLS) suite of the Biological Rhythms Analysis Software System (BRASS).

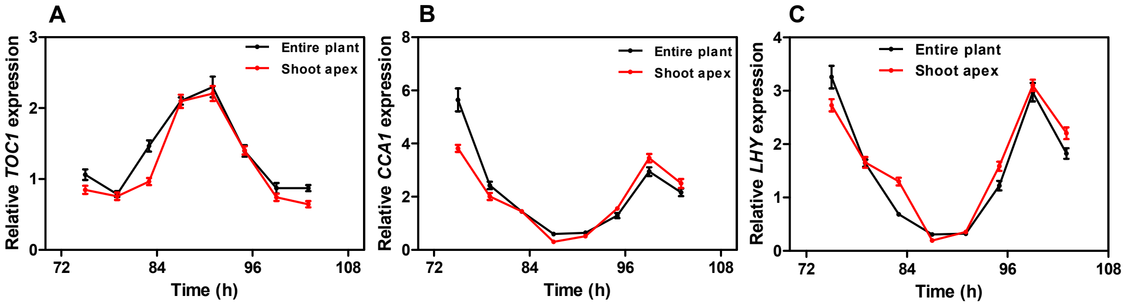

Figure 11. Time-course analysis of gene expression by RT-qPCR of *TOC1* (A), *CCA1* (B) and *LHY* (C). Plants were entrained under LD cycles followed by 2 days under LL conditions. Samples were taken every 4 hour over a 24 hour circadian cycle during the third day under LL. mRNA abundance was normalized to *PP2AA3* expression. Data represents means ± SEM of two biological replicates.

Furthermore, individual apexes showed highly similar waveforms (Figure 12 A and C), which is in clear contrast to the high degree of variability observed in individual leaf waveforms, manifested by a range of phases and amplitudes from the very first day under LL (Figure 12 B). As the size of the tissue might influence the circadian waveforms, we analyzed small sections of leaves (with sizes similar to those of the shoot apexes). Our results showed a similar variability to that displayed by full leaves (Figure 12 D), which suggests that the shoot apex homogeneity in waveforms is not due to the reduced sizes of the samples.

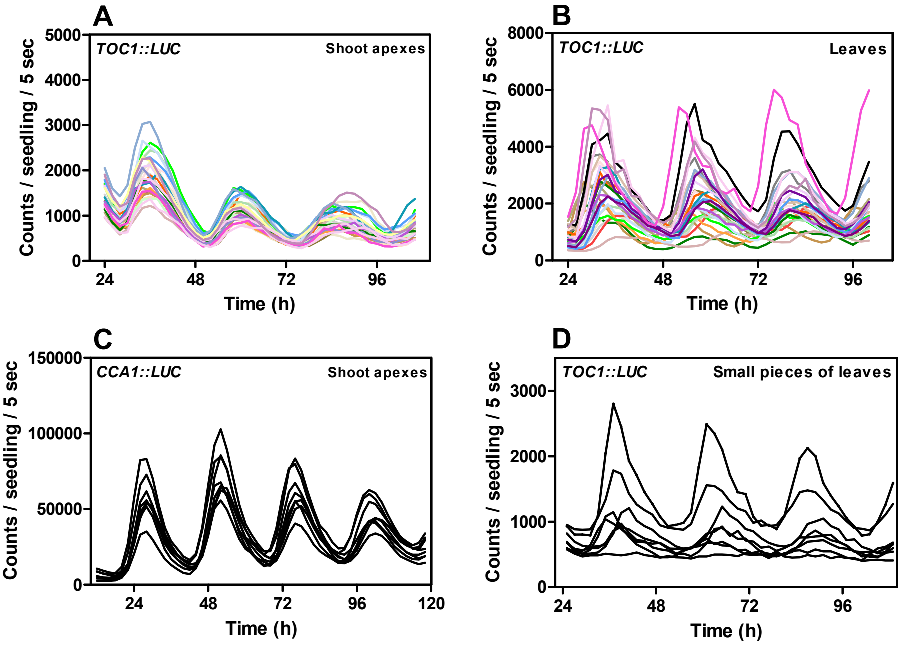

Figure 12. *In vivo* luminescence traces of *TOC1::LUC* (A, B and D) and *CCA1::LUC* (C) of individual excised shoot apexes (A and C), excised leaves (B) and small pieces of leaves (D) with similar sizes to shoot apexes. Plants were entrained under LD cycles and luminescence was recorded under LL.

The circadian phases clustered together in shoot apexes and to less extent in leaves (Figure 13 A and B). Similar conclusions were drawn when the average phase and the degree of phase coherence were calculated using the synchronization index “R”. The analysis showed high R values, close to 1, for the shoot apexes and lower values for leaves at all time points (Figure 13 C). Consistent with previous studies (Wenden et al., 2012), the R values in leaves were well above 0, which suggests a certain degree of coherence. Rhythms in excised organs were highly reproducible in four different biological replicates (each one with 6–12 samples), which reduces the possibility that results were due to indirect effects of the excision procedure.

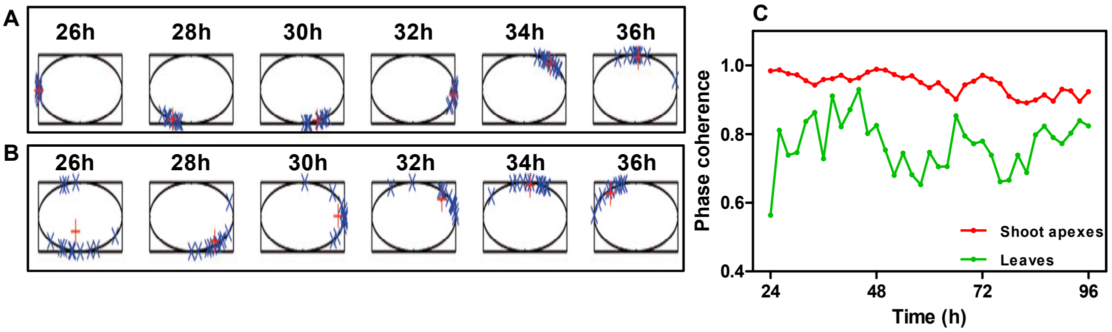

Figure 13. (A and B) Analysis of the phase synchrony among the different samples (blue crosses) of individual shoot apexes (A) and leaves (B) examined from 26 hour to 36 hour under LL. The red crosses indicate the means or circular variance (Mormann et al., 2000) at each time point. (C) Quantification of the phase coherence in shoot apexes and leaves by analysis of the synchronization index "R".

The circadian clock is not only a robust mechanism able to sustain rhythms in the absence of environmental changes but also a flexible system that resynchronizes and properly adjusts to changes in the environmental cycle (Harrington, 2010). To explore whether the differences between shoot apexes and leaves also extend to their capabilities for resynchronization and phase adjustment, we performed "jet-lag" experiments with an extended 12 hour dark period at dawn. In shoot apexes, rhythms showed similar timing for resynchronization to that of entire plants (Figure 14 A), although the shoot apex waveforms displayed very rapid declining at night for *TOC1::LUC* and an increased acute induction at dawn for *CCA1::LUC* (Figure 14 B). In leaves, rhythms showed a double peak for the first 2 days, reaching a stable phase at the third day after the extended night switch (Figure 14 C). Similar results for readjustment in time and waveforms were observed when "jet-lag" experiments were performed by extended day switch at dusk (Figure 14 D). These results reveal a different synchronizing behavior in leaves and shoot apexes. The specific waveforms in shoot apexes compared to the entire plant might also indicate a particular sensibility of shoot apexes to dawn and dusk resetting signals.

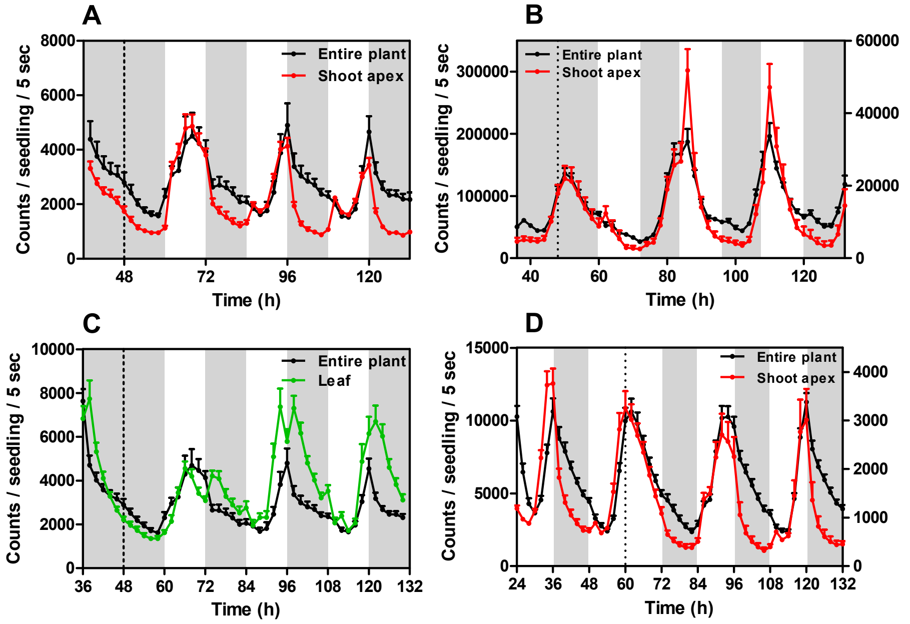

Figure 14. Average rhythms of *TOC1::LUC* (A, C and D) and *CCA1::LUC* (B) luminescence in shoot apexes (A, B and D) or leaves (C) subjected to a “jet-lag” experiment, with extended 12 hour darkness (extended night) at dawn (A-C) or extended 12 hour light (extended day) at dusk (D). Data are the means + SEM of the luminescence of 6–12 samples. Values of luminescence signals from shoot apexes are represented on the right Y axes. White boxes: light; Shaded boxes: dark.

3. Conserved molecular architecture of the circadian network at the shoot apex clocks

To determine organ-specific differences in the clock molecular composition, we examined whether different clock outputs and mutations in core clock genes were distinctively regulated in shoot apexes and leaves. Analysis of Wild-Type (WT) plants expressing the morning-phased clock output *CAB2 (CHLOROPHYLL A/B-BINDING PROTEIN 2)* (Millar et al., 1995) showed that in shoot apexes the phase was comparable to that in the entire plant, whereas increased heterogeneity and an average advanced phase were prevalent in leaves (Figure 15 A). Similar to entire plants, the shoot apexes and leaves of *cca1-11* mutants displayed persistent rhythms with shorter periods than WT shoot apexes and WT leaves, respectively (Figure 15 B-D). Similarly, the short period of the evening-expressed clock output *CCR2 (COLD, CIRCADIAN RHYTHM, AND RNA BINDING 2)* (Strayer et al., 2000) in *TOC1 RNA interference (RNAi)* plants (Más et al., 2003a) was also observed in shoot apexes and leaves (Figure 15 E and F). Therefore, circadian gene expression in shoot apexes and leaves with various reporter lines and clock mutant backgrounds did not render major differences in terms of the circadian network between the two organs.

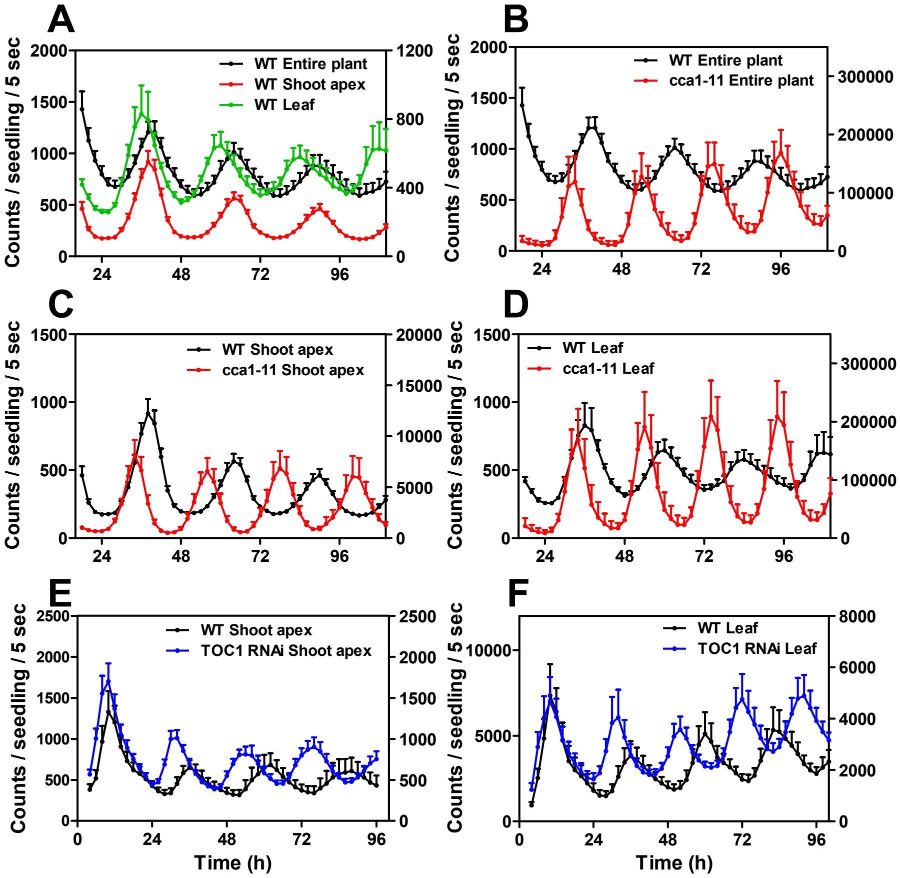

Figure 15. Average rhythms of *CAB2::LUC* (A-D) and *CCR2::LUC* (E and F) luminescence under LL in entire plants, shoot apexes, and leaves of WT (A), *cca1-11* mutants (B–D) and *TOC1 RNAi* (E and F). Plants were entrained under LD cycles. Data are the means + SEM of the luminescence of 6–12 samples. Values of luminescence signals from WT leaves (A) *cca1-11* mutant (B-D) and *TOC1 RNAi* (E and F) are represented on the right Y axes.

To profile the circadian transcriptional landscape at the shoot apex, we performed RNA sequencing (RNA-seq) analysis and used the JTK_CYCLE algorithm for precise definition of circadian expression (Hughes et al., 2010). After filtering out transcripts whose median expression across every sample was lower than 0.69 RPKM and those not differentially expressed, we identified over

1,400 genes with significant circadian fluctuations in mRNA abundance. Visual inspection of the data suggested that this may be a conservative estimation. However, the stringent analysis ensured the selection of the highest-confidence circadian hits. Rhythmic genes included all the previously described core clock components, genes involved in light signaling, and those involved in circadian outputs such as photosynthesis, photoperiodic flowering, and hormone signaling, among others (Figure 16 A-J). The waveforms oscillated with similar phases and amplitudes to those previously reported in entire plants (Figure 17 A-C), which suggests no fundamental differences in the global transcriptional circadian networks in the shoot apex and entire plants. It is noteworthy that shoot apexes display such strong and robust rhythms (both morning- and evening-expressed genes) as opposed to the uncoupled rhythms in veins (mainly evening) (Endo et al., 2014). Functional categorization of the rhythmic genes showed a wide range of biological functions, highlighting as most significantly enriched those genes involved in circadian rhythms and responses to environmental conditions, including different qualities of light, temperature, and radiation (Figure 18). This enrichment might explain the specific readjustment of shoot apexes to environmental changes observed in our "jet-lag" experiments.

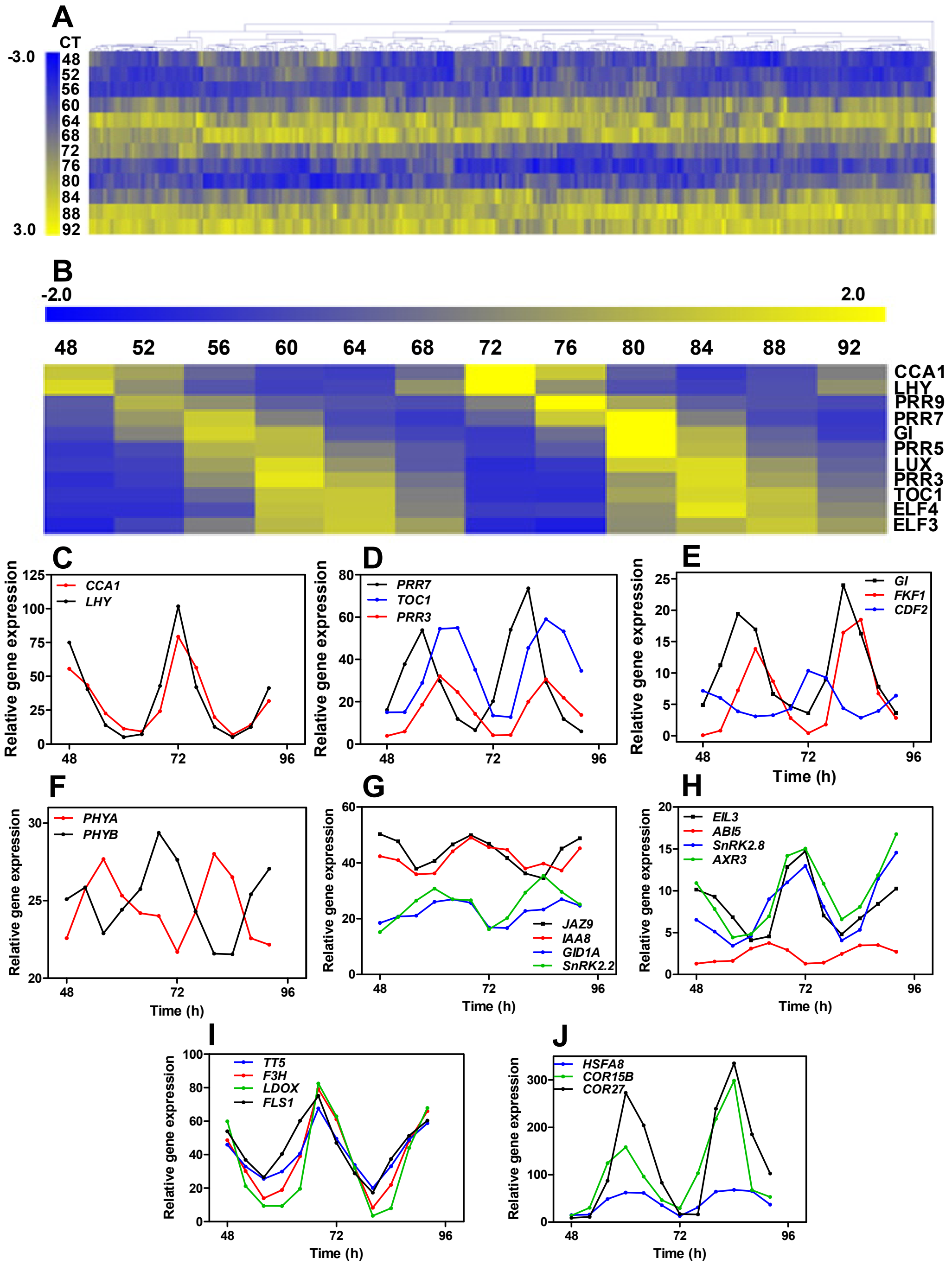

Figure 16. (A and B) Heatmap analysis of RNA-Seq data showing median-normalized gene expression at different circadian times (CT, vertical axis) for transcripts (horizontal axis) with a peak phase of expression at mid-late subjective night (A), and median-normalized oscillator gene expression at different circadian times (CT, horizontal axis) for transcripts (vertical axis) (B). Yellow indicates high expression and blue low expression. (C-G) Gene-expression analysis of *CCA1, LHY* (C), *PRR3, PRR7*,

TOC1 (D), *GIGANTEA* (*GI*), *FKF1, CYCLING DOF FACTOR 2* (*CDF2*) (E) *PHYA* and *PHYB* (F), *JASMONATE-ZIM-DOMAIN PROTEIN 9* (*JAZ9*), *INDOLEACETIC ACID-INDUCED PROTEIN 8* (*IAA8*), *GA INSENSITIVE DWARF 1A* (*GID1A*), *SNF1-RELATED PROTEIN KINASE 2.2* (*SnRK2.2*) (G), *ETHYLENE INSENSITIVE3-LIKE 3* (*EIL3*), *ABA INSENSITIVE 5* (*ABI5*), (*SNF1-RELATED PROTEIN KINASE 2.8*) (*SnRK2.8*), *AUXIN RESISTANT 5* (*AXR3*) (H), *TRANSPARENT TESTA 5* (*TT5*), *FLAVANONE 3-HYDROXYLASE* (*F3H*), *LEUCOANTHOCYANIDIN DIOXYGENASE* (*LDOX*), *FLAVONOL SYNTHASE 1* (*FLS1*) (I), and *HEAT SHOCK TRANSCRIPTION FACTOR A8* (*HSFA8*), *COLD REGULATED 15B* (*COR15B*), *COLD REGULATED GENE 27* (*COR27*) (J) in shoot apexes of WT plants grown under LD cycles followed by 2 days under LL.

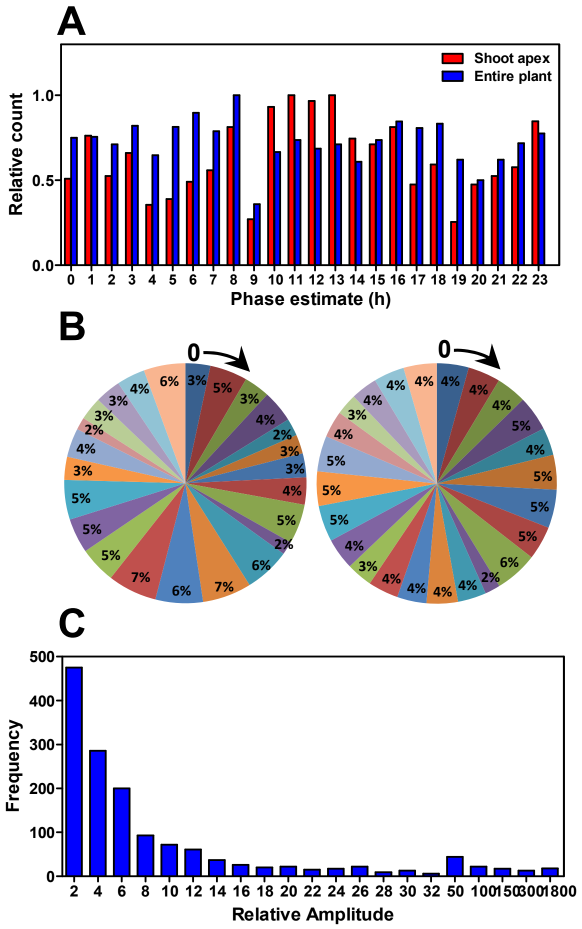

Figure 17. (A) Phase distribution of rhythmic genes in shoot apexes and entire plants. Phase enrichment was calculated using the web-based tool "Phaser." The phase estimates were represented relative to their maximum (A) and in pie charts (B) displaying the contribution of each phase to the total. Left chart: shoot apex; right chart: entire plants. (C) Distribution of amplitudes of cycling transcripts in shoot apexes calculated by using the algorithm JTK_Cycle.

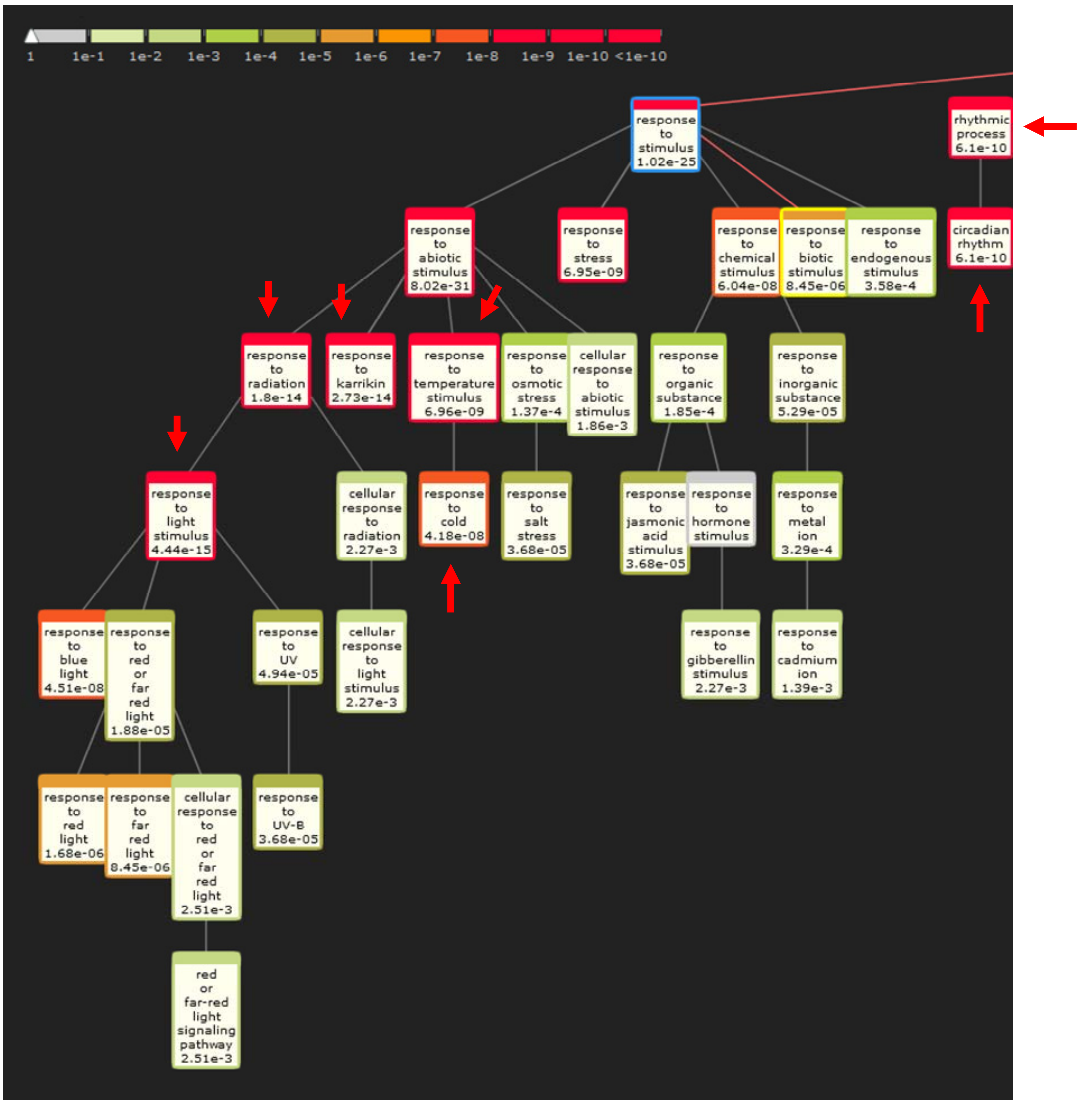
1 1e-1 1e-2 1e-3 1e-4 1e-5 1e-6 1e-7 1e-8 1e-9 1e-10 <1e-10
response to stimulus 1.02e-25
rhythmic process 6.1e-10
response to abiotic stimulus 8.02e-31
response to stress 6.95e-09
response to chemical stimulus 6.04e-08
response to biotic stimulus 8.45e-06
response to endogenous stimulus 3.58e-4
circadian rhythm 6.1e-10
response to radiation 1.8e-14
response to karrikin 2.73e-14
response to temperature stimulus 6.96e-09
response to osmotic stress 1.37e-4
cellular response to abiotic stimulus 1.86e-3
response to organic substance 1.85e-4
response to inorganic substance 5.29e-05
response to light stimulus 4.44e-15
cellular response to radiation 2.27e-3
response to cold 4.18e-08
response to salt stress 3.68e-05
response to jasmonic acid stimulus 3.68e-05
response to hormone stimulus
response to metal ion 3.29e-4
response to blue light 4.51e-08
response to red or far red light 1.88e-05
response to UV 4.94e-05
cellular response to light stimulus 2.27e-3
response to gibberellin stimulus 2.27e-3
response to cadmium ion 1.39e-3
response to red light 1.68e-06
response to far red light 8.45e-06
cellular response to red or far red light 2.51e-3
response to UV-B 3.68e-05
red or far-red light signaling pathway 2.51e-3

Figure 18. Functional categorization of the main circadian genes in the Arabidopsis shoot apex. The graphical output by “BioMaps” (Katari et al., 2010) shows the functional terms that are over-represented in the circadian gene list. The color code represents the statistical significance of the over-representation as specified in the legend on the upper left corner. Red arrows highlight the most over-represented terms related to circadian rhythms, response to light and temperature stimuli. format

4. Differences in synchrony of clock cells in various organs and tissues

To understand the cellular basis of the circadian rhythmicity at the shoot apex, we examined rhythms from individual cells of plants expressing CCA1-HA-EYFP under its own promoter (Yakir et al., 2009). We performed *in vivo* time-course analysis by confocal imaging of excised shoot apexes embedded in agarose (Más and Beachy, 1998). Fluorescent signals from individual nuclei of shoot apex cells sustained rhythmic oscillations. The circadian waveforms maintained good synchrony, manifested by similar timing in their rising and declining phases even after 3 days under LL (Figure 19 A and C). The results were also evident when the confocal imaging started at different time points (Figure 19 D). A similar pattern of highly synchronous waveforms was observed with single cells from shoot apexes of FLAG-PRR7-EGFP-expressing plants (Nakamichi et al., 2010) (Figure 19 E).

In contrast, and consistent with previous data (Yakir et al., 2011), the variation in the rhythmic accumulation of CCA1-HA-EYFP in individual leaf cells significantly increased after 2 days under LL (Figure 19 B and F). Differences in phase and amplitude were also clearly observed when fluorescent signals were not relativized to the maximum (Figure 19 G). We also measured fluorescence from the leaf vasculature, as previous studies have shown that these cells are coupled (Endo et al., 2014). We observed two distinguishable populations with slightly different phases (Figure 19 H). Individual cell-to-cell comparisons showed that both populations maintain a certain degree of synchrony (Figure 19 I and J). Synchrony appeared to be higher than that observed in leaf mesophyll cells but lower than in cells at the shoot apex. Quantitative analysis of the waveform correlation among individual cells confirmed that the correlation coefficient in shoot apex cells was higher than the one for vascular cells with the advanced (A) or delayed (D) phase (Figure 20 A and B). The group of cells with a delayed phase appeared to be more synchronous than the group with an advanced phase. The waveforms in leaf mesophyll cells displayed lower correlation values and increased heterogeneity.

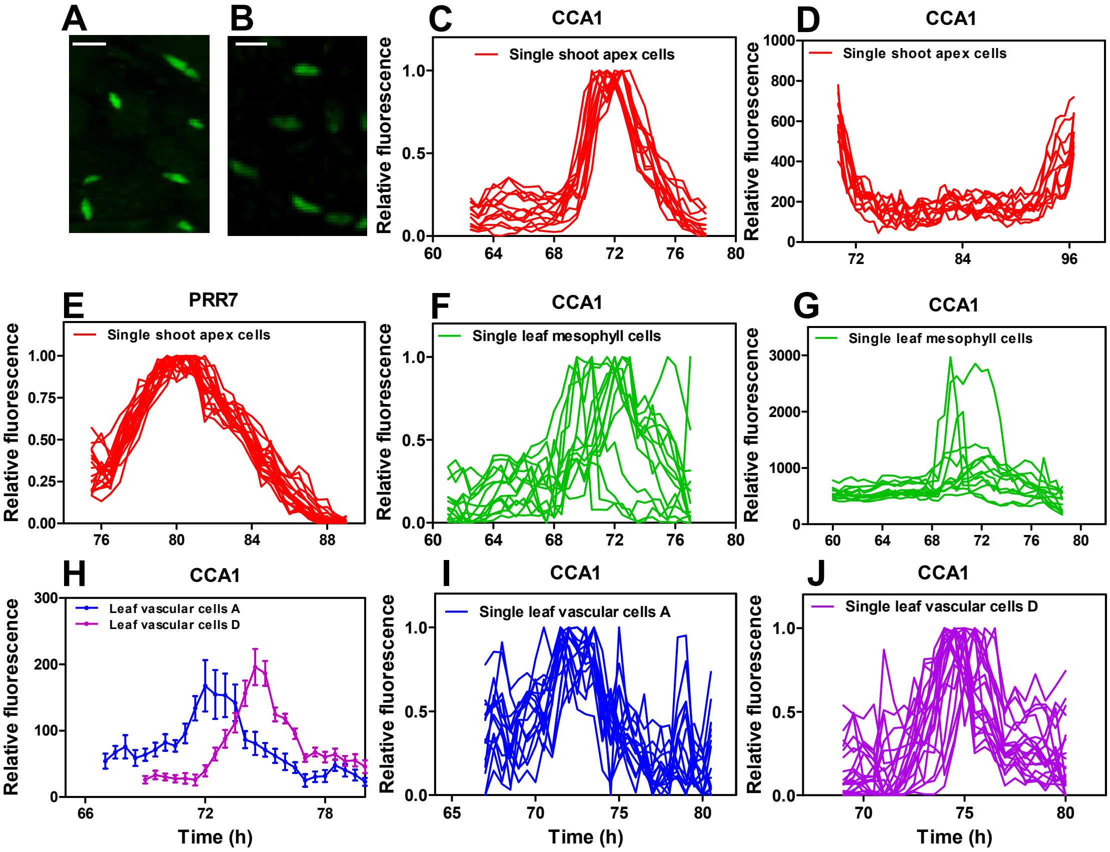

Figure 19. (A and B) Representative fluorescent signals from CCA1-HA-EYFP accumulation in nuclei of shoot apex cells (left panel) and leaf cells (right panel). Panels show representative cells from a larger picture containing other cells out of the shown field (scale bar, 20 µm). (C-J) *In vivo* time-course imaging of CCA1-HA-EYFP (C, D, F-J) and FLAG-PRR7-EGFP (E) fluorescent signals quantified in individual nuclei from shoot apex (C-E), leaf mesophyll (F) leaf mesophyll not relativized (G), and averaged signal of leaf vascular cells (H), signals in individual nuclei from vascular cells with advanced (I) and delayed (J) phases. Data are represented relative to the maximum value except (G). Samples were maintained under LL conditions at 60–100 µmol m^{-2}s^{-1}. Fluorescence quantification in the nuclei was analyzed using ImageJ software.

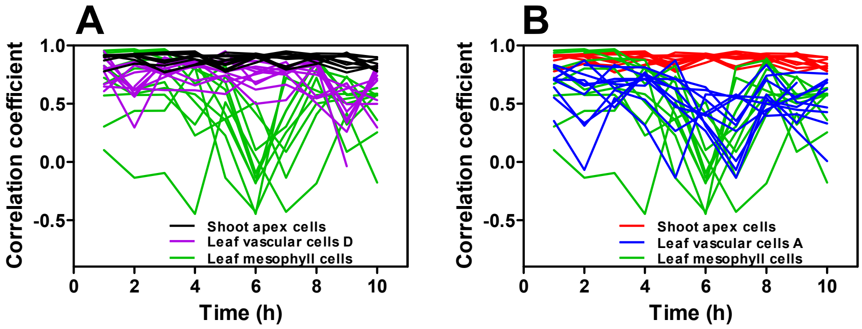

Figure 20. Correlation coefficients among the waveforms of CCA1-HA-EYFP fluorescent signals from individual nuclei in shoot apex, leaf mesophyll cells, and leaf vascular cells with advanced (A) and delayed (B) phases.

A higher synchrony in shoot apexes compared to vascular cells or the mesophyll cells adjacent to the leaf veins was also observed when an evening-expressed gene was examined (ELF3-EYFP) (Dixon et al., 2011). In this case, the separation of cells with advanced and delayed phases was not so evident in veins (Figure 21 A and B). Together, the results confirmed at the level of single cells and with three different reporters, our conclusions on the distinct degrees of synchrony in shoot apexes, leaf mesophyll cells, and veins.

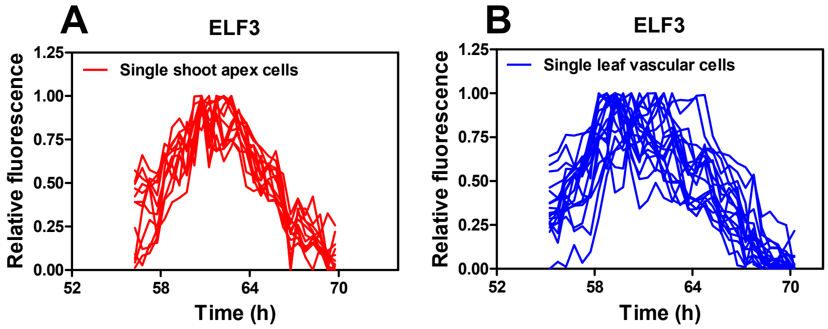

Figure 21. *In vivo* time-course imaging of ELF3-EYFP fluorescent signals quantified in individual nuclei of cells from the shoot apex (A) and leaf veins (B). Data are represented relative to the maximum value. Samples were maintained under LL

conditions at 60–100 µmol $m^{-2}s^{-1}$. Fluorescence quantification in the nuclei was analyzed using ImageJ software.

5. Intercellular circadian coupling among clock cells of the shoot apex

If coupling of shoot apex clocks is responsible for the waveform synchrony, then rhythms should be affected when the intercellular communication is disrupted. To explore this idea, we compared shoot apexes from intact tissues and from dissociated and diluted protoplasts. Rhythms in excised shoot apexes maintained good synchrony and were sustained for several days. However, in diluted shoot apex protoplasts, the oscillations persisted only for 2–3 days, increasing their heterogeneity over time (Figure 22 A). Further dilution of protoplasts increasingly advanced the timing of rhythmic dampening (Figure 22 B and C). Analysis of the R values in shoot apexes and in diluted protoplasts quantitatively confirmed that the phase coherence in protoplasts was only sustained for less than 2 days, reaching asynchrony afterward (Figure 22 D). As individual cells at the shoot apex are able to maintain rhythmic oscillations (Figure 19 C), one plausible explanation to our results is that dispersed cells do not sustain rhythms due to reduced intercellular communication and subsequent desynchronization over time.

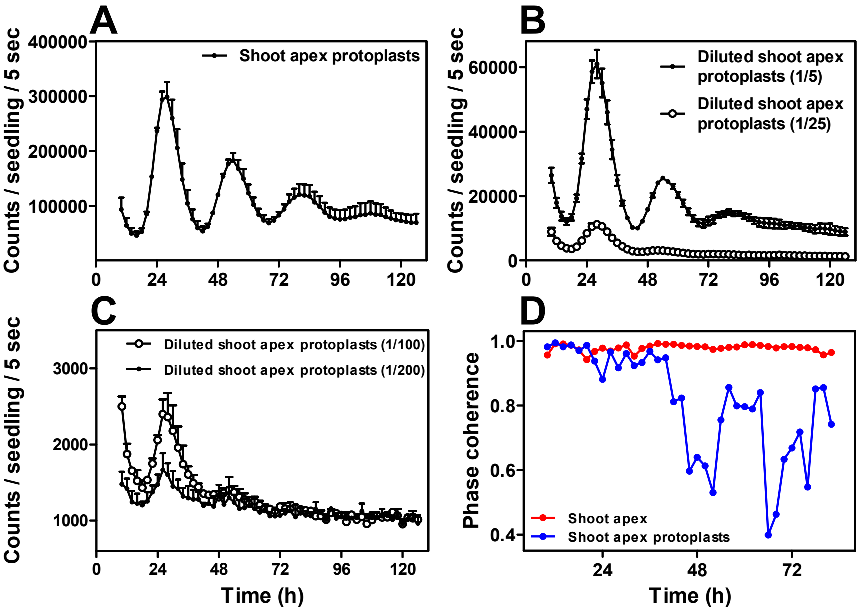

Figure 22. (A-C) Luminescence analysis of *CCA1::LUC* activity in dispersed (A) and further diluted series of protoplasts (B and C) from shoot apexes. Protoplasts were synchronized for an additional day under LD cycles before transferring to LL. Data are the means + SEM of the luminescence of 6–12 samples. (D) Quantification of the phase coherence in intact shoot apexes and in shoot apex protoplasts by calculating the synchronization index “R.”

In the mammalian circadian system, the clock components PER1 and CRY1 are required for sustained rhythms in peripheral tissues and in neurons dissociated from the SCN (Liu et al., 2007). However, cellular interactions at the SCN can compensate for *Per1* or *Cry1* deficiency (Liu et al., 2007; Evans et al., 2012). We found a similar scenario at the shoot apex of *lux* mutants. In contrast to the reported arrhythmia of *lux-2* plants, the *lux-2* shoot apexes were able to sustain rhythms to a certain degree. Although the rhythms were clearly compromised, rhythmicity at the *lux-2* shoot apex was better than in leaves (Figure 23 A-D). Thus, the absolute requirement of LUX function in leaves is not so apparent in shoot apexes. The differences are not due to changes in the circadian expression of *LUX* or the other components of the EC, *ELF3*, and *ELF4*, as verified by our RNA-seq analysis and by RT-qPCR (Figure 24 A-D).

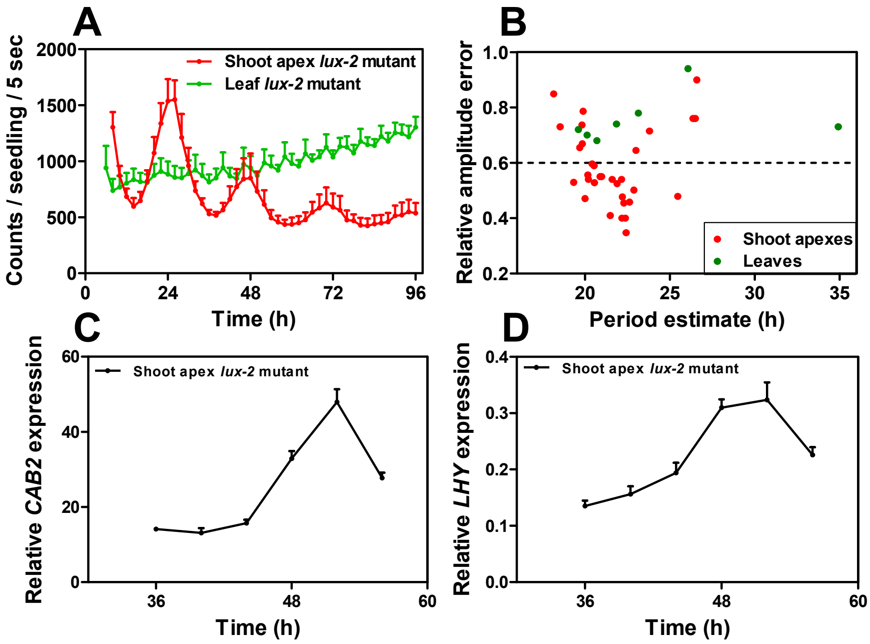

Figure 23. (A) Average luminescence of *CAB2::LUC* activity in shoot apexes and leaves of *lux-2* mutant plants. Data are means + SEM of the luminescence of six samples. (B) Period estimates and relative amplitude error of *CAB2*::*LUC* activity from individual traces. (C and D) RT-qPCR analysis of *CAB2* (C) and *LHY* (D) gene expression in the shoot apex of *lux-2* mutants grown under LD cycles followed by LL.

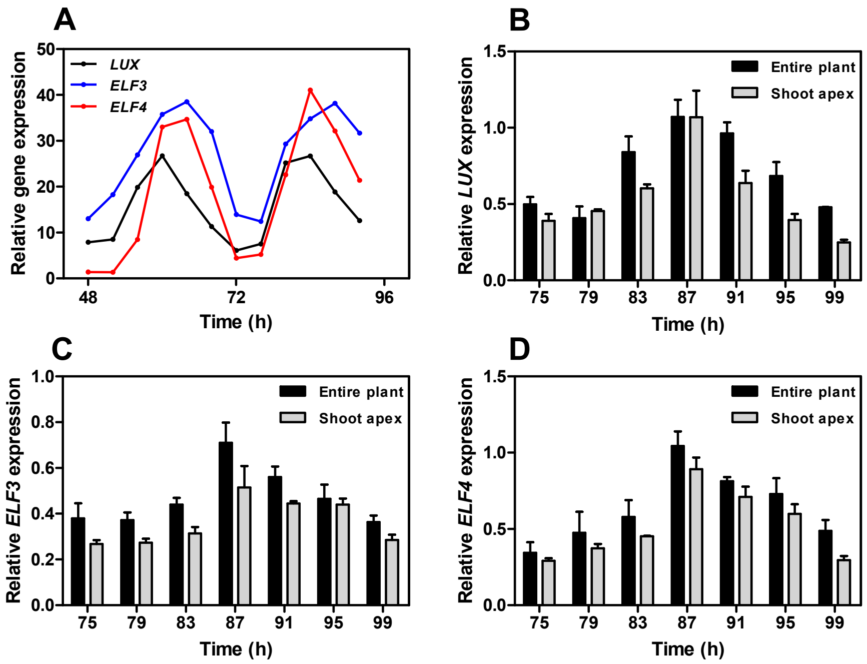

Figure 24. (A) Gene-expression analysis of *LUX*, *ELF3* and *ELF4* in the shoot apex of WT plants grown under LD cycles followed by 2 days under LL. (B-D) RT-qPCR analysis of *LUX* (B), *ELF3* (C), and *ELF4* (D) gene expression in entire plants and in shoot apexes. Plants were synchronized under LD cycles and the shoot apexes were excised and transferred to LL conditions for 3 days before sampling every 4 hour over a 24 hour circadian cycle. Data represents means + SEM of two biological replicates.

If in analogy to the mammalian system, effective intercellular coupling among the shoot apex cells is responsible for the distinctive phenotype, then disruption of the cellular communication should affect the rhythms. Indeed, shoot apex protoplasts from *lux-2* mutants were arrhythmic throughout the time-course analysis (Figure 25). We proposed that the arrhythmic phenotype in protoplasts is the result from the rapid desynchronization of the dispersed cells, each containing a semi-functional oscillator.

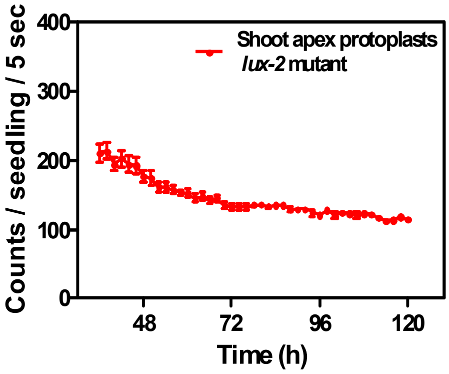

Figure 25. Luminescence analysis of *CAB2::LUC* activity in protoplasts from shoot apexes of *lux-2* mutant plants. Data represent means + SEM of 6–12 samples. Protoplasts were synchronized for an additional day under LD before transferring to LL.

Our results indicate that intercellular communication might be important for rhythms at the shoot apex. To mathematically explore the degree of intercellular coupling, we developed a predictive model by using barycentric coordinates for high-dimensional space (Hirata et al., 2015, please see Anex III). The model involves the use of linear programming that assigns different weights to neighboring cells and identifies the strength of coupling based on the accuracy of the predictions given the weights. We first tested the performance of the proposed methods using the Kuramoto (Kuramoto, 1975) and the coupled Rössler (Rössler, 1976) toy models. The examples showed that the weights of neighboring oscillators are higher when the coupling is stronger (Figure 26). When the model was used with the single-cell confocal data, we found that shoot apex clocks were highly coupled and had greater coupling strength than leaf vasculature or leaf mesophyll cells (Figure 26). Together, the results confirmed a gradation or hierarchy in the strength of the circadian communication in different parts of the plant.

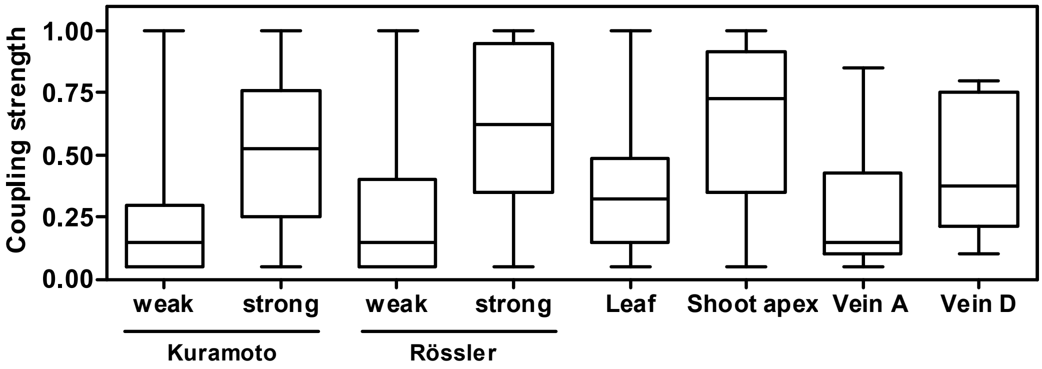

Figure 26. Mathematical analysis of the coupling strength by barycentric coordinates for high-dimensional space using the Kuramoto and coupled Rössler toy models and the in vivo CCA1-EYFP imaging data. The line in the middle of the box is plotted at the median. The whiskers represent the minimum and maximum values.

6. Relevance of the shoot apex clocks in the modulation of circadian oscillations in roots

We next addressed the possible role of the shoot apex controlling the circadian function in roots. We adapted the luminescence assay protocol (please check Materials and Methods) to examine rhythms in both shoots and roots of intact plants (Figure 27 A). We also used laser microdissection (LMD) to excise shoot apexes and examine rhythms in Δshoot apex plants (Figure 27 B).

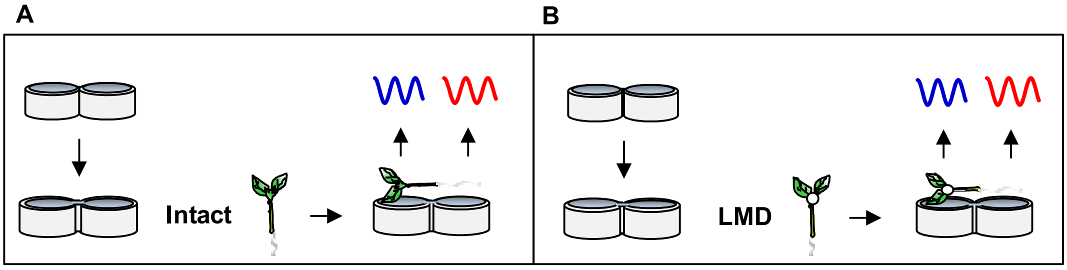

Figure 27. (A) Schematic drawing depicting the rhythmic analysis of shoots and roots from intact plants. (B) LMD was used to obtain Δshoot apex plants. Seedlings were horizontally positioned in serrated 96-well microplates so that rhythms could be examined in roots and shoots from the same plant.

Previous studies have reported that rhythms dampened low and waveforms broadened in entire plants after several days under free-running conditions (Yakir et al., 2011). We found that rhythms at the shoot apex were sustained for more than 7 days under LL (Figure 28), which suggests that intercellular coupling at the shoot apex might contribute to the rhythmic robustness after extended periods under LL.

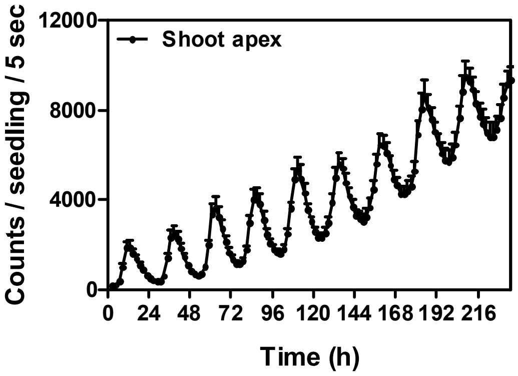

Figure 28. Average rhythms of *TOC1::LUC* luminescence in shoot apexes for extended days under LL following synchronization under LD. Data are the means + SEM of at least 6-12 individual samples.

When we examined rhythms in Δshoot apex plants, we observed an advanced average phase and increasing waveform variability, in a similar fashion to that of excised leaves (Figure 29 A and B). Application of auxin did not noticeably affect the rhythms in shoots of entire plants or Δshoot apex plants (Figure 29 C and D), which suggests that the Δshoot apex phenotypes are not due to changes in auxin flux. It is noteworthy that rhythms in plants that only lack the shoot apex are similar to the rhythms in leaves, whereas the small shoot apex is able to more precisely sustain rhythms. Unexpectedly, we also found that rhythms in plants without cotyledons or leaves were almost indistinguishable from the ones observed in intact plants (Figure 29 E and F).

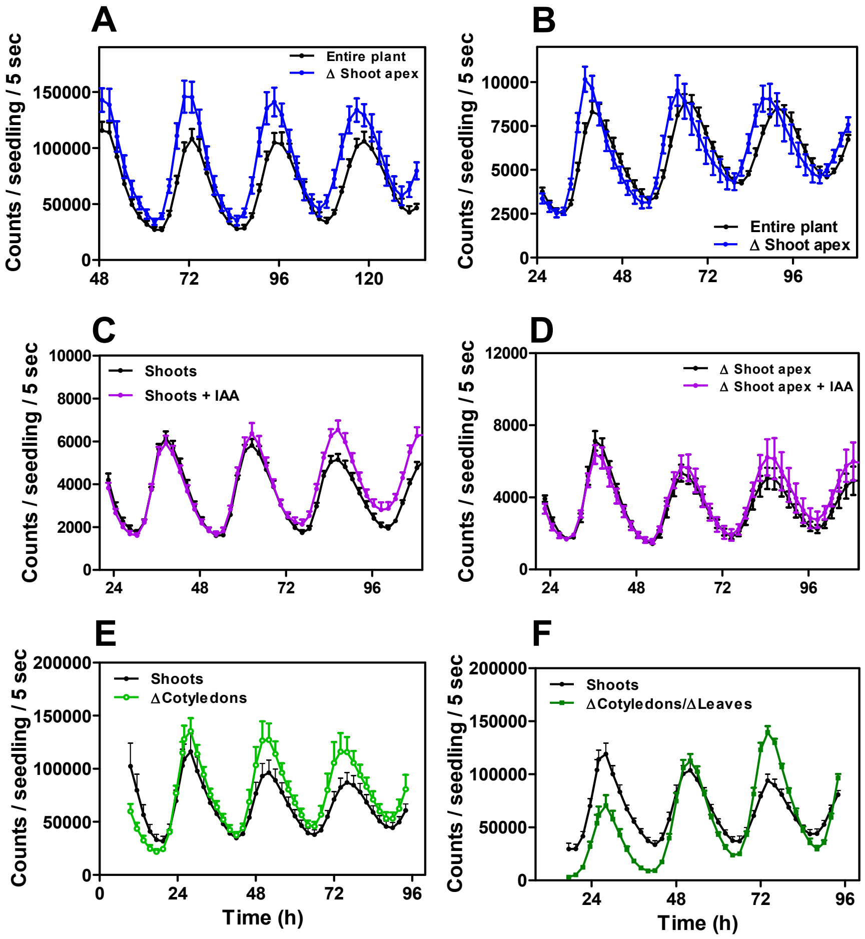

Figure 29. (A and B) Analysis of *CCA1::LUC* (A) and *TOC1::LUC* (B) luminescence in plants in which the shoot apexes were removed (Δshoot apex) by laser microdissection (LMD). (C and D) Rhythms in shoots from entire plants (C) and from Δshoot apex plants (D) treated with 20 μM of indole-3-acetic acid (IAA) on the shoot apex. (E and F) *CCA1::LUC* luminescence in plants in which the cotyledons (E) and leaves (F) were removed. Luminescence was recorded under LL following synchronization under LD. Data are the means + SEM of the luminescence of 6-12 samples.

Photosynthetic sucrose has been shown to modulate clock function (James et al., 2008; Haydon et al., 2013). Our studies revealed an initial phase delay and period lengthening that led to dampened rhythms in shoots from intact plants treated with the inhibitor of the photosynthetic electron transport

[3-(3,4-dichlorophenyl)-1,1-dimethylurea, DCMU] (Figure 30 A). When we applied the drug only in shoots and checked the effects on roots, we found a phase delay and dampened rhythms (Figure 30 B). These results confirmed that photosynthetic signals from shoots are important for the root clock. DCMU treatment in excised shoot apexes also led to eventual dampening of rhythms, but the early phase delay observed in whole shoots and roots was not so evident (Figure 30 C). These results suggest increased robustness against pharmacological perturbation of photosynthesis at the shoot apex.

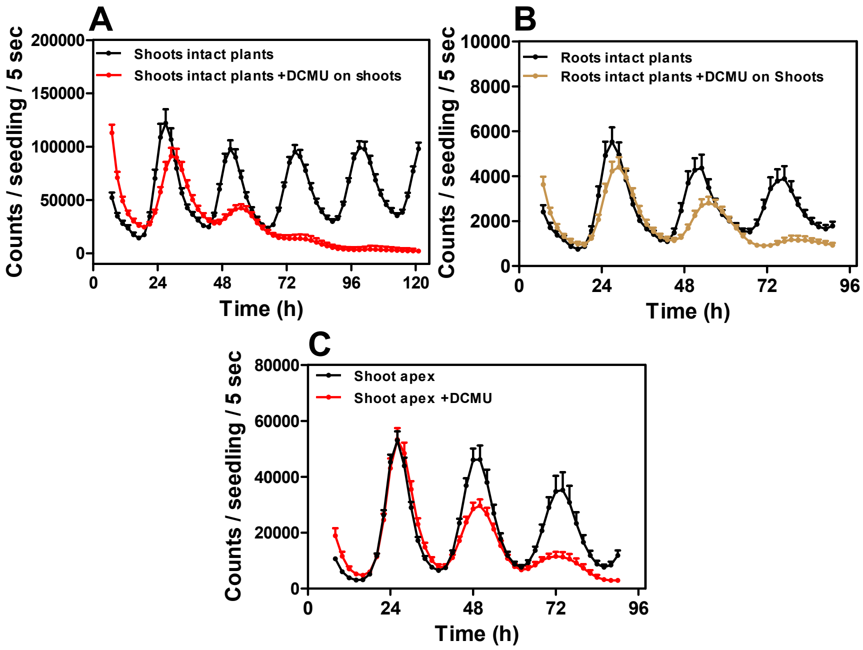

Figure 30. (A) Rhythms in shoots from entire plants following DCMU treatment on shoots. Intact plants were horizontally positioned on luminometer plate wells as shown in Figure 25. (B and C) Rhythms in roots from intact plants analyzed following DCMU treatment only on shoots (B) or in excised shoot apexes following treatment with DCMU (C). Luminescence was recorded under LL following synchronization under LD. Data are the means + SEM of the luminescence of 6-12 samples.

To further explore the importance of circadian communication, we used plants with reduced intercellular trafficking by means of *CALS3* gain-of-function mutations (*cals3-d*) that lead to reduced plasmodesmata aperture (Vatén et al., 2011). Our results showed that blocked trafficking clearly altered the rhythmic expression of core clock genes in roots, with no evident peak and trough expression as observed in WT roots (Figure 31 A-E).

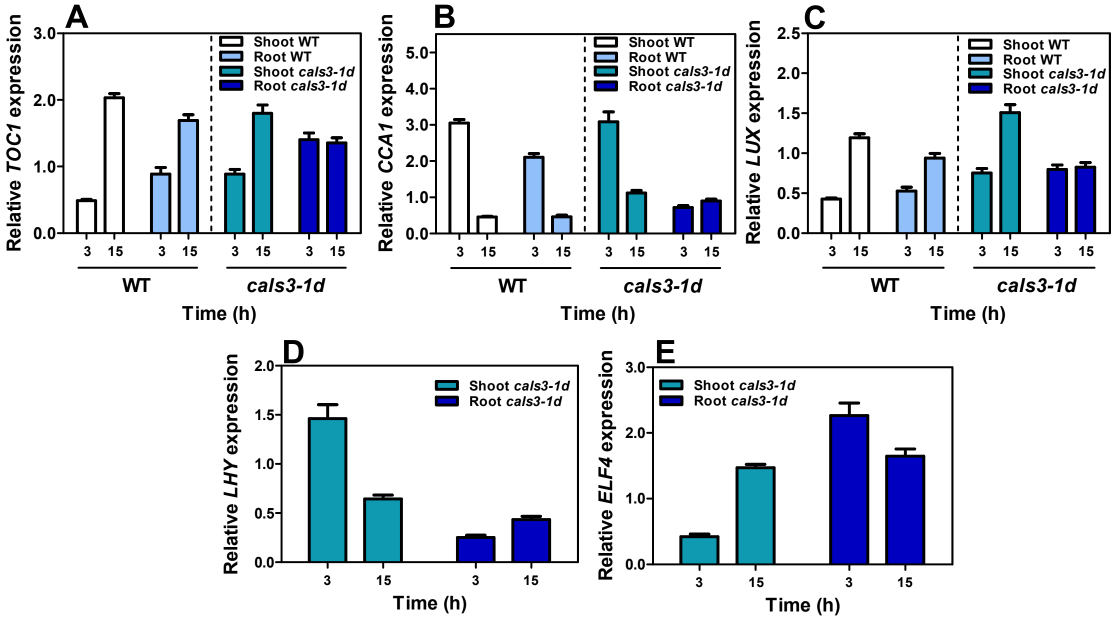

Figure 31. (A-C) RT-qPCR analysis of *TOC1* (A), *CCA1* (B) and *LUX* (C) expression in shoots and roots of WT and *cals3* mutant plants. (D and E) RT-qPCR analysis of and *LHY* (D), and *ELF4* (E) in shoots and roots of *cals3* mutant plants. Plants were synchronized under LD and samples were taken after 2 days under LL at CT3 and CT15.

We also examined rhythms in shoots and roots that were rapidly separated following 2 days of luminescence analysis of the intact plants (Figure 32 A). The separation led to dampening of rhythms in roots, indicating that rhythms in roots are altered very rapidly after separation from shoots. To ascertain the role of the shoot apex on root synchronization, we then examined circadian rhythms in roots from intact plants in which the shoot apex was removed (Δshoot apex plants) (Figure 27 B). Our results showed that rhythms were clearly affected, with an initial long-period phenotype that progressively led to arrhythmia (Figure 32 B). Rhythms in roots from plants in which leaves and cotyledons were removed were not severely affected and showed a slightly advanced phase compared with the rhythms in roots from intact plants (Figure 32 C). Noteworthy are also the results of "jet-jag" experiments showing that roots from intact plants were able to resynchronize with a pattern that more closely resembled the one in shoot apexes than the one in leaves (Figure 33 A and B).

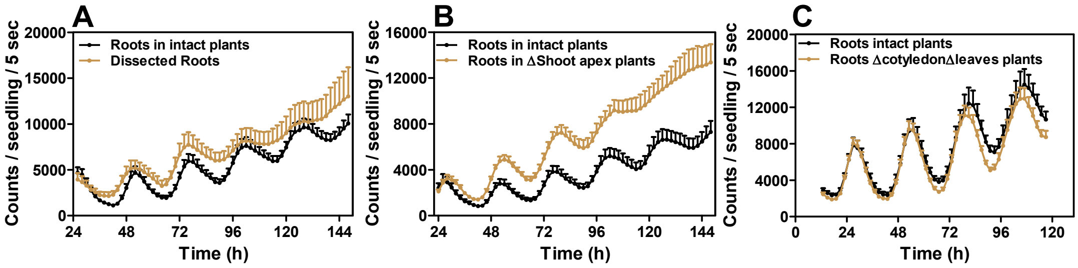

Figure 32. (A) *CCA1::LUC* luminescence from roots after rapid dissection from shoots. (B) *CCA1::LUC* luminescence in roots from intact plants and Δshoot apex plants. (C) *CCA1::LUC* rhythms in roots from intact plants and from plants in which the cotyledons and leaves were removed. Luminescence was recorded in presence of sucrose under LL following synchronization under LD. Data are represented as the means + SEM of the luminescence of 6-12 samples.

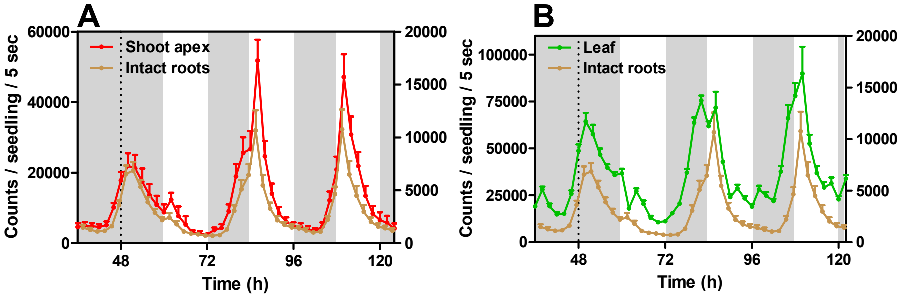

Figure 33. Comparisons of average rhythms of *CCA1::LUC* luminescence in roots from intact plants and excised shoot apexes (A) and leaves (B) subjected to a "jet-lag" experiment, with extended 12 hour darkness (extended night) at dawn. Data are the means + SEM of the luminescence of 6–12 samples. Values of luminescence signals of roots are represented on the right Y axes. White boxes: light; Shaded boxes: dark.

7. A hierarchical structure at the core of the Arabidopsis clock

Efficient micrografting of Arabidopsis seedlings is a powerful tool for studying long-distance signaling (Bainbridge et al., 2014). To conclusively determine the possible hierarchical nature of the plant circadian system, we performed micrografting with young Arabidopsis seedlings using the shoot apex as scion (Figure 34). We reasoned that grafting with different genotypes would provide definitive information on the role of shoot apexes on the root oscillation.

Micrografting and luminescence analysis were first tested on WT self-grafts (WT Shoot Apex–WT Roots, WT SA-WT Rt). The analysis showed that *CCA1::LUC* and *TOC1::LUC* rhythms followed a similar trend to that observed in entire non-grafted plants (Figure 35 A and B). Rhythms in roots exhibited a longer period compared to shoots, which also mirrored the observations in organs of non-grafted plants (Figure 6 G and H).

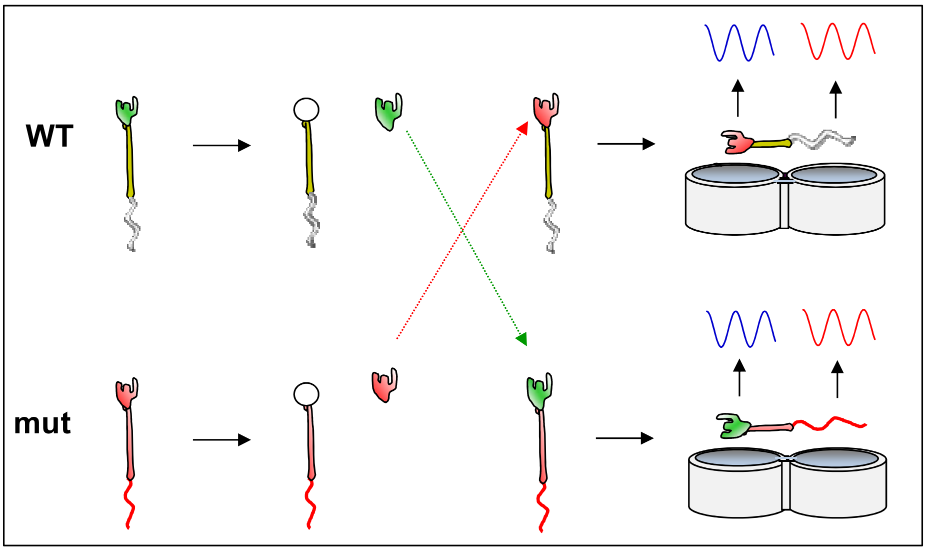

Figure 34. Schematic drawing depicting the rhythmic analysis of micrografted plants. Scions and rootstocks were isolated from seedlings of about 3-7 day old with a sterile razor blade, and joined together by very careful manipulation with tweezers. Grafts were horizontally positioned in serrated 96-well microplates so that rhythms could be examined in roots and shoots.

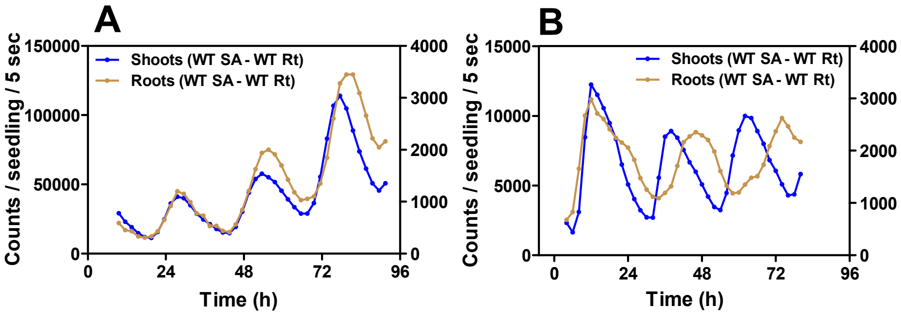

Figure 35. Analysis of *CCA1::LUC* (B) and *TOC1::LUC* (C) luminescence in shoots and roots of WT scion and WT rootstocks. Luminescence was recorded under LL following synchronization under LD. Values of luminescence signals from roots are represented on the right Y axes.

As these results suggested that the grafting procedure did not manifestly alter the circadian oscillation, we next grafted the shoot apex of arrhythmic plants into a WT rootstock. We reasoned that the lack of a functional clock in the shoot apex should alter the rhythms in roots. Indeed, grafting the shoot apex of the arrhythmic *cca1-1/lhy-11* plants (Mizoguchi et al., 2002; Portolés and Más, 2010) (Figure 36 A and B) disrupted the rhythms of WT roots (Figure 36 C). A similar alteration of WT root rhythms was observed with the shoot apex of *elf3-2* mutants (Hicks et al., 1996) (Figure 36 D). Although slight oscillations could be appreciated, the amplitude and robustness of the waveforms were clearly affected. These results confirmed that proper clock function in the shoot apex is important for the rhythmic activity in roots.

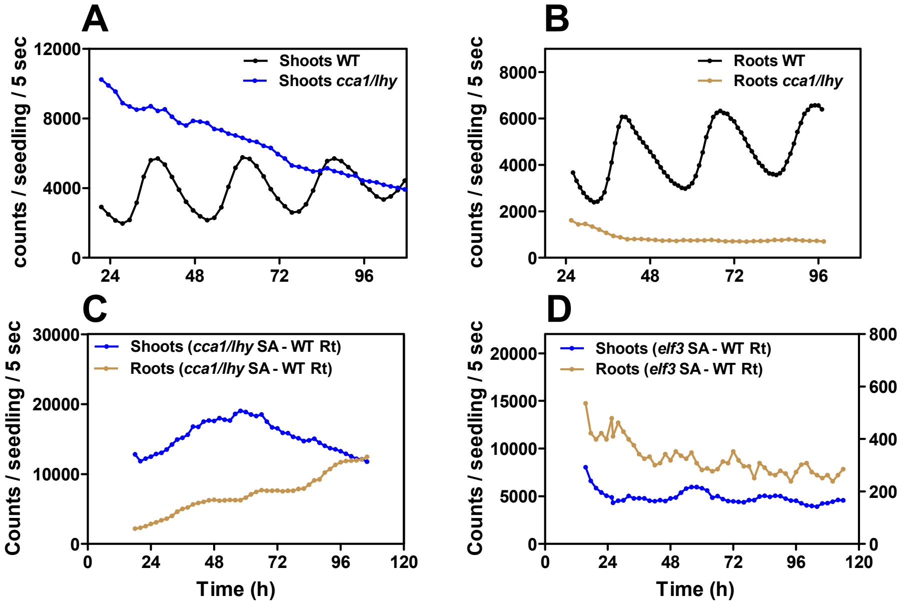

Figure 36. (A and B) Analysis of *TOC1::LUC* luminescence in shoots (A) and roots (B) of WT and *cca1/lhy* mutant plants. (C and D) Luminescence in shoots and roots of *cca1/lhy* mutant scion and WT rootstocks (C), *elf3* mutant scion with *CCA1::LUC* and WT rootstocks with *TOC1::LUC* (D) Luminescence was recorded under LL following synchronization under LD. Values of luminescence signals from roots are represented on the right Y axes for (D).

We then performed the reverse experiment in which WT shoot apexes were grafted into arrhythmic rootstocks to test the ability of shoot apex signals to reestablish the rhythms in roots. Remarkably, the arrhythmia of *cca1-1/lhy-11* or *elf3-2* roots could be partially restored by grafting the shoot apex of WT plants (Figure 37 A-C). The oscillations were not very robust, but the patterns were not as arrhythmic as the roots of non-grafted plants (Figure 36 B). Although we observed variability in the degree of restored rhythms (Figure 37 A and B), the recovery was quite evident. For WT SA-*cca1/lhy* Rt plants, a total of 120 grafting events were assayed, and approximately 50% of those were successfully grafted (possibly higher, but only faultlessly grafted plants were used for further analysis). Among 59 WT SA-*cca1/lhy* Rt successfully grafted plants, 50 showed a different degree of restoration in rhythmicity (approximately 85%, p value = 3.77×10^{-12} by Fisher's exact test, considering that none of the 20 *cca1/lhy* SA - *cca1/lhy* Rt plants displayed rhythms in roots). Altogether, we conclude that signals from the shoot apex are important for circadian oscillations in roots.

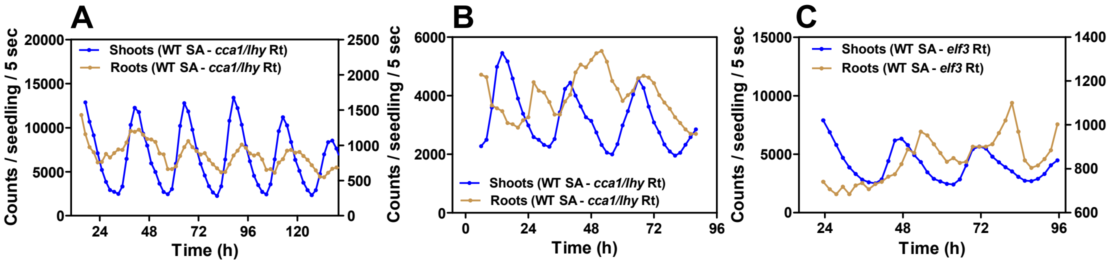

Figure 37. Luminescence in shoots and roots of WT scion and *cca1/lhy* mutant rootstocks (A and B), and WT scion and *elf3* mutant rootstocks (C). Luminescence was recorded under LL following synchronization under LD. Values of luminescence signals from roots are represented on the right Y axes for (A) and (C).

DISCUSSION

Discussion

We have addressed in our studies an important issue related to the circadian organization in plants. We have discovered that the cellular clocks at the shoot apex can (1) generate autonomous rhythms, (2) readjust to phase changes, (3) maintain synchrony to one another under free-running conditions, (4) provide robustness against genetic and pharmacological perturbations and (5) modulate the rhythmic activity in distal parts of the plant. Our study suggests that the plant clockwork might be closer to the mammalian circadian system than to the Drosophila clock, in which the rhythmic activity emerges from many independent oscillators (Yao and Shafer, 2014). Studies of topographically defined areas of circadian coupling and elucidation of the signals and mechanisms contributing to the circadian communication in plants will be central to fully define the spatio-temporal networks orchestrating physiology and development on each organ, tissue and cell.

A series of different protocols developed in this study has allowed us to follow the rhythmic expression in excised organs of the plant. Under sucrose, rhythms were sustained in all organs examined and the tissues continued growing normally after excision, which suggests that the excision did not manifestly affect the rhythms. The different excised organs displayed a wide range of circadian properties. Hypocotyls and roots lack precision and robustness, with long circadian periods and arrhythmia, whereas leaves lack synchrony among the different samples from plants similarly entrained. As roots are a sucrose sink, our results with excised roots (±sucrose) are consistent with previous studies (James et al., 2008; Haydon et al., 2013) and with the dampening of rhythms in roots when shoots are treated with DCMU. Analysis of root rhythms in Δshoot apex plants rendered similar results to those of excised roots, which confirmed the dependency of roots on the circadian communication with shoot apexes. The heterogeneity of circadian waveforms in leaves is also consistent with previous studies showing that bioluminescent signals from individual clocks in leaf cells cannot retain their synchrony under free-running conditions (Wenden et al., 2012). Phase heterogeneity might be due to differences in circadian coupling among various leaf cell types. Mesophyll cells in leaves are only weakly coupled, whereas the leaf vasculature synchronizes the neighboring mesophyll cells (Endo et al., 2014). This local synchronization raises the question about possible differences in rhythms of mesophyll cells close to the vasculature and those located far from the veins. Desynchronization between leaf stomatal and mesophyll cells (Yakir et al., 2011) could be another source of phase heterogeneity in leaves.

Shoot apexes displayed remarkable homogeneous rhythmicity with highly synchronous waveforms. Among the tissues examined, different patterns of waveform synchrony could be distinguished: the cells from the shoot apex with the highest synchrony, the intermediate synchrony in the vascular cells, and the lowest synchrony observed in leaf mesophyll cells. The fact that the synchrony is lost in dispersed, diluted shoot apex protoplasts suggests that the phase coherence and synchrony might be due to high intercellular coupling among shoot apex clocks. The development of a tailor-designed mathematical model using barycentric coordinates for high-dimensional space confirmed this notion. The method has been proven successful for a wide range of uses, from weather forecasting to creation of musical instruments with natural sounds (Hirata et al., 2015). Our studies also revealed that the intercellular coupling or circadian communication among shoot apex clocks confer robustness against genetic mutations and pharmacological perturbations. These properties closely resemble those of the circadian system in mammals in which intercellular coupling among neurons at the intact SCN can compensate for the absence of functional key clock components *Per1* or *Cry1* (Liu et al., 2007; Evans et al., 2012).

The molecular circadian network and phenotypes of core clock mutants at the shoot apex appear to be similar to those described in the whole plant. However, prevalence for morning- or evening-expressed genes has been shown for the clocks of leaf mesophyll cells and leaf veins, respectively (Endo et al., 2014). Uncoupled morning and evening oscillators for the clock in roots have been also previously proposed based on the shoot specific period shortening exhibited by *toc1* mutants, and arrhythmia of evening-phased genes in roots under constant light conditions (James et al., 2008). Our full time-course analysis by RNA-seq showed robust rhythms of circadian genes with similar peak phases and relative amplitudes to those reported in entire plants. The particular properties that we observed at the shoot apex clocks might result from their strong intercellular coupling rather than from a distinctive molecular network.

We also found a clear enrichment of genes involved in responses to environmental signals. This enrichment might be responsible for the distinctive waveforms in "jet-lag" experiments, as if the shoot apex clocks were highly sensible to perceive and respond to the changing environmental conditions. The enrichment might be particularly useful for the shoot apical cells that are buried and shielded from the environment. Intercellular coupling might also be an aid for circadian synchronization of cells with reduced light accessibility. The fact that genes responsible for perception of synchronizing signals such as light and temperature are enriched in our RNA-seq data is consistent with a main role of shoot apexes as a synchronizing master clock.

Grafting assays have been long used to study long-distance signaling in many different processes. Just two examples include for instance the use of Arabidopsis grafts between WT and mutants with increased branching that revealed the existence of a shoot branching signal able to move from roots to shoots (Turnbull et al., 2002). Another study used abscisic acid (ABA) deficient tomato grafts to show that stomatal closure in response to soil drying can occur in the absence of leaf water deficit and without requiring ABA production in roots (Holbrook, 2002). Our studies demonstrate the long-distance circadian signaling by micrografting approaches, and the influence of shoot apexes on the rhythmic activity of roots. The partial recovery of mutant rootstocks by grafting WT shoot apexes and, conversely, the arrhythmia of WT roots grafted with arrhythmic shoot apexes reflect the circadian hierarchy of shoot apexes. This situation is reminiscent of the circadian system in mammals in which genetic defects in peripheral clocks are phenotypically rescued by the hierarchical dominance of the SCN (Pando et al., 2002). The micrografting results were consistent with the shoot apex role influencing rhythms in roots, which was observed by other approaches used in this study (rapid dissection of shoots and roots, delta shoot apex plants, pharmacological treatments, and genetic analysis). The similar phenotypes reinforce the validity of the different procedures and the consistency of our conclusions.

A precise determination of mechanisms and factors responsible for short- and long-distance signaling awaits further investigation. One possible model is that changes in sugar flux at the vascular tissue is contributing to synchronize rhythms, using veins as the circadian traveling “highway” for the circadian coupling. This scenario certainly fits with previous reports showing that photosynthetic sugar has a marked effect on the entrainment and circadian rhythms (Haydon et al., 2013), application of sucrose affects the rhythms in roots (James et al., 2008), and our findings of the hierarchical structure in the circadian system.

Our studies also raise a question: how can the shoot apex govern the synchronization in distal parts of the plant? The shoot apex is a sucrose sink and thus it is unlikely that sugars locally photosynthesized at the shoot apex are directly regulating the circadian rhythms in other organs. A hint might be provided by a recent work showing that the shoot apex can regulate photosynthesis in distal leaves in tomato (Guo et al., 2016). The study describes a mechanism by which the photoreceptor PHYB perceives light at the shoot apex and triggers local IAA biosynthesis. Polar auxin transport drives then the movement of IAA to leaves, activating the cyclic electron flow around the photosystem I by changing the reduction-oxidation (redox) balance, increasing adenosine triphosphate (ATP) production, and fueling photosynthesis (Guo et al., 2016).

Just like in tomato, the shoot apex in Arabidopsis might also regulate the photosynthetic activity, modulating the sucrose flux. This would allow the shoot apex to indirectly modulate the photosynthetic-dependent circadian rhythms in distal parts of the plant. The components for this process are shared between these two species, and the enrichment of light input genes in our RNA-seq data also supports this idea. The circadian clock at the shoot apex might also directly drive photosynthetic activation, as several studies have shown the involvement of the clock within the PHYB signaling (Salomé and Michael, 2002), auxin pathway (Covington and Harmer, 2007), redox homeostasis (Lai et al., 2012) or ATP production (Karlsson et al., 2015).

Despite the possible important role of sugar flux on clock synchronization, supplemented sucrose was insufficient to completely synchronize circadian rhythms between shoots and roots under free-running conditions, indicating that the "time messenger" requires something else than sugar alone. Besides auxin, other phytohormones such as cytokinin could be involved in the long-distance communication between clocks. Indeed, exogenous application of cytokinin affects the oscillation of clock genes in Arabidopsis (Hanano et al., 2006; Salomé et al., 2006). A study showed that N^6-(Δ^2-isopentyl)adenine, one particular isoform of cytokinin, travels from shoots to roots and specifically regulates the vascular pattern in the root meristem, while not interfering with other cytokinin-regulated pathways (Bishopp et al., 2011). These findings could be expanded to the idea that shoot-derived cytokinins might deliver the temporal information to roots, enabling local coupling of clocks around the vasculature, similarly to those found in leaves (Endo et al., 2014). ABA signaling is also highly interconnected with the plant clock (Hanano et al., 2006). Intriguingly, osmotic stress perceived at the roots is shown to affect the expression of clock genes in shoots via an ABA-dependent pathway in barley (*Hordeum vulgare*) (Habte et al., 2014), suggesting the existence of a circadian signaling from roots to shoots in monocots under stress.

Non-coding RNAs (ncRNAs) can be added to the list of candidates for circadian coupling. In animals, some ncRNAs are rhythmically transcribed and function in the control of circadian rhythms (Kornfeld and Brüning, 2014). For example, *PER2* expression is regulated in mouse liver by an anti-sense long ncRNA called *asPER2* (Vollmers et al., 2012). In plants, many ncRNAs including natural anti-sense transcripts of *CCA1*, *LHY*, and *PRRs* are rhythmically expressed (Hazen et al., 2009). Although the actual function of these rhythmic ncRNAs are yet to be identified, they might function as signaling factors. In this sense, they might act similarly to the ncRNAs known to regulate phosphate homeostasis in plants (Pant et al., 2008).

Possibilities of "time messengers" are not limited to just molecules. Light perceived by roots has been proposed as a synchronizing signal, since the clock in separated roots are entrained by direct exposure to light/dark cycles (Bordage et al., 2016). Although roots are largely covered by soil in nature, light-piping through plant tissues could conduct low levels of light (Mandoli and Briggs, 1984) and light is able to penetrate the soil (Tester and Morris, 1987). Therefore, the direct effect of light on roots close to the surface might partly contribute to the synchronization of roots (Bordage et al., 2016).

Overall, our studies suggest that clocks at the shoot apex have a high degree of precision and synchrony, likely due to high intercellular coupling. Additionally, there is a long-distance communication between the clocks in shoot apexes and roots such that the shoot apex clocks can regulate the function of the root clocks. This circadian communication might be established by an orchestration of modulated sugar flux and signaling factors that act as “time messengers” able to coordinate rhythms at the whole plant level (Figure 38).

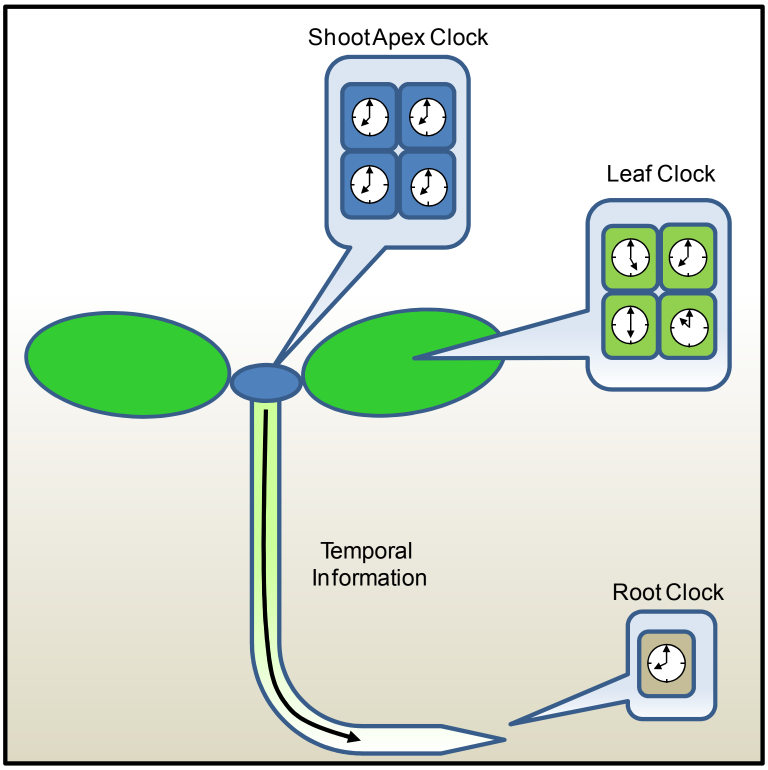
Shoot Apex Clock
Leaf Clock
Temporal Information
Root Clock

Figure 38. Graphical representation depicting the hierarchical structure of the circadian clock in Arabidopsis. Unlike leaves, clocks at the shoot apex are highly coupled, and can modulate circadian rhythms in root tissues.

CONCLUSIONS

Conclusions

The shoot apex clocks in Arabidopsis function in a similar way to that of the neurons from the suprachiasmatic nucleus in mammals. A strong circadian coupling within the clocks at the shoot apex defines the high degree of synchrony among them. Different plant organs exhibit variations in clock precision and circadian synchrony, with the clocks at the shoot apex influencing the circadian activity in roots. This situation parallels the hierarchical nature of the circadian system in mammals. Altogether, **we found that the circadian system in plants is hierarchical, with the clocks at the shoot apex functioning as master clocks synchronizing rhythms in roots**. A brief description of the main conclusions of these studies is summarized below:

1. The development of an *in vivo* luminescence approach has allowed us to discern the circadian function in different organs excised from the plant. We conclude from these studies that **there is a disparity of the circadian oscillations in excised Arabidopsis organs**, with hypocotyls, roots and leaves displaying reduced circadian precision.

2. *In vivo* luminescence assays with excised shoot apexes revealed that circadian rhythms were highly homogeneous among different samples, showing a high degree of synchronization. Our results show that **shoot apex clocks behave in a different way compared with other organs examined, and indicate that the shoot apex clocks are highly precise**.

3. The use of different clock mutants and reporter lines as well as analyses of the global circadian transcriptional landscape at the shoot apex revealed no fundamental changes of the components and regulatory networks compared to whole plants. Our results thus indicate that **the high degree of precision and synchrony of oscillations is not likely due to a molecular circadian network that is specific for the shoot apex**.

4. *In vivo* live-imaging of rhythmic single cells, desynchronization of dispersed protoplasts and mathematical analysis using barycentric coordinates for high-dimensional space revealed **a tight circadian coupling of cells at the shoot apex**. **The increased rhythmic synchrony confers robustness** against genetic and pharmacological perturbations **and particular capabilities for phase readjustments** during "jet-lag" experiments.

5. The development of a modified version of the *in vivo* luminescence approach has allowed us to examine rhythms in shoots and roots from the same plant. Rhythms in roots were affected by the removal of the shoot apex, by reducing the photosynthetic activity in shoots or by decreasing intercellular trafficking. Our results thus indicate **the importance of long-distance circadian communication between the clocks in shoots and roots**.

6. The use of micrografting assays with arrhythmic mutant shoots into Wild-Type roots clearly affected the rhythms in roots. More importantly, micrografting WT shoots into arrhythmic mutant roots resulted in a partial restoration of the circadian oscillation in roots. Thus, **signals from the shoot apex are able to modulate the circadian function of the root clocks**.

RESUMEN EN CASTELLANO

Resumen en Castellano

El reloj circadiano es un mecanismo celular responsable de la generación de ritmos biológicos con un periodo de 24 horas. La importancia de la función del reloj circadiano es evidente en casi todos los organismos estudiados hasta la fecha, desde bacterias hasta los seres humanos. Dado que las plantas son organismos sésiles, la función circadiana es particularmente relevante para su correcta adaptación al medio y supervivencia. Entender cómo el sistema circadiano de la planta se organiza en el contexto de células, tejidos y órganos surge como una de las preguntas fundamentales para comprender la fisiología y el metabolismo de la planta. Sin embargo, un gran desafío para los estudios de biología vegetal es descifrar cómo los relojes circadianos individuales están interconectados para generar ritmos en toda la planta. En esta Tesis Doctoral, demostramos que el ápice del brote aéreo de la planta *Arabidopsis thaliana* está compuesto por un conjunto de relojes acoplados que sincronizan los ritmos circadianos en la raíz. Una serie de diversos protocolos desarrollados en este estudio reveló una disparidad de oscilaciones circadianas en hipocotilos, raíces y hojas diseccionadas que exhibían una reducida precisión circadiana. En contraste, los análisis del ápice aéreo de la planta demostraron ritmos altamente sincronizados y precisos. El uso de diferentes mutantes de reloj y líneas de reporteros, así como el análisis global de la transcripción circadiana indicó que tal sincronía y precisión no era debida a una red circadiana molecular específica del ápice del brote. Sin embargo, los estudios *in vivo* de células individuales, la desincronización de protoplastos dispersos y el análisis matemático usando coordenadas baricéntricas para espacios multi-dimensionales demostraron que la precisión circadiana era debida al acoplamiento o comunicación entre las células del ápice del brote. La mayor sincronía rítmica confería precisión y robustez frente a perturbaciones genéticas y farmacológicas así como capacidades particulares para los reajustes de fase durante experimentos de "jet-lag". Los ritmos en raíces estaban alterados por la ablación del ápice y en estudios de microinjertos, sugiriendo que las señales del ápice pueden sincronizar órganos distales. De una forma similar a la organización circadiana en mamíferos, nuestros estudios demuestran que los ápices juegan un papel dominante dentro del sistema circadiano jerárquico en plantas.

MATERIALS AND METHODS

Materials and Methods

1. Plant material, seed sterilization and growing conditions

Different *Arabidopsis thaliana* lines were used in this study (Please see Table 1). For sterilization, seeds were placed in 1.5 mL microcentrifuge tubes and surface sterilized by soaking in 70% ethanol (v/v) with 0.1% (v/v) of Triton X-100 for 10 min, followed by several washes with 70% ethanol. Seeds were dried on sterile filter paper in a laminar flow cabinet and sown on plates containing Murashige and Skoog (MS) agar medium supplemented or not (as specified for each experiment) with 3% (w/v) sucrose. After 48 hours of stratification at 4ºC in the dark, plates were transferred to environmentally-controlled chambers (Inkoa Sistemas) and plants were grown under light/dark cycles (LD, 12 hour light:12 hour dark) with 60-100 µmol $m^{-2}s^{-1}$ of cool white fluorescent light at 22ºC.

2. Plant dissection

Seedlings of about 9-14 day-old were dissected with sterile surgical blades (#11 and #21) (Swann-Morton) to obtain excised shoots, roots, leaves, hypocotyls, and shoot apexes. LMD6000 laser microdissection system (Leica) was used to obtain plants without shoot apexes (Δshoot apex). Seedlings were placed on sterile plate lids containing MS medium on the microscope stage and tissues were cut with the UV laser (337 nm) using a 6.3x objective (Move and Cut mode), power 100 and specimen balance 0. Care was taken to preserve the integrity of the tissue.

Table 1. *Arabidopsis thaliana* plants used in this study

Line	**LUC Reporter**	**Ecotype**	**Reference**
WT	*CCA1::LUC*	Col-0	(Salomé and McClung, 2005)
WT	*CAB2::LUC*	C24	(Millar et al., 1995)
WT	*CAB2::LUC*	Ws	(Ding et al., 2007)
WT	*TOC1::LUC*	Col-0	(Perales and Más, 2007)
WT	*CCR2::LUC*	Col-0	(Strayer et al., 2000)
cca1-11	*CAB2::LUC*	Ws	(Ding et al., 2007)
cca1-1/lhy-11	*TOC1::LUC*	Ler	(Mizoguchi et al., 2002)
TOC1 RNAi	*CCR2::LUC*	Col-0	(Más et al., 2003a)
lux-2	*CAB2::LUC*	Col-0	(Hazen et al., 2005)
elf3-2	*CCA1::LUC*	Col-0	(Hicks et al., 1996)
CCA1-HA-EYFP/cca1-1	-	Col-0	(Yakir et al., 2009)
PRR7:FLAG-PRR7-EGFP	-	Col-0	(Nakamichi et al., 2010)
ELF3:ELF3-EYFP	-	Ws	(Dixon et al., 2011)
cals3-d	-	C24	(Vatén et al., 2011)

3. *In vivo* luminescence assays

Whole seedlings, excised organs or plants at about 9-14 days after the micrografting procedure were transferred to 96-well plates containing per well 180 µL of MS agar medium supplemented or not (as specified for each experiment) with 3% (w/v) sucrose, and 40 µL of luciferin solution consisting of 1.4 mM luciferin in 2.6 mM 2-(*N*-morpholino)ethanesulfonic acid (MES) at pH 5.8. Luminescence was monitored using a microplate luminometer LB-960 (Berthold Technologies) and the software Microwin, version 4.34 (Mikrotek 2 Laborsysteme). The period, phase and relative amplitude error of oscillations were calculated with the Fast Fourier Transform–Non-Linear Least-squares (FFT-NLLS) suite of the Biological Rhythms Analysis Software System (BRASS) package (http://millar.bio.ed.ac.uk/PEBrown/BRASS/BrassPage.htm).

For analysis of rhythms in roots from intact plants, Δshoot apex or Δleaf plants, one side of the walls of the plate wells was slightly serrated using heated surgical blades to allow communication between two adjacent wells. Seedlings were then horizontally positioned such that the shoot was placed in one well and the roots in the contiguous well. To decrease the possible effects following dissection and manipulation, samples were allowed to resynchronize for one day before luminescence analysis under constant light conditions (LL). Data from samples that appeared damaged or that eventually died after the treatments were excluded from the analysis. Luminescence analyses of pharmacological treatments were performed by applying to the shoots, shoot apexes or roots 20 µM of IAA or 20 µM of DCMU.

4. Micrografting

Seedlings were vertically grown on half strength MS agar medium supplemented with 0.5% (w/v) sucrose for 3-7 days. Seedlings were then transferred on top of wet filter papers or on 0.2 µm nitrocellulose membranes (Whatman) under the dissecting microscope in a laminar flow cabinet, as described (http://www.bio-protocol.org/e1164). Using sterile surgical blades (#11), cotyledons and hypocotyls were removed to obtain scions of shoot apexes. Rootstocks were obtained by cutting just below the shoot apex. The scion and rootstock cut stumps were joined together by very careful manipulation with tweezers, paying attention to align the two phloem strands. Plates containing grafted seedlings were sealed with two layers of micropore tape (3M) and then incubated minimum of 4-6 days in the growth chamber. Adventitious roots from scions, if present, were carefully removed under the dissecting microscope. Unsuccessful grafts or not clearly joint scions and rootstocks were discarded. A wet-lab protocol with a detailed step-by-step description of the micrografting experiments can be found in Anex I.

5. RNA extraction, RNA sequencing and analysis of circadian oscillations

Shoot apexes separated from 9-14 day old plants synchronized under LD cycles were transferred to LL conditions for 2 days. Samples were collected from the third day under LL, every 4 hours over two circadian cycles. Harvested samples were snap frozen by liquid nitrogen and stored at -80ºC. Total RNA was isolated using the RNeasy Plant Mini Kit (Qiagen) following the manufacturer's recommendations. RNA sequencing was performed by Genomix4life S.R.L. (Baronissi, Salerno, Italy). Indexed libraries were prepared from 500 ng purified RNA pool with TruSeq Stranded mRNA Sample Prep Kit (Illumina) according to the manufacturer’s instructions. Libraries were sequenced (paired‐end, 2 × 100 cycles) at a concentration of 8 pmol/L per lane on HiSeq1500 platform (Illumina) with a coverage of more than 30 million sequence reads/sample on average.

Sequence analysis was performed by Sequentia Biotech (Barcelona, Spain). The raw sequence files (.fastq files) were subjected to quality control analysis by using FastQC v0.10.1 (www.bioinformatics.babraham.ac.uk/projects/fastqc/) before trimming and removal of adapters with AdapterRemoval 1.5.2 and FASTX

Toolikt 0.0.13.2 (Lindgreen, 2012). The reads were then mapped against the *Arabidopsis thaliana* genome (TAIR10 Genome Release, ftp://ftp.arabidopsis.org/) with TopHat v2.0.11 (Kim et al., 2013), which provided the reference gene annotation with known transcripts. Cufflinks v2.2.0 (Trapnell et al., 2010) was then used to obtain RPKM expression for each annotated gene. Duplicated reads were removed from the mapped files (bam files) with Picard Tools 1.110 (http://picard.sourceforge.net) and the resulting files were merged to include the annotation of new transcripts by using Cufflinks v2.2.0 (Trapnell et al., 2010). Comparisons with the reference genome were performed by using Cuffmerge v1.0.0 (Trapnell et al., 2010). To identify oscillating genes regulated by the circadian clock, all genes with a RPKM median across the samples less than 0.69 were discarded. The BETR algorithm (Aryee et al., 2009) was applied to identify differentially expressed genes across the dataset ($p<0.05$).

The JTK_CYCLE algorithm (Hughes et al., 2010) was used to identify oscillating genes ($q<0.05$) with a period ranging from 20 to 28. The Integrative Genomics Viewer (IGV) was used to visualize the data (Robinson et al., 2011; Thorvaldsdóttir et al., 2013). The phases of circadian expression in shoot apexes and entire plants were analyzed using the publicly available Gene Phase Analysis Tool “PHASER” of the DIURNAL database (http://diurnal.mocklerlab.org/) (Mockler et al., 2007; Michael et al., 2008). Phase over-representation was calculated as the number of genes with a given phase divided by the total number of genes over the number of genes called rhythmic and divided by the total number of genes in the dataset. Circadian genes were classified into broad functional categories using the web tool “BIOMAPS” (Katari et al., 2010), which renders over-represented and significant functional terms (Gene Ontology or MIPS) as compared to the frequency of the term in the whole genome.

6. Gene expression analysis by RT-qPCR

Total RNA was prepared with a Maxwell 16 LEV simply RNA Tissue kit (Promega) and used for cDNA synthesis with iScript™ Reverse Transcription Supermix for RT-qPCR (BioRad) following the manufacturer's protocol. RT-qPCR was performed using 96-well CFX96 Touch Real-Time PCR Detection System (BioRad) with 10% diluted cDNA and iTaq Universal SYBR Green Supermix (BioRad). RT-qPCR thermal profile consisted of 30 seconds at 95ºC for one cycle, 39 cycles of 5 seconds at 95ºC followed by 30 seconds at 60ºC, with final steps from 65ºC to 95 ºC, 0.5ºC increments at 5 seconds per step. Primers used for gene expression analysis are listed in Table 2. The expression of genes was calculated by the comparative Ct method using *PP2AA3* (*Protein Phosphatase 2A subunit A3*) gene as the control (Kaufmann et al., 2010). Analyses by RT-qPCR were carried out with three technical replicates and at least two biological replicates.

Table 2. Primers used for gene expression analysis

Name		Sequence
TOC1	Forward	GAA GAT GTT GAT CGA CTG AC
	Reverse	GAG CCA ACA TTG CCT TAG AG
CCA1	Forward	TCA AGC TTC CAC ATG AGA CTC TA
	Reverse	GGA AAC AAA TAC AAA GGC CTC A
CAB2	Forward	AAT TCG AGT GAG AGA CAG GAG GAG
	Reverse	GTC TCT ACC ATC CAC CAC AAA CAC
LHY	Forward	ACA GCA ACA ACA ATG CAA CT
	Reverse	GAG AGC CTG AAA CGC TAT AC
LUX	Forward	GAC GAT GAT TCT GAT GAT AAG G
	Reverse	CAG TTT ATG CAC ATC ATA TGG G
ELF3	Forward	CGT AGT AAC AAC ACA AGC A
	Reverse	GAA GGA CAT TTG GGA GAC
ELF4	Forward	GAC AAT CAC CAA TCG AGA AT
	Reverse	ATG TTT CCG TTG AGT TCT TG
PP2AA3 (Control)	Forward	AAG CGG TTG TGG AGA ACA TGA TAC G
	Reverse	TGG AGA GCT TGA TTT GCG AAA TAC CG

7. Single cell confocal microscopy imaging

For *in vivo* single cell confocal imaging, we used a previously described method (Más and Beachy, 1998) with minor modifications. Briefly, isolated shoot apexes or leaves were embedded in 0.1% (w/v) low-melting-point agarose dissolved in MS medium. The embedded samples were placed on microscope slides with approximately 200 µL of liquid MS medium, which generated air bubbles within the liquid layer. Cover slips were placed on the samples, and edges were sealed with transparent adhesive tape, leaving some air spaces. Altogether, the system provided the aerobic environment and nutrients necessary for the survival of the tissues over the time course. Samples were maintained under LL conditions at 60-100 mol $m^{-2}s^{-1}$. Fluorescent signals from the shoot apex, leaf vascular and leaf mesophyll cells were imaged once every 30 minutes with an argon laser (transmissivity: 40%; excitation: 515 nm; emission range: 530-630 nm) in a FV-1000 confocal microscope (Olympus, Tokyo, Japan) with a 40x/1.3 oil immersion objective. About 15-20 serial optical sections (z stacks) were scanned using the scanned mode "XYZT" with image sizes of 640 x 640 (0.497 µm/pixel) and sampling speed of 4 µs/pixel. Sections of 2.0-3.0 µm step sizes perpendicular to the z-axis (microscope optical axis) were imaged using the filter mode Kalman line (set at 2). Fluorescence intensity quantification in the nuclei was analyzed using ImageJ software (https://imagej.nih.gov/ij/) using Mean Gray Value option. The results are representative of at least three biological replicates for shoot apex and leaf vascular cells and two biological replicates for leaf mesophyll cells. About 30-40 different nuclei were examined per experiment with each of the three different reporters (CCA1, PRR7 and ELF3). Signals from individual nuclei that moved or got out of focus were excluded from the analysis.

8. Protoplast preparation

Protoplasts were prepared as previously described (Yoo et al., 2007) with minor modifications. Briefly, 20-30 excised shoot apexes from 14 day old plants were transferred into 12-well plates containing the enzyme solution (400 mM mannitol, 20 mM KCl, 10 mM $CaCl_2$, 7.5 mg/ml cellulase RS and 3 mg/ml macerozyme R10). The plates were incubated in a shaker with slow agitation overnight at room temperature. An ethanol sterilized nylon mesh (4 cm x 4 cm) was used as a filter to transfer the released protoplasts to 1.5 ml tubes. Protoplasts were spun at 250g for 2 minutes and subsequently washed three times in W5 solution (154 mM NaCl, 125 mM $CaCl_2$, 5 mM KCl, 2 mM MES pH 5.6) before final collection of the protoplasts. The dispersed cells were initially diluted to approximately a concentration of $1x10^3$ cells per well. Protoplasts were resynchronized for one additional day before *in vivo* analysis by luminescence assays.

9. Mathematical analysis

Mathematical analyses were performed by Dr. Yoshito Hirata and Dr. Kazuyuki Aihara. Details of the procedures are described in (Hirata et al., 2015; Takahashi et al., 2015). Please also check Anex II and III.

ANNEXES

Annexes

Annex I: Protocol of micrografting assays with Arabidopsis seedlings

Materials & Equipments:

- *Arabidopsis thaliana* seedlings [vertically grown for 3-7 days on 0.5^2 agar medium (0.5x Murashige and Skoog, MS, agar medium with 0.5% sucrose]
- Sterile 100 mm x 20 mm Petri plates (CELLSTAR)
- micropore tape (3 M)
- Strips of autoclaved filter paper (sizes of approximately 7 cm x 1 cm)
- #11 sterile surgical blades (Swann-Morton)
- Sterile fine point tweezers (i.e. Dumont #55 Biologie tweezers)
- Sterile micropipettes (Gilson)
- Alcohol lamp
- Dissecting microscope (Zeiss, Stemi SV6)
- Laminar flow cabinet
- 96% Ethanol
- Tissue paper
- Sterile water

Methods:

*All the procedures should be carried out under the laminar flow cabinet.

Step 0: Preparation for micrografting

Set up the dissecting microscope under the laminar flow cabinet. Rinse your hands with 96% ethanol. Then, use tissue paper soaked with Ethanol to gently wipe the surface of the microscope.

Place strips of autoclaved filter paper onto the surface of the 0.5^2 medium plates as shown in Figure 1. Make sure the filter paper becomes wet.

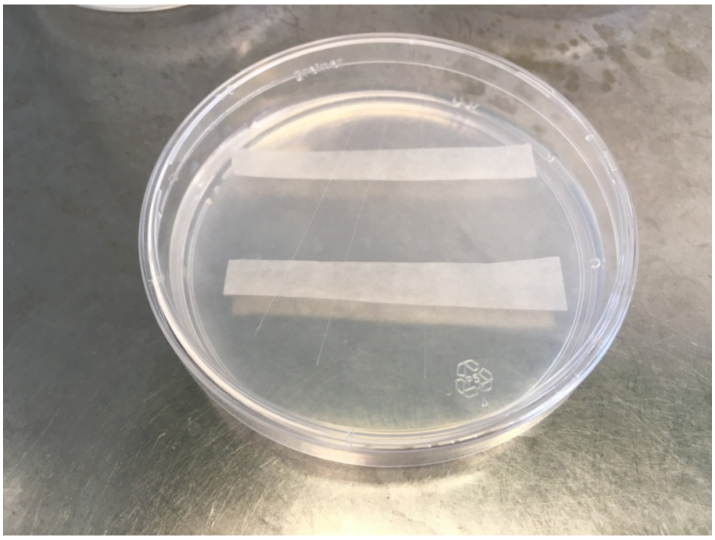

Figure 1. Placement of filter paper strips on 0.5^2 medium plates.

Step1: Transfer of seedlings

Apply small amount of 96% ethanol to the tip of tweezers and flame sterilize with the alcohol lamp for few seconds. Press the tip of the tweezers into the agar medium to cool down. Use then the tweezers to transfer the seedlings that will be used as rootstocks onto the 0.5^2 medium plates prepared at step 0 as shown in Figure 2. Pay extra attention not to let the roots to dry out as it might cause the development of adventitious roots after grafting. Sterile water can be added to roots or alternatively, very gently bury the roots in the medium.

Transfer the seedlings to be used as scion and placed them onto the filter paper in an inverse position to the rootstock seedlings as shown in Figure 2.

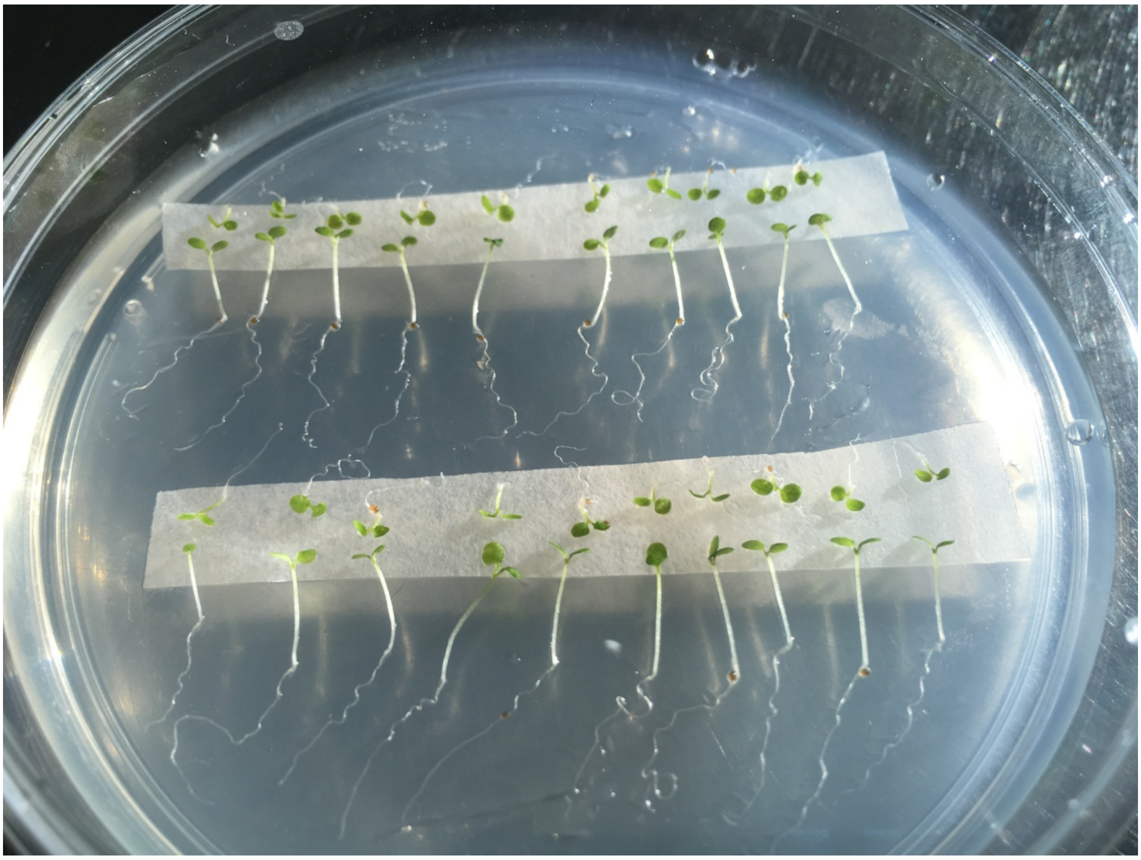

Figure 2. Position of seedlings on the filter paper strips. Seedlings on the top will be used as scions while the ones on the bottom will be rootstocks.

Step 2: Cutting

Using the tweezers and the #11 blades, carefully remove on the filter paper the cotyledons from seedlings to be scions. The same blade can be used for all samples. Next, very carefully cut off the hypocotyls from scion seedlings using the #11 blades. It is highly recommended to change blades every 10 cuttings. Cross sections must be clean, sharp and horizontal to the hypocotyls. Leave scions on the filter paper until rootstocks are cut (Figure 3). Make sure scions are kept moisturized.

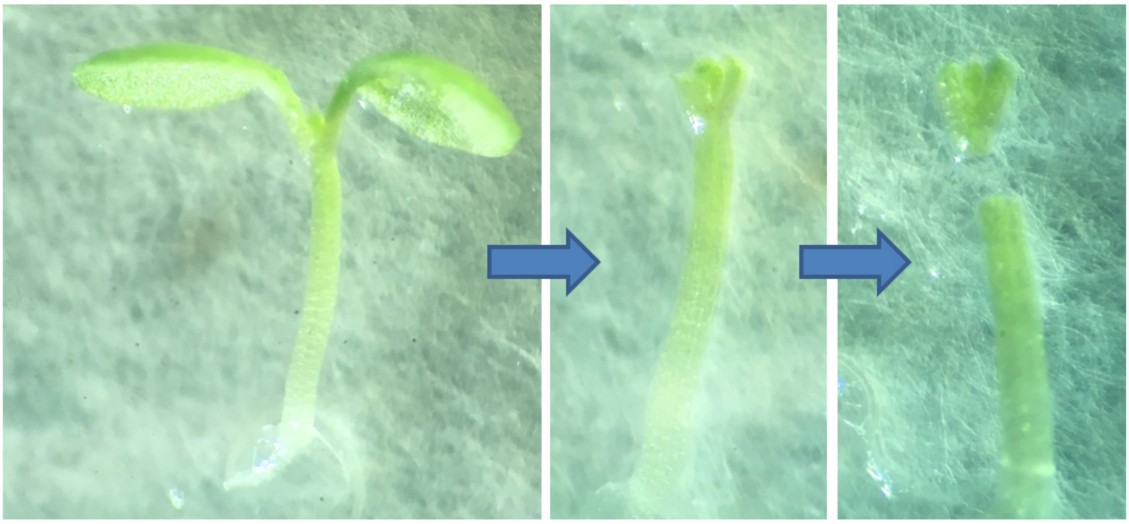

Figure 3. Cutting the scion from the seedling.

Next, cut hypocotyls of rootstock seedlings with the #11 blades. It is also strongly recommended to change the blades every 10 cuttings. Cuts must be clean, sharp and horizontal to the hypocotyls (Figure 4). In this procedure, it is not required to remove cotyledons (unless scions will be isolated from these plants for reciprocal grafting).

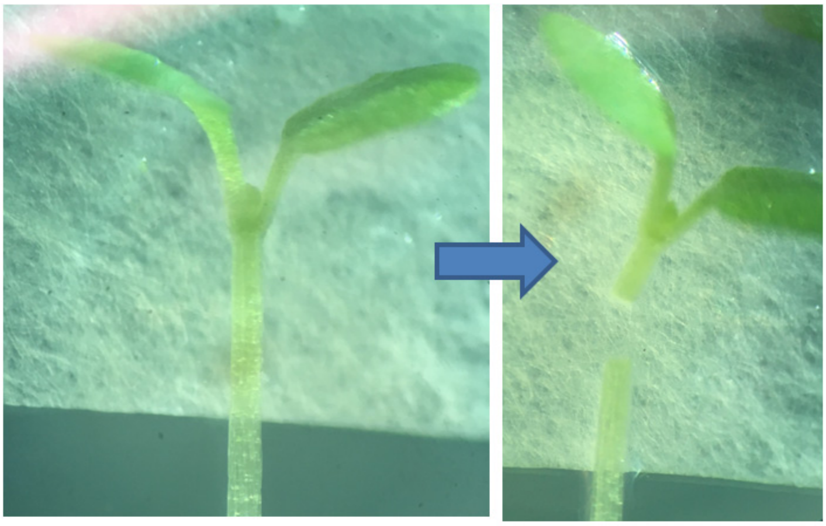

Figure 4. Cutting the rootstock seedling.

Step 3: Connecting scions and rootstocks after cutting

Once cuttings are completed, slide the filter paper upwards to allow tips of rootstocks to touch the MS medium as shown in Figure 5. This procedure prevents the cross sections to be dried out. Next, use the tweezers to transfer the scions close to the rootstocks. Avoid grabbing or pinching. If scions are gently touched with the tips of the tweezers, they will transiently adhere to tweezers. After transferring all scions in the vicinity of the rootstocks, remove the filter paper from the plate.

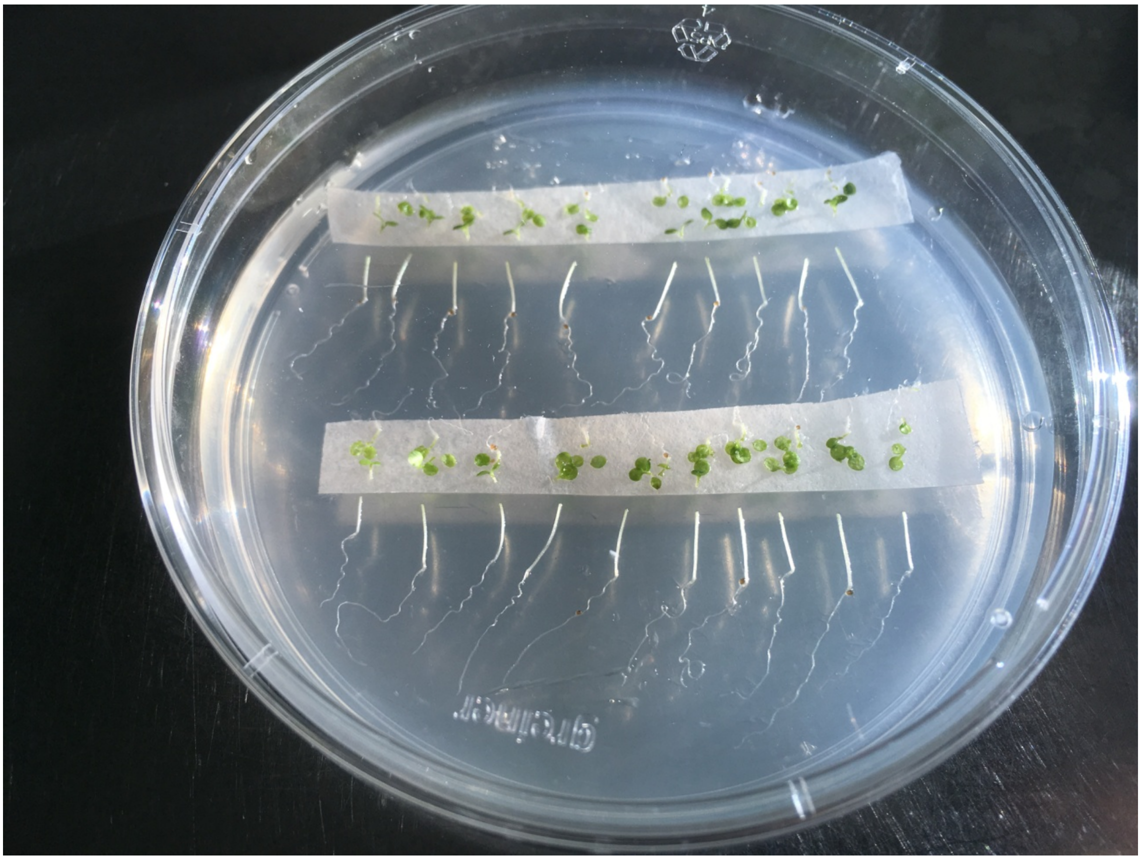

Figure 5. Upward sliding of filter paper strips. This allows rootstocks to touch the MS medium and keep cross sections moisturized.

Using the tip of the tweezers, gently push scions and join them together with the rootstocks. Pay extra attention to align the two phloem strands (Figure 6). It is more likely to be successful when grafts have rootstock and scion well-matched for size, and cross sections are very clean and horizontal so that cut ends of rootstock and scion can be easily joined together.

When grafting is completed, seal the plate with micropore tape and incubate vertically in the growth chamber under 12 hour light:12 hour dark or 16 hour light:8 hour dark cycles with 60-100 µmol $m^{-2}s^{-1}$ of cool white fluorescent light at 22ºC. Grafts are likely to be established as early as 6 days after the procedure.

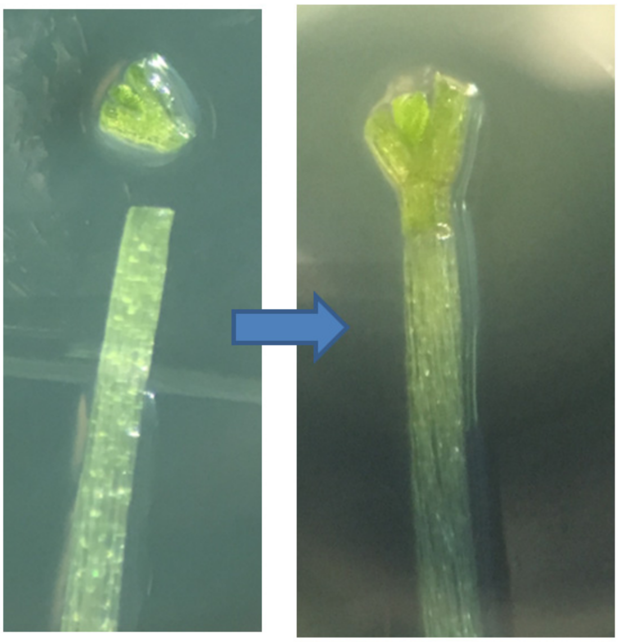

Figure 6. Joining of scion and rootstock.

Additional Step: Removal of adventitious roots.

Adventitious roots could emerge from grafted plants. This will become apparent approximately 1 week after the procedure. This frequently occurs if conditions of grafted roots are suboptimal. If adventitious roots are observed, remove them with the sterile tweezers and the #11 blades under the dissecting microscope. Grab the tip of the adventitious roots with the tweezers and carefully cut as closer to the shoots as possible. If adventitious roots are short enough, they can be squashed with tweezers.

References:

Grafting *Arabidopsis*
Tonni Grube Andersen, Dacheng Liang, Barbara Ann Halkier and Rosemary White
http://www.bio-protocol.org/e1164

Plant Methods. 2013 May 4;9(1):14. doi: 10.1186/1746-4811-9-14.
An efficient flat-surface collar-free grafting method for Arabidopsis thaliana seedlings.
Marsch-Martínez N[1], Franken J, Gonzalez-Aguilera KL, de Folter S, Angenent G, Alvarez-Buylla ER.
http://www.ncbi.nlm.nih.gov/pubmed/23641687

J Plant Res. 2009 Mar;122(2):201-14. doi: 10.1007/s10265-008-0209-1. Epub 2009 Jan 15.
Adaptation of a seedling micro-grafting technique to the study of long-distance signaling in flowering of Arabidopsis thaliana.
Notaguchi M[1], Daimon Y, Abe M, Araki T.
http://www.ncbi.nlm.nih.gov/pubmed/19145404

Plant J. 2002 Oct;32(2):255-62.
Micrografting techniques for testing long-distance signalling in Arabidopsis.
Turnbull CG[1], Booker JP, Leyser HM.
http://www.ncbi.nlm.nih.gov/pubmed/12383090

Annex II:

Cell
Article

A Hierarchical Multi-oscillator Network Orchestrates the *Arabidopsis* Circadian System

Graphical Abstract

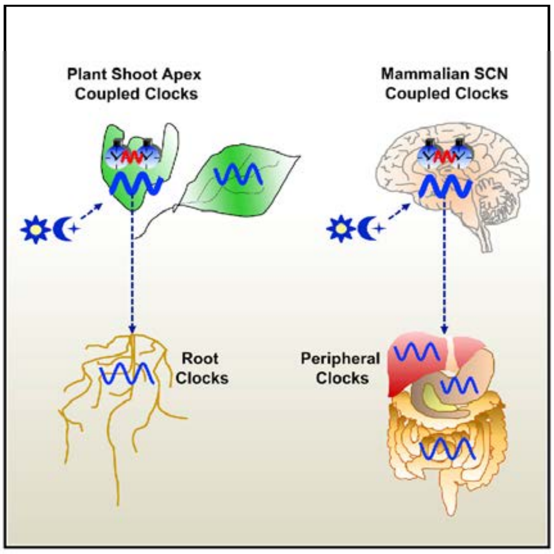

Authors

Nozomu Takahashi, Yoshito Hirata, Kazuyuki Aihara, Paloma Mas

Correspondence

paloma.mas@cragenomica.es

In Brief

The plant shoot apex clocks resemble the suprachiasmatic nucleus in mammals in their coupling properties and their capacity to synchronize circadian rhythms in distal organs.

Highlights

- Shoot apex clocks function as the suprachiasmatic nucleus neurons in mammals
- Circadian coupling defines the high degree of synchrony among shoot apex clocks
- The shoot apex clocks influence the circadian activity in roots
- Different plant organs exhibit variations in clock precision and circadian synchrony

Takahashi et al., 2015, Cell *163*, 148–159
September 24, 2015 ©2015 Elsevier Inc.
http://dx.doi.org/10.1016/j.cell.2015.08.062

Article

A Hierarchical Multi-oscillator Network Orchestrates the *Arabidopsis* Circadian System

Nozomu Takahashi,[1] Yoshito Hirata,[2] Kazuyuki Aihara,[2] and Paloma Mas[1,3,*]
[1]Centre for Research in Agricultural Genomics (CRAG), CSIC-IRTA-UAB-UB, Campus UAB, Bellaterra, 08193 Barcelona, Spain
[2]Institute of Industrial Science, The University of Tokyo, 4-6-1 Komaba, Meguro-ku, Tokyo 153-8505, Japan
[3]Consejo Superior de Investigaciones Científicas (CSIC), 08028 Barcelona, Spain
*Correspondence: paloma.mas@cragenomica.es
http://dx.doi.org/10.1016/j.cell.2015.08.062

SUMMARY

Short- and long-distance circadian communication is essential for integration of temporal information. However, a major challenge in plant biology is to decipher how individual clocks are interconnected to sustain rhythms in the whole plant. Here we show that the shoot apex is composed of an ensemble of coupled clocks that influence rhythms in roots. Live-imaging of single cells, desynchronization of dispersed protoplasts, and mathematical analysis using barycentric coordinates for high-dimensional space show a gradation in the strength of circadian communication in different tissues, with shoot apex clocks displaying the highest coupling. The increased synchrony confers robustness of morning and evening oscillations and particular capabilities for phase readjustments. Rhythms in roots are altered by shoot apex ablation and micrografting, suggesting that signals from the shoot apex are able to synchronize distal organs. Similarly to the mammalian suprachiasmatic nucleus, shoot apexes play a dominant role within the plant hierarchical circadian structure.

INTRODUCTION

The circadian clock is a cellular mechanism able to generate rhythms in biological processes. A key function of circadian clocks is the synchronization of metabolism, physiology, and development in anticipation of the diurnal and seasonal environmental changes (Young and Kay, 2001). Over the last years, biochemical and genetic studies have provided a complex view of the circadian organization and function in several clock systems, including mammals, insects, plants, fungi, and cyanobacteria (Wijnen and Young, 2006). Rhythms in most organisms are generated by reciprocal regulations among core clock components that produce 24 hr oscillations in gene expression, mRNA processing, protein abundance, and activity (Harmer et al., 2001). Changes in chromatin architecture have also emerged as a central mechanism coupled to the rhythmic oscillation of clock gene expression (Nakahata et al., 2007; Ripperger and Merrow, 2011; Stratmann and Más, 2008).

Plants as sessile organisms perceive and adapt to the environmental changes for optimal growth and survival. Consistently, nearly all stages of plant development and many essential aspects of growth and metabolism are regulated by the clock (de Montaigu et al., 2010; Yakir et al., 2007). Among others, processes such as photo-protection, responses to biotic attacks, or the photoperiodic regulation of flowering are controlled by the clock (Kinmonth-Schultz et al., 2013). Mechanistically, a number of regulatory transcriptional modules have been defined at the basis of the *Arabidopsis thaliana* circadian oscillator. Two single MYB-domain transcription factors expressed early in the morning, known as CIRCADIAN CLOCK ASSOCIATED 1 (CCA1) (Wang and Tobin, 1998) and LATE ELONGATED HYPOCOTYL (LHY) (Schaffer et al., 1998), negatively regulate the expression (Alabadí et al., 2001) of the evening-phased *PSEUDO-RESPONSE REGULATOR 1 (PRR1)* or *TIMING OF CAB EXPRESSION 1* (*TOC1*) (Makino et al., 2002; Strayer et al., 2000). TOC1 (Gendron et al., 2012; Huang et al., 2012) and the other members of the PRR family (PRR5, PRR7, and PRR9) (Nakamichi et al., 2010) also bind to the promoters of *CCA1* and *LHY* to repress their expression. Additional components such as EARLY FLOWERING3 (ELF3), ELF4, and LUX ARRYTHMO (LUX) interact to form the Evening Complex (EC) that represses the expression of the early day-phased clock gene *PRR9* (Helfer et al., 2011; Nusinow et al., 2011).

At a cellular level, it has been assumed that virtually every plant cell might contain an endogenous clock. However, their possible circadian communication or coupling has been a matter of debate. Circadian analysis using cell cultures (Kim and Somers, 2010; Nakamichi et al., 2003), records of different rhythmic markers (Sai and Johnson, 1999), studies of clock synchronization (Wenden et al., 2012), and circadian characterization of guard cells (Yakir et al., 2011) have suggested that plant cellular clocks might be only weakly coupled. However, luminescence assays in *Arabidopsis* and analysis of chlorophyll fluorescence in *Kalanchoe daigremontiana* have shown a certain degree of cellular coupling in different parts of leaves (Fukuda et al., 2007; Rascher et al., 2001). A recent interesting report has also described particular properties of clocks in leaf veins that are able to communicate with the adjacent leaf mesophyll cells (Endo et al., 2014). Intercellular coupling opens the question about long-distance signaling and synchronization. Indeed, circadian oscillations in roots seem to be entrained by signals from shoots (James et al., 2008). This situation resembles that of the mammalian circadian system in which a master clock

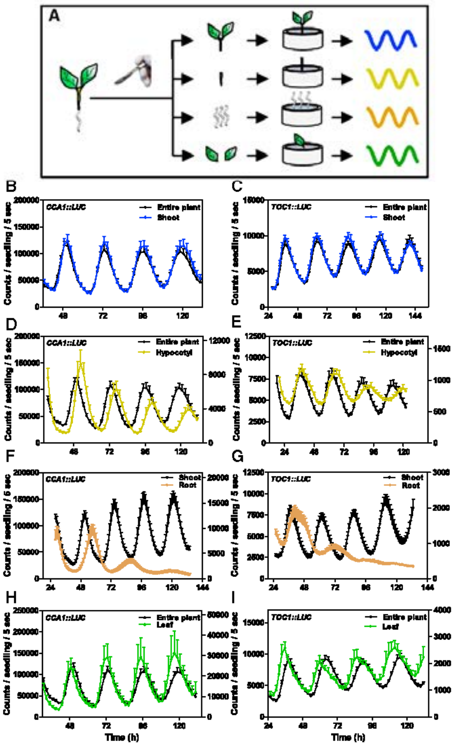

Figure 1. Disparity in the Precision and Robustness of Circadian Rhythms in Various Organs Excised from the Plant

(A) Schematic drawing depicting the dissection of the different parts of the plant and the subsequent analysis by luminescence assays. Seedlings were dissected to separate shoots, hypocotyls, roots, and leaves.

(B–I) In vivo circadian analysis of luminescent rhythms under LL from *CCA1::LUC* (B, D, F, and H) and *TOC1::LUC* (C, E, G, and I) in shoots (B and C), hypocotyls (D and E), roots (F and G), and leaves (H and I). Data are the means + SEM of the luminescence of 6–12 individual samples. Values of luminescence signals from hypocotyls, roots, and leaves are represented on the right y axes. See also Figure S1.

located at the suprachiasmatic nucleus (SCN) synchronizes peripheral clocks dispersed throughout the body (Aton and Herzog, 2005; Welsh et al., 2010).

The functional structure of a circadian system consists of a complex assembly of components and mechanisms that are precisely coordinated in cells, tissues, and organs. Intercellular coupling of circadian clocks might provide an efficient way for local synchronization in a particular tissue while long-distance signaling can aid in synchronizing distal parts. In this study, we have focused on these two particular aspects of circadian communication in *Arabidopsis* and found that the shoot apex might act as a master clock that influences rhythms in roots.

RESULTS

Differences in Robustness and Precision of Circadian Rhythms in Dissected Organs

To determine organ-specific circadian function, we analyzed rhythms in different organs excised from the plant (Figure 1A and Supplemental Experimental Procedures). Promoter activity was monitored by in vivo luminescence assays of plants expressing the morning- (*CCA1*) and evening-phased (*TOC1*) gene promoters fused to the *LUCIFERASE* (*LUC*). Under constant light conditions (LL), *CCA1::LUC* and *TOC1::LUC* expression in excised shoots robustly oscillated without evident dampening. Circadian waveforms closely matched those of whole plants (Figures 1B and 1C), suggesting that root excision did not manifestly affect oscillations in shoots. Excised hypocotyls sustained rhythms albeit with a long circadian period (27.02 ± 0.64 versus 24.61 ± 0.25 in entire plants) and a progressive decrease in amplitude over the days (Figures 1D and 1E). Rhythms in excised roots were only sustained for about 2 days, dampening low afterward (Figures 1F and 1G). The fact that oscillations in roots do not persist in the absence of sucrose could be due to energy limitation, as excised roots are a sucrose sink. Indeed, the use of the same procedure for root excision but using medium with sucrose revealed that rhythms were sustained for more than 4 days (Figure S1) with a significantly longer period (26.21 ± 0.33) than in shoots (24.63 ± 0.22). The sustained oscillations suggest that the excision per se was not responsible for the dampened rhythms observed without sucrose. Adding sucrose to non-sucrose grown and arrhythmic excised roots did not restore the oscillatory pattern (Figure S1), suggesting that sugar cannot compensate for the arrhythmia. When excised leaves were analyzed in the absence (Figures 1H and 1I) or in the presence (Figure S1) of sucrose, we observed an averaged advanced phase compared to entire plants or shoots.

Specific Properties for Synchronization and Phase Readjustments of Shoot Apex Clocks

We next performed similar analysis with excised shoot apexes (Figure 2A) and found that the phase, period, and amplitude remained synchronized (Figures 2B and 2C), with rhythms very similar to those of the entire plants (Figure S2) and with highly synchronous individual waveforms (Figure 2D). These results are in clear contrast with the high degree of variability observed in individual leaf waveforms, manifested by a range of phases and amplitudes from the very first day under LL (Figure 2E). As the size of the tissue might influence the circadian waveforms, we analyzed small sections of leaves (with sizes similar to those of the shoot apexes). Our results showed a similar variability to that displayed by full leaves (Figure S2), which suggests that the shoot apex homogeneity in waveforms is not due to the reduced sizes of the samples. The circadian phases clustered together in shoot apexes and to much less extent in leaves (Figures 2F and 2G). Similar conclusions were drawn when the average phase and the degree of phase coherence were calculated using the synchronization index “R” (see Supplemental

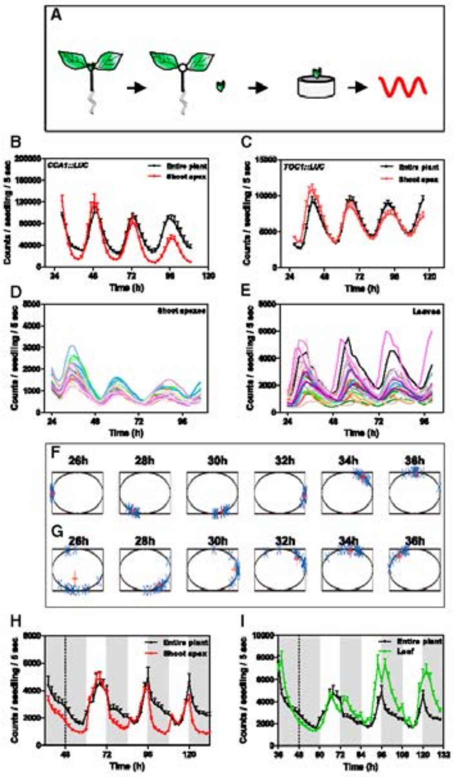

Figure 2. High Degree of Synchrony and Responsiveness to Environmental Changes of Shoot Apex Clocks

(A) Schematic drawing depicting the rhythmic analysis of excised shoot apexes.

(B and C) In vivo circadian analysis of luminescent rhythms under LL from *CCA1::LUC* (B) and *TOC1::LUC* (C) in shoots apexes.

(D and E) *TOC1::LUC* luminescence traces of individual excised shoot apexes (D) and excised leaves (E).

(F and G) Analysis of the phase synchrony among the different samples (blue crosses) of individual shoot apexes (F) and leaves (G) examined from 26 hr to 36 hr under LL. The red crosses indicate the means or circular variance (Mormann et al., 2000) at each time point.

(H and I) Average rhythms of *TOC1::LUC* luminescence in shoot apexes (H) and leaves (I) subjected to a "jet-lag" experiment, with extended 12 hr darkness (extended night) at dawn.

Data are the means + SEM of the luminescence of 6–12 samples. White boxes: light; shaded boxes: dark. See also Figure S2.

Experimental Procedures). The analysis showed high R values, close to 1, for the shoot apexes and lower values for leaves at all time points (Figure S2). Consistent with previous studies (Wenden et al., 2012), the R values in leaves were well above 0, which suggests a certain degree of coherence. Rhythms in excised organs were highly reproducible in four different biological replicates (each one with 6–12 samples), which reduces the possibility that results were due to indirect effects of the excision procedure.

The circadian clock is not only a robust mechanism able to sustain rhythms in the absence of environmental transitions but also a flexible system that resynchronizes and properly adjusts to changes in the environmental cycle (Harrington, 2010). To explore whether the differences between shoot apexes and leaves also extend to their capabilities for resynchronization and phase adjustment, we performed "jet-lag" experiments. In shoot apexes, rhythms showed similar timing for resynchronization to that of entire plants (Figure 2H), although the shoot apex waveforms displayed very rapid declining at night for *TOC1::LUC* and an increased acute induction at dawn for *CCA1::LUC* (Figure S2). In leaves, rhythms showed a double peak for the first 2 days, reaching a stable phase at the third day after the extended night switch (Figure 2I). These results reveal different synchronizing behavior in leaves and shoot apexes. The specific waveforms in shoot apexes compared to the entire plant might also indicate a particular sensibility of shoot apexes to dawn and dusk resetting signals.

Conserved Molecular Architecture of the Circadian Network at the Shoot Apex Clocks

To determine organ-specific differences in the clock molecular composition, we examined whether different clock outputs and mutations in core clock genes were distinctively regulated in shoot apexes and leaves. Analysis of WT plants expressing the morning-phased clock output *CAB2 (CHLOROPHYLL A/B-BINDING PROTEIN 2)* (Millar et al., 1995) showed that in shoot apexes the phase was comparable to that in the entire plant, whereas increased heterogeneity and an average advanced phase were prevalent in leaves (Figure 3A). Similar to entire plants, the shoot apexes and leaves of *cca1-11* mutants displayed persistent rhythms with shorter periods than WT shoot apexes and WT leaves, respectively (Figures 3B–3D). Similarly, the short period of the evening-expressed clock output *CCR2 (COLD, CIRCADIAN RHYTHM, AND RNA BINDING 2)* (Strayer et al., 2000) in *TOC1 RNAi* plants (Huang et al., 2012) was also observed in shoot apexes and leaves (Figures 3E and 3F). Therefore, circadian gene expression in shoot apexes and leaves with various reporter lines and clock mutant backgrounds did not render major differences between the two organs.

To profile the circadian transcriptional landscape at the shoot apex, we performed RNA sequencing (RNA-seq) analysis and used the JTK_CYCLE algorithm for precise definition of circadian expression (Hughes et al., 2010). After filtering out transcripts whose median expression across every sample was lower than 0.69 RPKM and those not differentially expressed, we identified over 1,400 genes with significant circadian fluctuations in mRNA abundance. Visual inspection of the data suggested that this may be a conservative estimation. However, the stringent analysis ensured the selection of the highest-confidence circadian hits. Rhythmic genes included all the

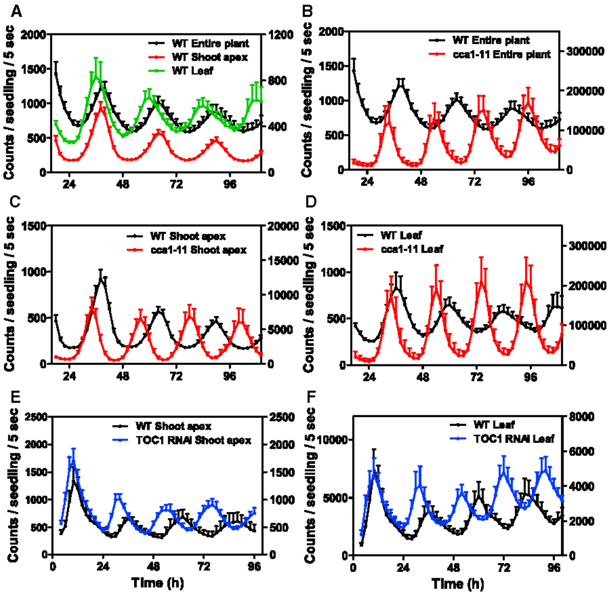

Figure 3. Phenotypes of Core Clock Mutations in Shoot Apexes and Leaves

Average rhythms of *CAB2::LUC* (A–D) and *CCR2::LUC* (E and F) luminescence under LL in entire plants, shoot apexes, and leaves of WT, *cca1-11* mutants (A–D) and *TOC1 RNAi* (E and F). Plants were entrained under LD cycles and processed as detailed in the Supplemental Experimental Procedures. Data are the means + SEM of the luminescence of 6–12 samples. Values of luminescence signals from *cca1-11* mutant and *TOC1 RNAi* are represented on the right y axes.

previously described core clock components, genes involved in light signaling, and those involved in circadian outputs such as photosynthesis, photoperiodic flowering, and hormone signaling, among others (Figures 4A–4D and S3). The waveforms oscillated with similar phases and amplitudes to those previously reported in entire plants (Figures 4E–4G), which suggests no fundamental differences in the global transcriptional circadian networks in the shoot apex and entire plants. It is noteworthy that shoot apexes display such strong and robust rhythms (both morning- and evening-expressed genes) as opposed to the uncoupled rhythms in roots (only morning) (James et al., 2008) and in veins (mainly evening) (Endo et al., 2014). Functional categorization of the rhythmic genes showed a wide range of biological functions, highlighting as most significantly enriched those genes involved in circadian rhythms and responses to environmental conditions, including different qualities of light, temperature, and radiation (Figure S3). This enrichment might explain the specific readjustment of shoot apexes to environmental changes observed in our jet-lag experiments.

Differences in Synchrony of Clock Cells in Various Organs and Tissues

To understand the cellular basis of the circadian rhythmicity at the shoot apex, we examined rhythms from individual cells of plants expressing CCA1-HA-EYFP under its own promoter (Yakir et al., 2009). We performed in vivo time-course analysis by confocal imaging of excised shoot apexes embedded in agarose (Mas and Beachy, 1998). Fluorescent signals from individual nuclei of shoot apex cells sustained rhythmic oscillations. The circadian waveforms maintained good synchrony, manifested by similar timing in their rising and declining phases even after 3 days under LL (Figure 5A, left panel and Figure 5B). The results were also evident when the confocal imaging started at different time points (Figure S4). A similar pattern of highly synchronous waveforms was observed with single cells from shoot apexes of FLAG-PRR7-EGFP-expressing plants (Nakamichi et al., 2010) (Figure S4). In contrast, and consistent with previous data (Yakir et al., 2011), the variation in the rhythmic accumulation of CCA1-HA-EYFP in individual leaf cells significantly increased after 2 days under LL (Figure 5A, right panel and Figure 5C). Differences in phase and amplitude were also clearly observed when fluorescent signals were not relativized to the maximum (Figure S4). We also measured fluorescence from the leaf vasculature, as previous studies have shown that these cells are coupled (Endo et al., 2014). We observed two distinguishable populations with slightly different phases (Figure S4). Individual cell-to-cell comparisons showed that both populations maintain a certain degree of synchrony (Figures 5D and 5E). Synchrony appeared to be higher than that observed in leaf mesophyll cells but lower than in cells at the shoot apex. Quantitative analysis of the waveform correlation among individual cells confirmed that the correlation coefficient in shoot apex cells was higher than the one for vascular cells with the advanced (A) or delayed (D) phase (Figures 5F and 5G). The group of cells with a delayed phase appeared to be more synchronous than the group with an advanced phase. The waveforms in leaf mesophyll cells displayed lower correlation values and increased heterogeneity. A higher synchrony in shoot apexes compared to vascular cells or the mesophyll cells adjacent to the leaf veins (Figure S4) was also observed when an evening-expressed gene was examined (ELF3-EYFP) (Dixon et al., 2011). In this case, the separation of cells with advanced and delayed phases was not so evident in veins (Figure S4). Together, the results confirmed at the level of single cells and with three different reporters our conclusions

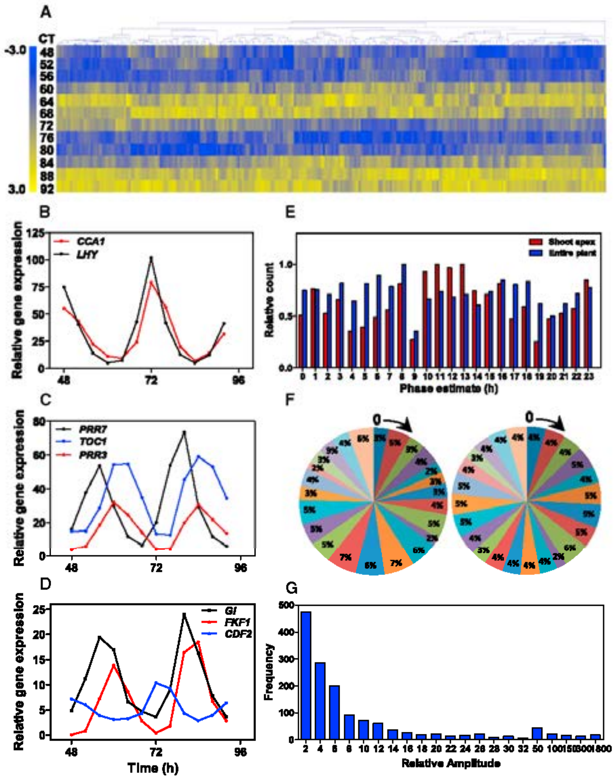

Figure 4. Transcriptional Profiling of the Circadian Program at the Shoot Apex

(A) Heatmap showing median-normalized gene expression at different circadian times (CT, vertical axis) for transcripts (horizontal axis) with a peak phase of expression at mid-late subjective night. Yellow indicates high expression and blue low expression.

(B–D) Gene-expression analysis of *CCA1*, *LHY* (B), *PRR3*, *PRR7*, *TOC1* (C), and *GI*, *FKF1*, *CDF2* (D) in shoot apexes of WT plants grown under LD cycles followed by 2 days under LL.

(E and F) Phase distribution of rhythmic genes in shoot apexes and entire plants. Phase enrichment was calculated using the web-based tool "Phaser." The phase estimates were represented relative to their maximum (E) and in pie charts (F) displaying the contribution of each phase to the total. Left chart: shoot apex; right chart: entire plants.

(G) Distribution of amplitudes of cycling transcripts in shoot apexes calculated by using the algorithm JTK_Cycle.

See also Figure S3.

on the distinct degrees of synchrony in shoot apexes, leaf mesophyll cells, and veins.

Intercellular Circadian Coupling among Clock Cells of the Shoot Apex

If coupling of shoot apex clocks is responsible for the waveform synchrony, then rhythms should be affected when the intercellular communication is disrupted. To explore this idea, we compared shoot apexes from intact tissues and from dissociated and diluted protoplasts. Rhythms in excised shoot apexes maintained good synchrony and were sustained for several days. However, in diluted shoot apex protoplasts, the oscillations persisted only for 2–3 days, increasing their heterogeneity over time (Figure 5H). Further dilution of protoplasts increasingly advanced the timing of rhythmic dampening (Figures 5I and S4). Analysis of the R values in shoot apexes and in diluted protoplasts quantitatively confirmed that the phase coherence in protoplasts was only sustained for less than 2 days, reaching asynchrony afterward (Figure 5J). As individual cells at the shoot apex are able to maintain rhythmic oscillations (Figure 5B), one plausible explanation to our results is that dispersed cells do not sustain rhythms due to reduced intercellular communication and subsequent desynchronization over time.

In the mammalian circadian system, the clock components PER1 and CRY1 are required for sustained rhythms in peripheral tissues and in neurons dissociated from the SCN (Welsh et al., 2010). However, cellular interactions at the SCN can compensate for *Per1* or *Cry1* deficiency (Evans et al., 2012; Liu et al., 2007). We found a similar scenario at the shoot apex of *lux* mutants. In contrast to the reported arrhythmia of *lux-2* plants, the *lux-2* shoot apexes were able to sustain rhythms to a certain degree. Although the rhythms were clearly compromised, rhythmicity at the *lux-2* shoot apex was better than in leaves (Figures 5K, 5L, and S4). Thus, the absolute requirement of LUX function in leaves is not so apparent in shoot apexes. The differences are not due to changes in the circadian expression of *LUX* or the other components of the EC, *ELF3*, and *ELF4*, as verified by our RNA-seq analysis and by qRT-PCR (Figure S4). If in analogy to the mammalian system, effective intercellular coupling among the shoot apex cells is responsible for the distinctive phenotype, then disruption of the cellular communication should affect the rhythms. Indeed, shoot apex protoplasts from *lux-2* mutants were arrhythmic throughout the time-course analysis (Figure 5M). We proposed that the arrhythmic phenotype in protoplasts is the result from the rapid desynchronization of the dispersed cells, each containing a semi-functional oscillator.

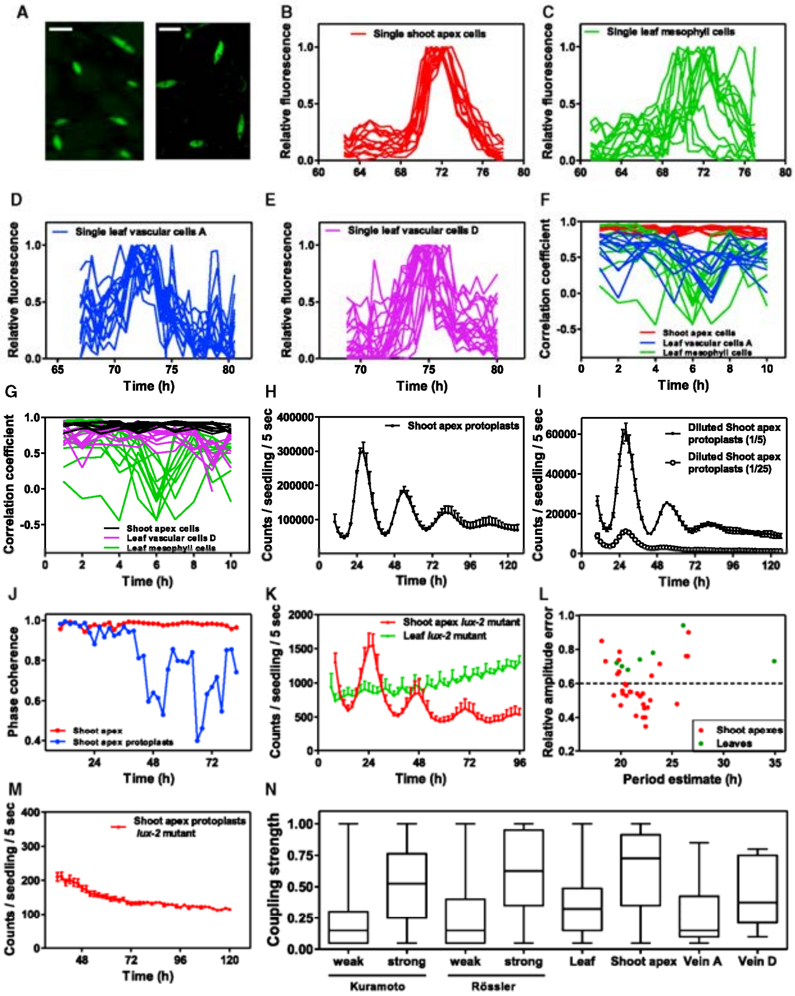

Figure 5. Circadian Coupling Defines the High Synchrony of Shoot Apex Clock Cells

(A) Representative fluorescent signals from CCA1-HA-EYFP accumulation in nuclei of shoot apex cells (left panel) and leaf cells (right panel). Panels show representative cells from a larger picture containing other cells out of the shown field (scale bar, 20 μm).

(B–E) In vivo time-course imaging of CCA1-HA-EYFP fluorescent signals quantified in individual nuclei from shoot apex (B), leaf mesophyll (C), and leaf vascular cells with advanced (D) and delayed (E) phases. Data are represented relative to the maximum value.

(F and G) Correlation coefficients among the waveforms of individual nuclei in shoot apex, leaf mesophyll cells, and leaf vascular cells with advanced (F) and delayed (G) phases.

(H and I) Luminescence analysis of *CCA1::LUC* activity in diluted (H) and further diluted series of protoplasts (I) from shoot apexes. Protoplasts were synchronized for an additional day under LD before transferring to LL. Data are the means + SEM of the luminescence of 6–12 samples.

(J) Quantification of the phase coherence in intact shoot apexes and in shoot apex protoplasts by calculating the synchronization index “R.”

(legend continued on next page)

Our results indicate that intercellular communication might be important for rhythms at the shoot apex. To mathematically explore the degree of intercellular coupling, we developed a predictive model by using barycentric coordinates for high-dimensional space (Hirata et al., 2015). The model involves the use of linear programming that assigns different weights to neighboring cells and identifies the strength of coupling based on the accuracy of the predictions given the weights. We first tested the performance of the proposed methods using the Kuramoto (Kuramoto, 1975) and the coupled Rössler (Rössler, 1976) toy models. The examples showed that the weights of neighboring oscillators are higher when the coupling is stronger (Figure 5N). When the model was used with the single-cell confocal data, we found that shoot apex clocks were highly coupled and had greater coupling strength than leaf vasculature or leaf mesophyll cells (Figure 5N). Together, the results confirmed a gradation or hierarchy in the strength of the circadian communication in different parts of the plant.

Relevance of the Shoot Apex Clocks in the Modulation of Circadian Oscillations in Roots

We next addressed the possible role of the shoot apex controlling the circadian function in roots. We adapted the luminescence assay protocol to examine rhythms in both shoots and roots of intact plants (Figure 6A). We also used laser microdissection (LMD) to excise shoot apexes and examine rhythms in Δshoot apex plants (Figure 6B). Previous studies have reported that rhythms dampened low and waveforms broadened in entire plants after several days under free-running conditions (Yakir et al., 2011). We found that rhythms at the shoot apex were sustained for more than 7 days under LL (Figure 6C), which suggests that intercellular coupling at the shoot apex might contribute to the rhythmic robustness after extended periods under LL. When we examined rhythms in Δshoot apex plants, we observed an advanced average phase and increasing waveform variability, in a similar fashion to that of excised leaves (Figures 6D and S5). Application of auxin did not noticeably affect the rhythms in shoots of entire plants or Δshoot apex plants (Figure S5), which suggests that the Δshoot apex phenotypes are not due to changes in auxin flux. It is noteworthy that rhythms in plants that only lack the shoot apex are similar to the rhythms in leaves, whereas the small shoot apex is able to more precisely sustain rhythms. Unexpectedly, we also found that rhythms in plants without cotyledons or leaves were almost indistinguishable from the ones observed in intact plants (Figures 6E and 6F).

Photosynthetic sucrose has been shown to modulate clock function (Haydon et al., 2013; James et al., 2008). Our studies revealed an initial phase delay and period lengthening that led to dampened rhythms in shoots from intact plants treated with the inhibitor of the photosynthetic electron transport [3-(3,4-dichlorophenyl)-1,1-dimethylurea, DCMU) (Figure S5). When we applied the drug only in shoots and checked the effects on roots, we found a phase delay and dampened rhythms (Figure S5). These results confirmed that photosynthetic signals from shoots are important for the root clock. DCMU treatment in excised shoot apexes also led to eventual dampening of rhythms, but the early phase delay observed in whole shoots and roots was not so evident (Figure S5). These results suggest increased robustness against pharmacological perturbation of photosynthesis at the shoot apex.

To further explore the importance of circadian communication, we used plants with reduced intercellular trafficking by means of *CALS3* gain-of-function mutations (*cals3-d*) that lead to reduced plasmodesmata aperture (Vatén et al., 2011). Our results showed that blocked trafficking clearly altered the rhythmic expression of core clock genes in roots, with no evident peak and trough expression as observed in WT roots (Figures 6G, 6H, and S5). We also examined rhythms in shoots and roots that were rapidly separated following 2 days of luminescence analysis of the intact plants (Figure 6I). The separation led to dampening of rhythms in roots, indicating that rhythms in roots are altered very rapidly after separation from shoots. To ascertain the role of the shoot apex on root synchronization, we then examined circadian rhythms in roots from intact plants in which the shoot apex was removed (Δshoot apex plants) (Figure 6B). Our results showed that rhythms were clearly affected, with an initial long-period phenotype that progressively led to arrhythmia (Figure 6J). Rhythms in roots from plants in which leaves and cotyledons were removed were not severely affected and showed a slightly advanced phase compared with the rhythms in roots from intact plants (Figure S5). Noteworthy are also the results of jet-jag experiments showing that roots from intact plants were able to resynchronize with a pattern that more closely resembled the one in shoot apexes than the one in leaves (Figure S5).

A Hierarchical Structure at the Core of the *Arabidopsis* Clock

Efficient micrografting of *Arabidopsis* seedlings is a powerful tool for studying long-distance signaling (Bainbridge et al., 2014). To conclusively determine the possible hierarchical nature of the plant circadian system, we performed micrografting with young *Arabidopsis* seedlings using the shoot apex as scion (Figure 7A). We reasoned that grafting with different genotypes would provide definitive information on the role of shoot apexes on the root oscillation.

Micrografting and luminescence analysis were first tested on WT self-grafts (WT Shoot Apex–WT Roots, WT SA-WT Rt). The analysis showed that *CCA1::LUC* and *TOC1::LUC* rhythms followed a similar trend to that observed in entire non-grafted

---

(K) Average luminescence of *CAB2::LUC* activity in shoot apexes and leaves of *lux-2* mutant plants. Data are means + SEM of the luminescence of six samples.

(L) Period estimates of *CAB2::LUC* activity from individual traces analyzed as detailed in the Supplemental Experimental Procedure.

(M) Luminescence analysis of *CAB2::LUC* activity in protoplasts from shoot apexes of *lux-2* mutant plants. Data represent means + SEM of 6–12 samples. Protoplasts were synchronized for an additional day under LD before transferring to LL.

(N) Mathematical analysis of the coupling strength by barycentric coordinates for high-dimensional space using the Kuramoto and coupled Rössler toy models and the in vivo CCA1-EYFP imaging data. The line in the middle of the box is plotted at the median. The whiskers represent the minimum and maximum values. See also Figure S4.

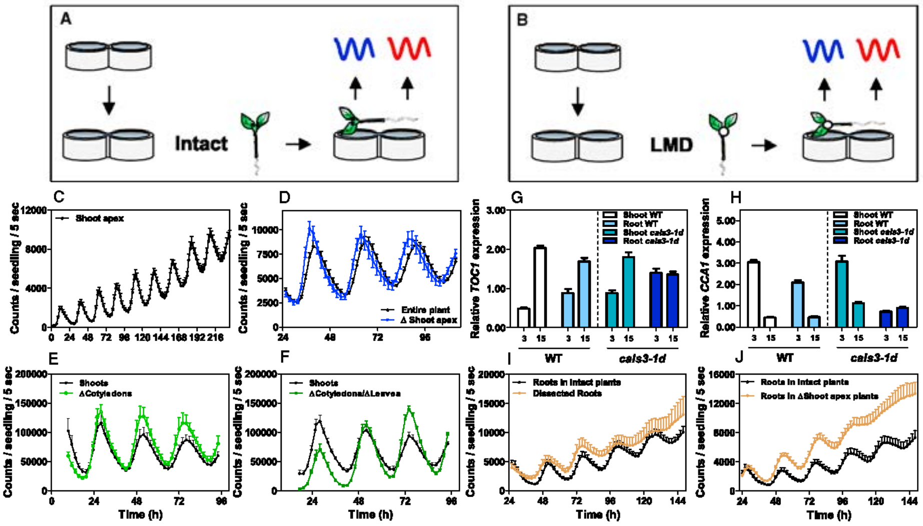

Figure 6. Rhythms at the Shoot Apex Influence the Circadian Activity in Roots

(A) Schematic drawing depicting the rhythmic analysis of shoots and roots from intact plants.

(B) LMD was used to obtain Δshoot apex plants. Seedlings were horizontally positioned in serrated 96-well microplates so that rhythms could be examined in roots and shoots.

(C) Average rhythms of *TOC1::LUC* luminescence in shoot apexes for extended days under LL.

(D) *TOC1::LUC* luminescence in plants in which the shoot apexes were removed by LMD.

(E and F) *CCA1::LUC* luminescence in plants in which the cotyledons (E) and leaves (F) were removed.

(G and H) qRT-PCR analysis of *TOC1* (G) and *CCA1* (H) expression in shoots and roots of WT and *cals3* mutant plants. Plants were synchronized under LD, and samples were taken after 2 days under LL at CT3 and CT15.

(I) *CCA1::LUC* luminescence from roots after rapid dissection from shoots.

(J) *CCA1::LUC* luminescence in roots from intact plants and Δshoot apex plants. Luminescence was recorded under LL following synchronization under LD. Data are represented as the means + SEM. See also Figure S5.

plants (Figures 7B and 7C). Rhythms in roots exhibited a longer period compared to shoots, which also mirrored the observations in organs of non-grafted plants (Figure S1). As these results suggested that the grafting procedure did not manifestly alter the circadian oscillation, we next grafted the shoot apex of arrhythmic plants into a WT rootstock. We reasoned that the lack of a functional clock in the shoot apex should alter the rhythms in roots. Indeed, grafting the shoot apex of the arrhythmic *cca1-1/lhy-11* plants (Mizoguchi et al., 2002; Portolés and Más, 2010) (Figure S6) disrupted the rhythms of WT roots (Figure 7D). A similar alteration of WT root rhythms was observed with the shoot apex of *elf3-2* mutants (Hicks et al., 1996) (Figure 7E). Although slight oscillations could be appreciated, the amplitude and robustness of the waveforms were clearly affected. These results confirmed that proper clock function in the shoot apex is important for the rhythmic activity in roots. We then performed the reverse experiment in which WT shoot apexes were grafted into arrhythmic rootstocks to test the ability of shoot apex signals to reestablish the rhythms in roots. Remarkably, the arrhythmia of *cca1-1/lhy-11* or *elf3-2* roots could be partially restored by grafting the shoot apex of WT plants (Figures 7F and 7G). The oscillations were not very robust, but the patterns were not as arrhythmic as the roots of non-grafted plants (Figure S6). Although we observed variability in the degree of restored rhythms (Figure S6), the recovery was quite evident. Altogether, we conclude that signals from the shoot apex are important for circadian oscillations in roots.

DISCUSSION

A series of different protocols developed in this study has allowed us to follow the rhythmic expression in excised organs of the plant. Under sucrose, rhythms were sustained in all organs examined and the tissues continued growing normally after excision, which suggests that the excision did not manifestly affect the rhythms. The different excised organs displayed a wide range of circadian properties. Hypocotyls and roots lack precision and robustness, with long circadian periods and

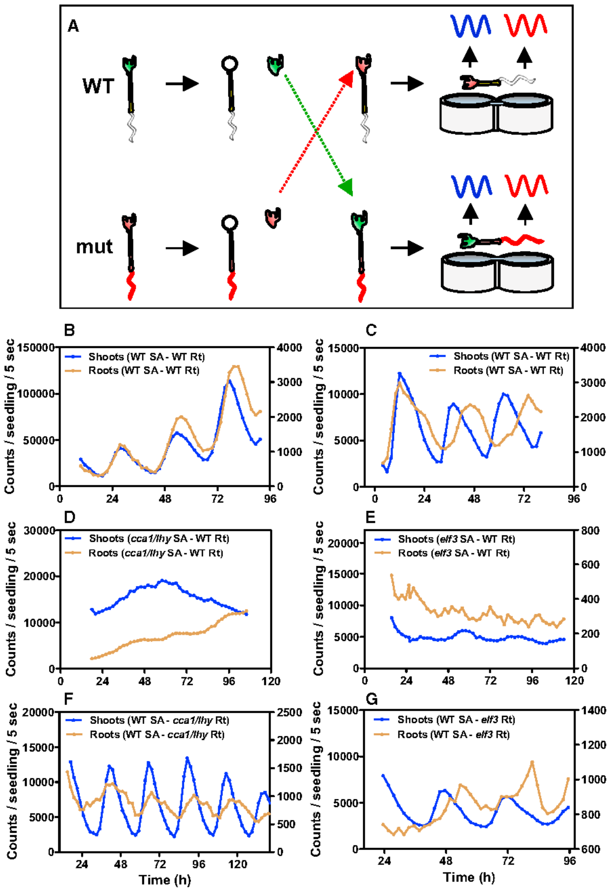

Figure 7. A Hierarchical Dominance of the Shoot Apex Clocks

(A) Schematic drawing depicting the rhythmic analysis of micrografted plants as detailed in Experimental Procedures.

(B and C) Analysis of *CCA1::LUC* (B) and *TOC1::LUC* (C) luminescence in shoots and roots of WT scion and WT rootstocks.

(D–G) Luminescence in shoots and roots of *cca1/lhy* mutant scion and WT rootstocks (D), *elf3* mutant scion and WT rootstocks (E), WT scion and *cca1/lhy* mutant rootstocks (F), and WT scion and *elf3* mutant rootstocks (G). Luminescence was recorded under LL following synchronization under LD. Values of luminescence signals from roots are represented on the right y axes.

See also Figure S6.

arrhythmia, whereas leaves lack synchrony among the different samples from plants similarly entrained. As roots are a sucrose sink, our results with excised roots (±sucrose) are consistent with previous studies (Haydon et al., 2013; James et al., 2008) and with the dampening of rhythms in roots when shoots are treated with DCMU. Analysis of root rhythms in ∆shoot apex plants rendered similar results to those of excised roots, which confirmed the dependency of roots on the circadian communication with shoot apexes. The heterogeneity of circadian waveforms in leaves is also consistent with previous studies (Wenden et al., 2012). Phase heterogeneity might be due to differences in circadian coupling among various leaf cell types. Mesophyll cells in leaves are only weakly coupled, whereas the leaf vasculature synchronizes the neighboring mesophyll cells (Endo et al., 2014). This local synchronization raises the question about possible differences in rhythms of mesophyll cells close to the vasculature and those located far from the veins. Desynchronization between leaf stomatal and mesophyll cells (Yakir et al., 2011) could be another source of phase heterogeneity in leaves.

Shoot apexes displayed remarkable homogeneous rhythmicity with highly synchronous waveforms. Among the tissues examined, different patterns of waveform synchrony could be distinguished: the cells from the shoot apex with the highest synchrony, the intermediate synchrony in the vascular cells, and the lowest synchrony observed in leaf mesophyll cells. The fact that the synchrony is lost in dispersed, diluted shoot apex protoplasts suggests that the phase coherence and synchrony might be due to high intercellular coupling among shoot apex clocks. The development of a tailor-designed mathematical model using barycentric coordinates for high-dimensional space confirmed this notion. The method has been proven successful for a wide range of uses, from weather forecasting to creation of musical instruments with natural sounds (Hirata et al., 2015). Our studies also revealed that the intercellular coupling or circadian communication among shoot apex clocks confer robustness against genetic mutations and pharmacological perturbations. These properties closely resemble those of the circadian system in mammals in which intercellular coupling among neurons at the SCN can compensate for the absence of functional key clock components (Evans et al., 2012; Liu et al., 2007).

The molecular circadian network and phenotypes of core clock mutants at the shoot apex appear to be similar to those described in the whole plant. However, prevalence for morning- or evening-expressed genes has been shown for the clocks of leaf mesophyll cells and leaf veins, respectively (Endo et al., 2014). Uncoupled morning and evening oscillators have been also previously reported for the clock in roots (James et al., 2008). Our full time-course analysis by RNA-seq showed robust rhythms of circadian genes with similar peak phases and relative amplitudes to those reported in entire plants. The particular properties that we observed at the shoot apex clocks might result from their strong intercellular coupling rather than from a distinctive molecular network. We also found a clear enrichment of genes involved in responses to environmental signals. This enrichment might be responsible for the distinctive waveforms in jet-lag experiments, as if the shoot apex clocks were highly sensible to perceive and respond to the changing environmental conditions. The enrichment might be particularly useful for the shoot apical cells that are buried and shielded from the environment. Intercellular coupling might also be an aid for circadian synchronization of cells with reduced light accessibility. The fact that genes responsible for perception of synchronizing signals such as light and temperature are enriched in our RNA-seq data is consistent with a main role of shoot apexes as a synchronizing master clock.

Grafting has been used to study long-distance signaling in different processes, for instance shoot branching (Turnbull et al., 2002) or stress responses (Holbrook et al., 2002). The studies presented here demonstrate the long-distance circadian signaling by micrografting approaches. Our results have revealed the influence of shoot apexes on the rhythmic activity of roots. A plausible idea is that changes in auxin flux could be responsible for synchronizing rhythms in roots. However, our results suggest that auxin signaling has a minor, if any, role in the long-distance circadian communication. The partial recovery of mutant rootstocks by grafting WT shoot apexes and, conversely, the arrhythmia of WT roots grafted with arrhythmic shoot apexes reflect the circadian hierarchy of shoot apexes. This situation is reminiscent of the circadian system in mammals in which genetic defects in peripheral clocks are phenotypically rescued by the hierarchical dominance of the SCN (Pando et al., 2002). The micrografting results were consistent with the shoot apex role influencing rhythms in roots, which was observed by other approaches used in this study (rapid dissection of shoots and roots, delta shoot apex plants, pharmacological treatments, and genetic analysis). The similar phenotypes reinforce the validity of the different procedures and the consistency of our conclusions.

Based on the recently discovered role of the plant vasculature (Endo et al., 2014), a very interesting possibility is that veins are used as the circadian traveling “highway” in which the synchronizing signals circulate from shoot apexes to roots. In analogy with the mammalian circadian system, the shoot apex clock cells might function as the SCN neurons, whereas the plant vasculature could be comparable to blood veins and arteries. Further studies of topographically defined areas of circadian coupling and elucidation of the signals and mechanisms contributing to the circadian communication will be central to fully define the spatio-temporal networks orchestrating plant physiology and development on each organ, tissue, and cell.

EXPERIMENTAL PROCEDURES

Organ Dissection and Micrografting Experiments

Organ dissection was performed as detailed in the Supplemental Experimental Procedures. For micrografting experiments, *Arabidopsis* seedlings were grown vertically on half-strength Murashige and Skoog (MS) agar medium with 0.5% sucrose for 3–7 days. Seedlings were placed on wet filters under the dissecting microscope in a laminar flow cabinet as described (http://www.bio-protocol.org/e1164). Cotyledons were removed, and both scion and rootstock seedlings were horizontally cut with a razor blade just below the shoot apex. With forceps, and very gently, the scion and rootstock cut stumps were joined together, paying attention to match up the two phloem strands. When grafting was completed, plates were sealed with two layers of micropore tape and returned to the growth chamber for at least 4–6 more days. If present, adventitious roots on the scions were removed before luminescence analysis. The unsuccessful grafted seedlings were identified as the grafts failed to properly join together. In cases when the successful grafting was not clear, the resulting plants were discarded. A total of 120 grafting events were assayed for WT SA–*cca1/lhy* Rt plants. The percentage of successfully micrografted plants was about 50% (possibly higher but only faultlessly grafted plants were examined). From the 59 successfully grafted WT SA - *cca1/lhy* Rt plants, 50 (i.e., around 85%) showed different degrees of restored rhythms (p value = 3.77×10^{12} by Fisher’s exact test, considering that none of the 20 *cca1/lhy* SA - *cca1/lhy* Rt plants displayed rhythms in roots). For the control WT SA–WT Rt grafting, 22 out of 24 successfully grafted plants showed very robust rhythms.

RNA Extraction and RNA-Seq Analysis

RNA extraction and RNA-seq analysis were performed as detailed in the Supplemental Experimental Procedures.

Single-Cell Confocal Microscopy Imaging

For in vivo confocal imaging at a single-cell resolution, excised shoot apexes or leaves were embedded just after dissection in low-melting-point agarose dissolved in MS medium as previously described (Mas and Beachy, 1998). Further details are described in the Supplemental Experimental Procedures.

Protoplast Preparation and Gene-Expression Analysis

Protoplast preparation (Yoo et al., 2007) and gene-expression analysis (Malapeira et al., 2012) were performed as described. Details are described in the Supplemental Experimental Procedures.

Mathematical Analysis

Mathematical analysis was performed as described in Hirata et al. (2015). See further details in the Supplemental Experimental Procedures.

SUPPLEMENTAL INFORMATION

Supplemental Information includes Supplemental Experimental Procedures and six figures and can be found with this article online at http://dx.doi.org/10.1016/j.cell.2015.08.062.

AUTHOR CONTRIBUTIONS

N.T. performed the biological experiments. Y.H. and K.A. designed and performed the mathematical analysis. P.M. designed the biological experiments and wrote the manuscript. All authors read, revised, and approved the manuscript.

ACKNOWLEDGMENTS

We thank Professor Y. Helariutta for the *cals3* seeds, Professor K. Kornacker for help with the JTK_CYCLE algorithm, Professor R. Green for CCA1-HA-EYP plants, and M. Amenós for help with the confocal microscope. This work was supported by research grants to P.M. from the Spanish Ministry of Economy and Competitiveness, from the Generalitat de Catalunya (AGAUR), from the

Global Research Network of the National Research Foundation of Korea, and from the European Commission Marie Curie Research Training Network (ChIP-ET). Y.H. and K.A. are supported by the Platform Project for Supporting in Drug Discovery and Life Science Research (Platform for Dynamic Approaches to Living System) from the Ministry of Education, Culture, Sports, Science (MEXT) and Japan Agency for Medical Research and development (AMED). K.A. is also partially supported by CREST, JST, Japan. N.T. is supported by a CRAG fellowship.

Received: March 13, 2015
Revised: July 1, 2015
Accepted: August 6, 2015
Published: September 24, 2015

REFERENCES

Alabadí, D., Oyama, T., Yanovsky, M.J., Harmon, F.G., Más, P., and Kay, S.A. (2001). Reciprocal regulation between *TOC1* and *LHY/CCA1* within the Arabidopsis circadian clock. Science *293*, 880–883.

Aton, S.J., and Herzog, E.D. (2005). Come together, right...now: synchronization of rhythms in a mammalian circadian clock. Neuron *48*, 531–534.

Bainbridge, K., Bennett, T., Crisp, P., Leyser, O., and Turnbull, C. (2014). Grafting in Arabidopsis. In Arabidopsis Protocols, J.J. Sanchez-Serrano and J. Salinas, eds. (New York: Humana Press), pp. 155–163.

de Montaigu, A., Tóth, R., and Coupland, G. (2010). Plant development goes like clockwork. Trends Genet. *26*, 296–306.

Dixon, L.E., Knox, K., Kozma-Bognar, L., Southern, M.M., Pokhilko, A., and Millar, A.J. (2011). Temporal repression of core circadian genes is mediated through EARLY FLOWERING 3 in *Arabidopsis*. Curr. Biol. *21*, 120–125.

Endo, M., Shimizu, H., Nohales, M.A., Araki, T., and Kay, S.A. (2014). Tissue-specific clocks in Arabidopsis show asymmetric coupling. Nature *515*, 419–422.

Evans, J.A., Pan, H., Liu, A.C., and Welsh, D.K. (2012). Cry1-/- circadian rhythmicity depends on SCN intercellular coupling. J. Biol. Rhythms *27*, 443–452.

Fukuda, H., Nakamichi, N., Hisatsune, M., Murase, H., and Mizuno, T. (2007). Synchronization of plant circadian oscillators with a phase delay effect of the vein network. Phys. Rev. Lett. *99*, 098102.

Gendron, J.M., Pruneda-Paz, J.L., Doherty, C.J., Gross, A.M., Kang, S.E., and Kay, S.A. (2012). Arabidopsis circadian clock protein, TOC1, is a DNA-binding transcription factor. Proc. Natl. Acad. Sci. USA *109*, 3167–3172.

Harmer, S.L., Panda, S., and Kay, S.A. (2001). Molecular bases of circadian rhythms. Annu. Rev. Cell Dev. Biol. *17*, 215–253.

Harrington, M. (2010). Location, location, location: important for jet-lagged circadian loops. J. Clin. Invest. *120*, 2265–2267.

Haydon, M.J., Mielczarek, O., Robertson, F.C., Hubbard, K.E., and Webb, A.A.R. (2013). Photosynthetic entrainment of the Arabidopsis thaliana circadian clock. Nature *502*, 689–692.

Helfer, A., Nusinow, D.A., Chow, B.Y., Gehrke, A.R., Bulyk, M.L., and Kay, S.A. (2011). LUX ARRHYTHMO encodes a nighttime repressor of circadian gene expression in the Arabidopsis core clock. Curr. Biol. *21*, 126–133.

Hicks, K.A., Millar, A.J., Carré, I.A., Somers, D.E., Straume, M., Meeks-Wagner, D.R., and Kay, S.A. (1996). Conditional circadian dysfunction of the *Arabidopsis early-flowering 3* mutant. Science *274*, 790–792.

Hirata, Y., Shiro, M., Takahashi, N., Aihara, K., Suzuki, H., and Mas, P. (2015). Approximating high-dimensional dynamics by barycentric coordinates with linear programming. Chaos Interdisc. J. Nonlinear Sci. *25*, 013114.

Holbrook, N.M., Shashidhar, V.R., James, R.A., and Munns, R. (2002). Stomatal control in tomato with ABA-deficient roots: response of grafted plants to soil drying. J. Exp. Bot. *53*, 1503–1514.

Huang, W., Pérez-García, P., Pokhilko, A., Millar, A.J., Antoshechkin, I., Riechmann, J.L., and Mas, P. (2012). Mapping the core of the Arabidopsis circadian clock defines the network structure of the oscillator. Science *336*, 75–79.

Hughes, M.E., Hogenesch, J.B., and Kornacker, K. (2010). JTK_CYCLE: an efficient nonparametric algorithm for detecting rhythmic components in genome-scale data sets. J. Biol. Rhythms *25*, 372–380.

James, A.B., Monreal, J.A., Nimmo, G.A., Kelly, C.L., Herzyk, P., Jenkins, G.I., and Nimmo, H.G. (2008). The circadian clock in Arabidopsis roots is a simplified slave version of the clock in shoots. Science *322*, 1832–1835.

Katari, M.S., Nowicki, S.D., Aceituno, F.F., Nero, D., Kelfer, J., Thompson, L.P., Cabello, J.M., Davidson, R.S., Goldberg, A.P., Shasha, D.E., et al. (2010). VirtualPlant: A Software Platform to Support Systems Biology Research. Plant Physiol. *152*, 500–515.

Kim, J., and Somers, D.E. (2010). Rapid assessment of gene function in the circadian clock using artificial microRNA in Arabidopsis mesophyll protoplasts. Plant Physiol. *154*, 611–621.

Kinmonth-Schultz, H.A., Golembeski, G.S., and Imaizumi, T. (2013). Circadian clock-regulated physiological outputs: dynamic responses in nature. Semin. Cell Dev. Biol. *24*, 407–413.

Kuramoto, Y. (1975). Self-entrainment of a population of coupled nonlinear oscillators. Lect. N. Phys. *39*, 420–422.

Liu, A.C., Welsh, D.K., Ko, C.H., Tran, H.G., Zhang, E.E., Priest, A.A., Buhr, E.D., Singer, O., Meeker, K., Verma, I.M., et al. (2007). Intercellular coupling confers robustness against mutations in the SCN circadian clock network. Cell *129*, 605–616.

Makino, S., Matsushika, A., Kojima, M., Yamashino, T., and Mizuno, T. (2002). The APRR1/TOC1 quintet implicated in circadian rhythms of Arabidopsis thaliana: I. Characterization with APRR1-overexpressing plants. Plant Cell Physiol. *43*, 58–69.

Malapeira, J., Khaitova, L.C., and Mas, P. (2012). Ordered changes in histone modifications at the core of the Arabidopsis circadian clock. Proc. Natl. Acad. Sci. USA *109*, 21540–21545.

Mas, P., and Beachy, R.N. (1998). Distribution of TMV movement protein in single living protoplasts immobilized in agarose. Plant J. *15*, 835–842.

Millar, A.J., Carré, I.A., Strayer, C.A., Chua, N.H., and Kay, S.A. (1995). Circadian clock mutants in *Arabidopsis* identified by luciferase imaging. Science *267*, 1161–1163.

Mizoguchi, T., Wheatley, K., Hanzawa, Y., Wright, L., Mizoguchi, M., Song, H.R., Carré, I.A., and Coupland, G. (2002). *LHY* and *CCA1* are partially redundant genes required to maintain circadian rhythms in *Arabidopsis*. Dev. Cell *2*, 629–641.

Mormann, F., Lehnertz, K., David, P., and Elger, C.E. (2000). Mean phase coherence as a measure for phase synchronization and its application to the EEG of epilepsy patients. Physica D *144*, 358–369.

Nakahata, Y., Grimaldi, B., Sahar, S., Hirayama, J., and Sassone-Corsi, P. (2007). Signaling to the circadian clock: plasticity by chromatin remodeling. Curr. Opin. Cell Biol. *19*, 230–237.

Nakamichi, N., Kiba, T., Henriques, R., Mizuno, T., Chua, N.-H., and Sakakibara, H. (2010). PSEUDO-RESPONSE REGULATORS 9, 7, and 5 are transcriptional repressors in the Arabidopsis circadian clock. Plant Cell *22*, 594–605.

Nakamichi, N., Matsushika, A., Yamashino, T., and Mizuno, T. (2003). Cell autonomous circadian waves of the APRR1/TOC1 quintet in an established cell line of Arabidopsis thaliana. Plant Cell Physiol. *44*, 360–365.

Nusinow, D.A., Helfer, A., Hamilton, E.E., King, J.J., Imaizumi, T., Schultz, T.F., Farré, E.M., and Kay, S.A. (2011). The ELF4-ELF3-LUX complex links the circadian clock to diurnal control of hypocotyl growth. Nature *475*, 398–402.

Pando, M.P., Morse, D., Cermakian, N., and Sassone-Corsi, P. (2002). Phenotypic rescue of a peripheral clock genetic defect via SCN hierarchical dominance. Cell *110*, 107–117.

Portolés, S., and Más, P. (2010). The functional interplay between protein kinase CK2 and CCA1 transcriptional activity is essential for clock temperature compensation in Arabidopsis. PLoS Genet. *6*, e1001201.

Rascher, U., Hütt, M.-T., Siebke, K., Osmond, B., Beck, F., and Lüttge, U. (2001). Spatiotemporal variation of metabolism in a plant circadian rhythm: the biological clock as an assembly of coupled individual oscillators. Proc. Natl. Acad. Sci. USA *98*, 11801–11805.

Ripperger, J.A., and Merrow, M. (2011). Perfect timing: epigenetic regulation of the circadian clock. FEBS Lett. *585*, 1406–1411.

Rössler, O.E. (1976). An equation for continuous chaos. Phys. Lett. A *57*, 397–398.

Sai, J., and Johnson, C.H. (1999). Different circadian oscillators control Ca(2+) fluxes and lhcb gene expression. Proc. Natl. Acad. Sci. USA *96*, 11659–11663.

Schaffer, R., Ramsay, N., Samach, A., Corden, S., Putterill, J., Carré, I.A., and Coupland, G. (1998). The late elongated hypocotyl mutation of Arabidopsis disrupts circadian rhythms and the photoperiodic control of flowering. Cell *93*, 1219–1229.

Stratmann, T., and Más, P. (2008). Chromatin, photoperiod and the Arabidopsis circadian clock: a question of time. Semin. Cell Dev. Biol. *19*, 554–559.

Strayer, C., Oyama, T., Schultz, T.F., Raman, R., Somers, D.E., Más, P., Panda, S., Kreps, J.A., and Kay, S.A. (2000). Cloning of the Arabidopsis clock gene *TOC1*, an autoregulatory response regulator homolog. Science *289*, 768–771.

Turnbull, C.G.N., Booker, J.P., and Leyser, H.M.O. (2002). Micrografting techniques for testing long-distance signalling in Arabidopsis. Plant J. *32*, 255–262.

Vatén, A., Dettmer, J., Wu, S., Stierhof, Y.-D., Miyashima, S., Yadav, S.R., Roberts, C.J., Campilho, A., Bulone, V., Lichtenberger, R., et al. (2011). Callose biosynthesis regulates symplastic trafficking during root development. Dev. Cell *21*, 1144–1155.

Wang, Z.Y., and Tobin, E.M. (1998). Constitutive expression of the *CIRCADIAN CLOCK ASSOCIATED 1* (*CCA1*) gene disrupts circadian rhythms and suppresses its own expression. Cell *93*, 1207–1217.

Welsh, D.K., Takahashi, J.S., and Kay, S.A. (2010). Suprachiasmatic nucleus: cell autonomy and network properties. Annu. Rev. Physiol. *72*, 551–577.

Wenden, B., Toner, D.L.K., Hodge, S.K., Grima, R., and Millar, A.J. (2012). Spontaneous spatiotemporal waves of gene expression from biological clocks in the leaf. Proc. Natl. Acad. Sci. USA *109*, 6757–6762.

Wijnen, H., and Young, M.W. (2006). Interplay of circadian clocks and metabolic rhythms. Annu. Rev. Genet. *40*, 409–448.

Yakir, E., Hilman, D., Harir, Y., and Green, R.M. (2007). Regulation of output from the plant circadian clock. FEBS J. *274*, 335–345.

Yakir, E., Hilman, D., Kron, I., Hassidim, M., Melamed-Book, N., and Green, R.M. (2009). Posttranslational regulation of CIRCADIAN CLOCK ASSOCIATED1 in the circadian oscillator of Arabidopsis. Plant Physiol. *150*, 844–857.

Yakir, E., Hassidim, M., Melamed-Book, N., Hilman, D., Kron, I., and Green, R.M. (2011). Cell autonomous and cell-type specific circadian rhythms in Arabidopsis. Plant J. *68*, 520–531.

Yoo, S.-D., Cho, Y.-H., and Sheen, J. (2007). Arabidopsis mesophyll protoplasts: a versatile cell system for transient gene expression analysis. Nat. Protoc. *2*, 1565–1572.

Young, M.W., and Kay, S.A. (2001). Time zones: a comparative genetics of circadian clocks. Nat. Rev. Genet. *2*, 702–715.

Supplemental Figures

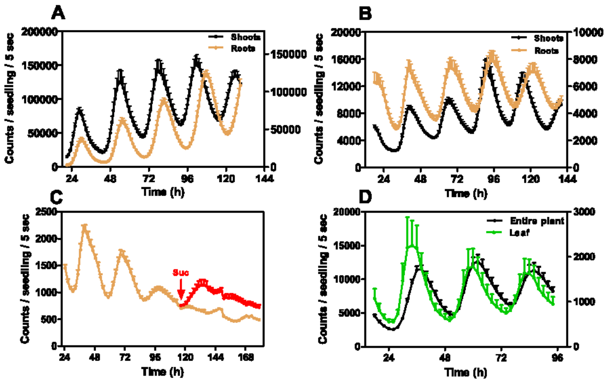

Figure S1. Rhythms in Different Organs Excised from the Plant, Related to Figure 1

Average rhythms of *CCA1::LUC* (A) and *TOC1::LUC* (B, C, and D) luminescence in shoots and roots. Plants were grown and analyzed in medium with sucrose as described in Supplemental Experimental Procedures. Luminescence was recorded under LL conditions. Data are the means + SEM of the luminescence of 6–12 individual samples. Values of luminescence signals from roots (A and B) and leaves (D) are represented on the right y axes. (C) Luminescence of excised roots after adding sucrose to roots grown in medium without sucrose. (D) Luminescence rhythms in excised leaves from plants grown in medium with sucrose.

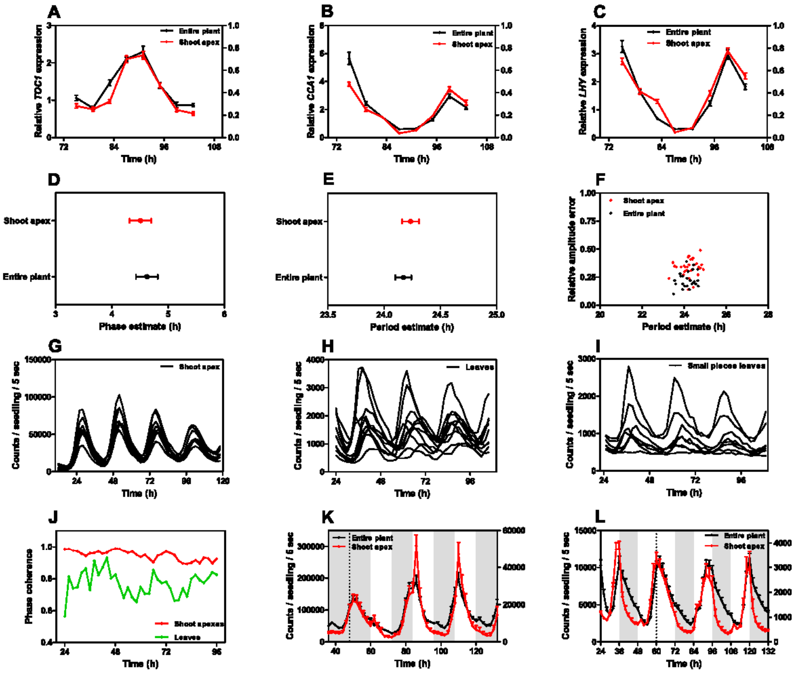

Figure S2. Comparison of Circadian Rhythmicity in Entire Plants, Shoot Apexes, and Leaves, Related to Figure 2

(A–C) Time-course analysis of gene expression by qRT-PCR of *TOC1* (A), *CCA1* (B) and *LHY* (C). Plants were entrained under LD followed by two days under LL conditions. Samples were taken every 4 hr over a 24 hr circadian cycle during the third day under LL. mRNA abundance was normalized to *PP2AA3* (At1g13320) expression. Data represents means ± SEM of two biological replicates.

(D–F) Phase (D), period (E and F), and relative amplitude (F) estimates of circadian rhythms in shoot apexes and entire plants using the Fast Fourier Transform–Non-Linear Least-squares (FFT-NLLS) suite of the Biological Rhythms Analysis Software System (BRASS).

(G–I) In vivo luminescence traces of *CCA1::LUC* and *TOC1::LUC* of individual shoot apexes (G), leaves (H), and small pieces of leaves (I) with similar sizes to shoot apexes. Plants were entrained under LD cycles and excised as detailed in Supplemental Experimental Procedures. Luminescence was recorded under LL.

(J) Quantification of the phase coherence in shoot apexes and leaves by analysis of the synchronization index "R" (see Supplemental Experimental Procedures).

(K and L) Average rhythms of *CCA1::LUC* (K) and *TOC1::LUC* (L) luminescence in entire plants and shoot apexes subjected to a "jet-lag" experiment, with extended 12 hr darkness (extended night) at dawn (K) or extended 12 hr light (extended day) at dusk (L).

Data are the means + SEM of the luminescence of 6–12 samples. Values of luminescence signals from shoot apexes are represented on the right Y axes. White boxes: light; Shaded boxes: dark.

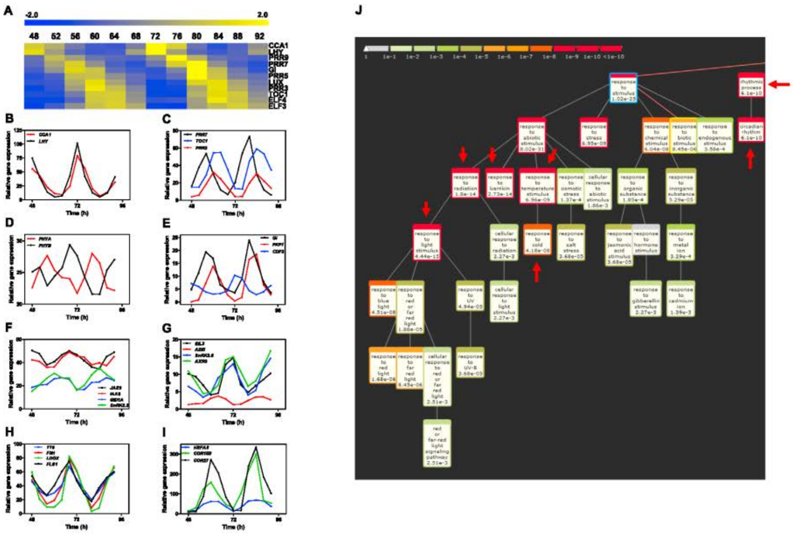

Figure S3. RNA-Seq Analyses of Circadian Rhythms at the Shoot Apex, Related to Figure 4

(A) Heatmap analysis of RNA-Seq data showing median-normalized oscillator gene expression at different circadian times (CT, horizontal axis) for transcripts (vertical axis). Yellow indicates high expression and blue low expression.

(B–I) Gene-expression analysis of *CCA1*, *LHY* (B), *PRR3, PRR7*, *TOC1* (C), PHYA and PHYB (D), *GI, FKF1, CDF2* (E), JAZ9, IAA8, GID1A, SnRK2.2 (F), EIL3, ABI5, SnRK2.8, AXR3 (G), TT5, F3H, LDOX, FLS1 (H), and HSFA8, COR15B, COR27 (I) in shoot apexes of WT plants grown under LD cycles followed by two days under LL.

(J) Functional categorization of the main circadian genes in the *Arabidopsis* shoot apex. The graphical output by "BioMaps" (Katari et al., 2010) shows the functional terms that are over-represented in the circadian gene list. The color code represents the statistical significance of the over-representation as specified in the legend on the upper left corner. Red arrows highlight the most over-represented terms related to circadian rhythms, response to light and temperature stimuli.

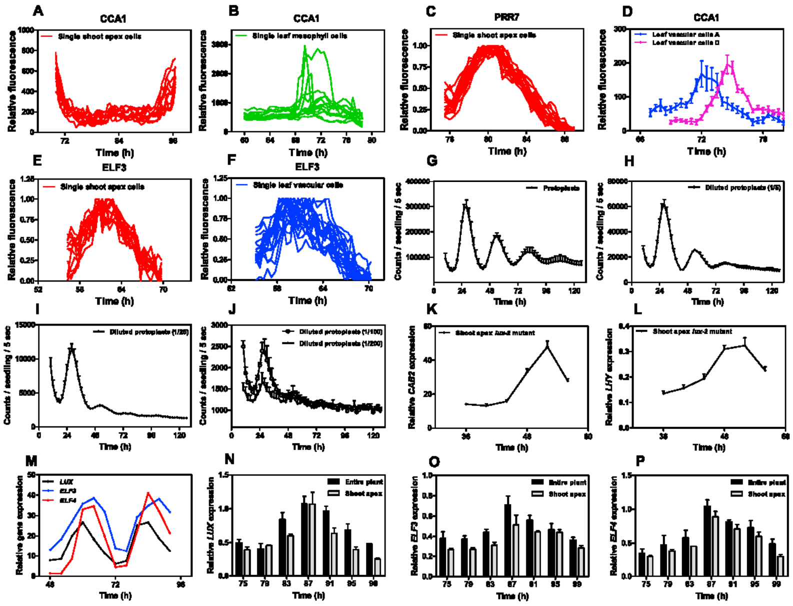

Figure S4. Rhythmic Expression in Single Cells and in Shoot Apex Protoplasts, Related to Figure 5

(A–F) In vivo time-course imaging of CCA1-HA-EYFP (A, B, and D), FLAG-PRR7-EGFP (C), and ELF3-EYFP (E and F) fluorescent signals quantified in individual nuclei of cells from the shoot apex (A, C, and E) and from leaf mesophyll cells (B) and leaf veins (D and F) embedded in agarose. Images were taken every 30 min for about 24 hr under LL. Fluorescent signals were detected with the 488 nm argon laser (excitation: 515 nm, emission: 530–630 nm). Samples were maintained under LL conditions at 60–100 μmol $m^{-2}s^{-1}$. Fluorescence quantification in the nuclei was analyzed using ImageJ software.

(G–J) Luminescence analysis of *CCA1::LUC* activity in dispersed, diluted cells (protoplasts) under LL conditions. Protoplasts were prepared as described in Supplemental Experimental Procedures from shoot apexes of plants synchronized under LD cycles. Luminescence of *CCA1::LUC* activity in serially diluted protoplasts as indicated.

(K and L) Protoplasts were synchronized for an additional day under LD before transferring to LL. qRT-PCR analysis of *CAB2* (K) and *LHY* (L) gene expression in the shoot apex of *lux-2* mutants grown under LD cycles followed by 2 days under LL.

(M) Gene-expression analysis of *LUX*, *ELF3* and *ELF4* in the shoot apex of WT plants grown under LD cycles followed by 2 days under LL.

(N–P) Comparison of *LUX* (N), *ELF3* (O), and *ELF4* (P) gene expression in entire plants and in shoot apexes. Plants were synchronized under LD cycles and the shoot apexes were excised and transferred to LL conditions for 2 days before sampling every 4 hr over a 24 hr circadian cycle.

Data represents means + SEM of two biological replicates.

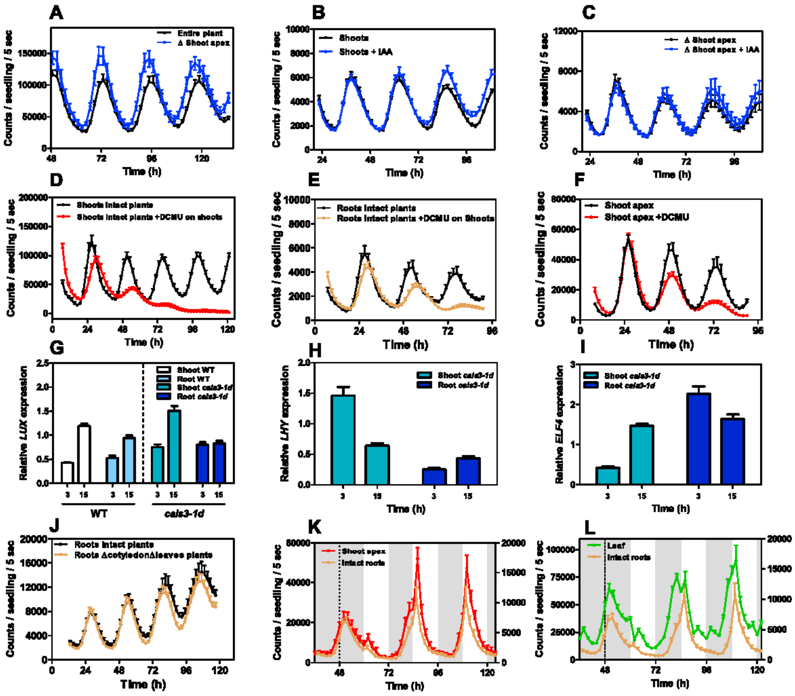

Figure S5. Rhythmic Analysis in Different Parts of the Plant and under Different Conditions, Related to Figure 6

Analysis of *CCA1::LUC* luminescence in plants in which the shoot apexes were removed by laser microdissection (Δshoot apex) (A). Plants were processed and analyzed as detailed in Supplemental Experimental Procedures.

(B and C) Rhythms in shoots from entire plants (B) and from Δshoot apex plants (C) treated with 20 μM of indole-3-acetic acid (IAA) on the shoot apex.

(D) Rhythms in shoots from entire plants following DCMU treatment on shoots. Intact plants were horizontally positioned on luminometer plate wells as described in Supplemental Experimental Procedures and depicted on Figure 6.

(E and F) Rhythms in roots from intact plants analyzed following DCMU treatment only on shoots (E) or in excised shoot apexes following treatment with DCMU (F).

(G–I) qRT-PCR analysis of *LUX* (G), *LHY* (H), and *ELF4* (I) in shoots and roots of *cals3* mutant plants. Plants were synchronized under LD and samples were taken after 2 days under LL at CT3 and CT15.

(J) *CCA1::LUC* rhythms in roots from intact plants and from plants in which the cotyledons and leaves were removed. Luminescence was recorded under LL following synchronization under LD.

(K and L) Comparisons of average rhythms of *CCA1::LUC* luminescence in roots from intact plants and excised shoot apexes (K) and leaves (L) subjected to a jet-lag experiment, with extended 12 hr darkness (extended night) at dawn.

Data are the means + SEM of the luminescence of 6–12 samples. Values of luminescence signals of roots are represented on the right y axes. White boxes: light; Shaded boxes: dark.

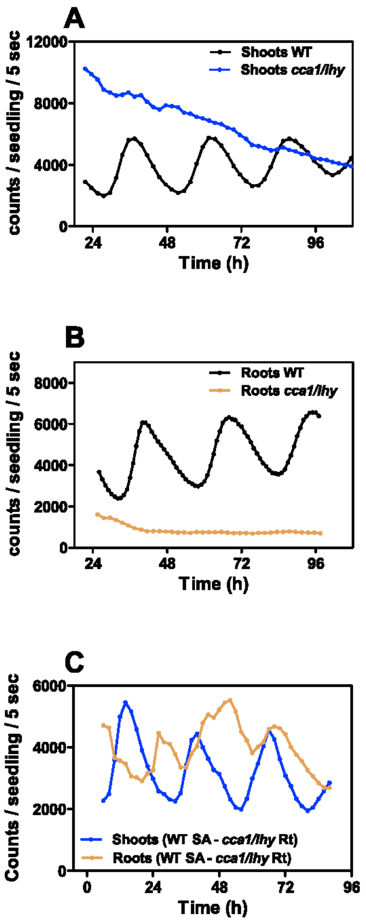

Figure S6. Rhythmic Analyses of Micrografted Plants, Related to Figure 7

(A and B) Analysis of *TOC1::LUC* luminescence in shoots (A) and roots (B) of WT and *cca1/lhy* mutant plants.

(C) Luminescence in shoots and roots of WT scion and *cca1/lhy* mutant rootstocks micrografted plants. Luminescence was recorded under LL following synchronization under LD.

Cell

Supplemental Information

A Hierarchical Multi-oscillator Network Orchestrates the *Arabidopsis* Circadian System

Nozomu Takahashi, Yoshito Hirata, Kazuyuki Aihara, and Paloma Mas

SUPPLEMENTAL INFORMATION

EXTENDED EXPERIMENTAL PROCEDURES

Plant material and organ dissection

Arabidopsis thaliana seedlings were grown on Murashige and Skoog (MS) agar medium supplemented or not (as specified for each experiment) with 3% sucrose. Seedlings were synchronized under Light:Dark cycles (LD, 12h light:12h dark) with 60-100 µmol $m^{-2}s^{-1}$ of cool white fluorescent light at 22°C. The *CCA1::LUC* (Salomé and McClung, 2005), *CAB2::LUC* (Millar et al., 1995), *TOC1::LUC* (Perales and Más, 2007) and *CCR2::LUC* (Strayer et al., 2000) reporter lines and the *cca1-11* (Ding et al., 2007), *cca1-1/lhy-11* (Mizoguchi et al., 2002), *TOC1 RNAi* (Más et al., 2003), *lux-2* (Hazen et al., 2005), *elf3-2* (Hicks et al., 1996), CCA1-HA-EYFP/*cca1-1* (Yakir et al., 2009), PRR7:FLAG-PRR7-EGFP (Nakamichi et al., 2010), ELF3:ELF3-EYFP (Dixon et al., 2011) and *cals3-d* (Vatén et al., 2011) were described elsewhere. For luminescence analysis of dissected organs, 9-14 day-old seedlings were dissected with a sterile razor blade to separate roots, hypocotyls, cotyledons, leaves and shoots. The dissected organs (or the plants without cotyledons or leaves) were placed in 96-well microplates containing Murashige and Skoog (MS) agar medium supplemented with luciferin (Biothema). A Leica Laser Microdissection system (Leica Microsystems, Inc.) was used for separating the shoot apexes and to obtain the ΔShoot apex plants. Seedlings were placed on sterile plate lids containing MS medium on the microscope stage and tissues were cut with the UV laser (337 nm) using a 6.3x objective (Move and Cut mode), power 100 and specimen balance 0. Care was taken to preserve the integrity of the tissue. For analysis of rhythms in roots from intact plants and Δshoot apex plants, one side of the walls of the 96-wells was slightly serrated to allow communication between two adjacent wells. Seedlings were then horizontally positioned such that the shoot was placed in one well and the roots in the contiguous well. For all experiments, and to decrease the possible resetting effects following dissection and manipulation, samples were allowed to resynchronize for one day before luminescence analysis was performed under constant light conditions (LL). Data from samples that appeared damaged or that eventually died after the treatments were excluded from the analysis. Pharmacological treatments were performed by applying to the shoots, shoot apexes or roots 20 µM of IAA or 20 µM of DCMU.

In vivo luminescence assays

Luminescence was examined as previously described (Malapeira et al., 2012) using a microplate luminometer LB-960 (Berthold Technologies) and the software Microwin, version 4.34 (Mikrotek

Laborsysteme). Amplitude, period, phase and relative amplitude error (RAE) were estimated with the Fast Fourier Transform–Non-Linear Least Squares (FFT-NLLS) suite (Plautz et al., 1997) using the Biological Rhythms Analysis Software System (BRASS, http://www.amillar.org). For "jet-lag" experiments, entire plants, leaves, shoot apexes as well as roots from intact plants synchronized under LD cycles (12h light:12h dark) were subjected at dawn to an additional period of 12 hour darkness (extended night) or at dusk to an additional period of 12 hour light (extended day).

RNA extraction, RNA-Seq and circadian oscillation analysis

Shoot apexes dissected from plants synchronized under LD cycles were transferred to LL conditions for two days. Samples were taken from the third day under LL, every four hours over two circadian cycles. Total RNA was isolated using the RNeasy Plant Mini Kit (Qiagen) following the manufacturer's recommendations. RNA sequencing was performed by Genomix4life S.R.L. (Baronissi, Salerno, Italy). Indexed libraries were prepared from 500 ng purified RNA pool with TruSeq Stranded mRNA Sample Prep Kit (Illumina) according to the manufacturer's instructions. Libraries were sequenced (paired-end, 2x100 cycles) at a concentration of 8pmol/L per lane on HiSeq1500 platform (Illumina) with a coverage of more than 30 million sequence reads/sample on average. Sequence analysis was performed by Sequentia Biotech (Barcelona, Spain). The raw sequence files (.fastq files) were subjected to quality control analysis by using *FastQC v0.10.1* (www.bioinformatics.babraham.ac.uk/projects/fastqc/) before trimming and removal of adapters with *AdapterRemoval 1.5.2* and *FASTX Toolikt 0.0.13.2* (Lindgreen, 2012). The reads were then mapped against the *Arabidopsis thaliana* genome (TAIR10 Genome Release, ftp://ftp.arabidopsis.org/) with TopHat v2.0.11 (Kim et al., 2013), which provided the reference gene annotation with known transcripts. Cufflinks v2.2.0 (Trapnell et al., 2010) was then used to obtain RPKM expression for each annotated gene. Duplicated reads were removed from the mapped files (bam files) with Picard Tools 1.110 (http://picard.sourceforge.net) and the resulting files were merged to include the annotation of new transcripts by using Cufflinks v2.2.0 (Trapnell et al., 2010). Comparisons with the reference genome were performed by using Cuffmerge v1.0.0 (Trapnell et al., 2010). To identify oscillating genes regulated by the circadian clock, all genes with a RPKM median across the samples less than 0.69 were discarded. The BETR algorithm (Aryee et al., 2009) was applied to identify differentially expressed genes across the dataset ($p<0.05$). The JTK_Cycle algorithm (Hughes et al., 2010) was used to identify oscillating genes ($q<0.05$) with a period ranging from 20 to 28. The Integrative Genomics Viewer (IGV) was used to visualize the data (Robinson et al., 2011; Thorvaldsdóttir et al., 2013).

The phases of circadian expression in shoot apexes and entire plants were analyzed using the publicly available Gene Phase Analysis Tool "PHASER" of the DIURNAL database (http://diurnal.mocklerlab.org/) (Michael et al., 2008; Mockler et al., 2007). Phase over-representation is calculated as the number of genes with a given phase divided by the total number of genes over the number of genes called rhythmic and divided by the total number of genes in the dataset. Circadian genes were classified into broad functional categories using the web tool "BIOMAPS" (Katari et al., 2010), which renders over-represented and significant functional terms (Gene Ontology or MIPS) as compared to the frequency of the term in the whole genome.

Mathematical analysis

The synchronization index R (Kuramoto, 1975), known as the order parameter was determined to quantitatively analyze the degree of synchronization and was calculated as

$$R(t) = \frac{1}{N}\left|\sum_{n} e^{\sqrt{-1}\theta_n(t)}\right|,$$

where θ_n represents the phases of each individual sample obtained by applying the Hilbert transform to the difference for two successive measurements within a population of size N. The synchronization index R values range from 0 and 1, where values close to 1 indicate high synchronization and values close to 0 indicate desynchronization.

For mathematical analysis of cellular coupling, we extended the barycentric coordinates to high-dimensional space by employing linear programming (Hirata et al., 2015) and by directly expressing the approximation errors. The barycentric coordinates approximate a point in phase space by a linear combination of neighboring points. Each coefficient for the linear combination is between 0 and 1. The next point is predicted by using the linear combination of the neighboring points with the corresponding coefficients. The extension allows proper modeling of high-dimensional dynamics, providing accurate mid-term predictions for high-dimensional time series.

By following Hirata et al. (2015), we identified the strength of coupling for *Arabidopsis* based on the accuracy of prediction. Let $x_i(t)$ be the value for the ith component ($i \in \{1,2,\ldots,I\}$) at time t ($1 \le t \le T$). Then, we constructed the prediction based on the following barycentric coordinates. We use weighted delay coordinates defined as

$$z_i(t,w) = (z_{i,j}(t,w)) = \left(y_{i,1}(t-d+1,w), y_{i,1}(t-d+2,w), \ldots, y_{i,1}(t,w), y_{i,2}(t-d+1,w), \ldots., y_{i,I}(t,w)\right) ,$$

and

$$y_{i,j}(t,w) = \begin{cases} x_i(t), & j = i, \\ wx_j(t), & j \neq i, \end{cases}$$

to find the K nearest neighbors for the i th component whose time indices are denoted by $I_i(t,w) = \{I_{i,1}(t,w), I_{i,2}(t,w), \ldots, I_{i,K}(t,w)\} \subset \{d, d+1, \ldots, 18\}$; we set $d = 8$ and $K = 3$ throughout the paper. Namely, we assume that there is uniform coupling among cells. Then, for predicting $x_i(t+1)$ at $t = 19$, the modeling by the barycentric coordinates can be written as

$$\hat{\lambda}(t,i,w) = \underset{\lambda=(\lambda_1,\lambda_2,\ldots,\lambda_K)}{\operatorname{argmin}} \ \varepsilon$$

$$s.t.$$

$$\left| z_{i,j}(t,w) - \sum_{k\in\{1,2,\ldots,K\}} \lambda_k z_{i,j}(I_{i,k}(t,w),w) \right| \leq \varepsilon, \text{ for } j \in \{1,2,\ldots,dI\},$$

$$0 \leq \lambda_k \leq 1, \text{ for } k \in \{1,2,\ldots,K\} \text{ and } \sum_{k\in\{1,2,\ldots,K\}} \lambda_k = 1.$$

This problem can be solved by linear programming easily. The prediction is given by

$$\hat{x}_i(t+1,w) = \sum_{k\in\{1,2,\ldots,K\}} \hat{\lambda}_k(t,i,w) x_i(I_{i,k}(t,w)+1).$$

For predicting $x_i(t+1)$ at $19 < t < T$, we apply the similar calculation iteratively to obtain $\hat{x}_i(t+1,w)$.

We evaluated the prediction error by $\sum_{t\geq 19} \left|\hat{x}_i(t+1,w) - x_i(t+1)\right|$. The coupling strength for the i th component was obtained by $\hat{w}_i = \underset{w\in\{0.05,0.1,\ldots,1\}}{\operatorname{argmin}} \sum_{t\geq 19} \left|\hat{x}_i(t+1,w) - x_i(t+1)\right|$.

Protoplast preparation

Protoplasts were prepared as previously described (Yoo et al., 2007) with modifications. Briefly, 20-30 excised shoot apexes from two-week old plants were rapidly transferred into 12-well plates containing the enzyme solution (400 mM mannitol, 20 mM KCl, 10 mM CaCl2, 7.5mg/ml cellulase RS and 3 mg/ml macerozyme R-10). The plates were incubated in a shaker with slow agitation overnight at room temperature. An ethanol sterilized nylon mesh (4cm x 4cm) was used as a filter to transfer the released protoplasts to 1.5ml tubes. Protoplasts were spin at 250g for 2 min and subsequently washed three times in W5 solution (154 mM NaCl, 125 mM CaCl2, 5 mM KCl, 2 mM MES pH 5.6) before final collection of the protoplasts. The dispersed cells were initially diluted to approximately a concentration of $0.1x10^3$ cells per well. Protoplasts were resynchronized for one additional day before in vivo analysis by luminescence assays.

Single cell confocal microscopy imaging

For *in vivo* confocal imaging at a single cell resolution, excised shoot apexes or leaves were embedded just after dissection in low-melting-point agarose dissolved in MS medium as previously described (Mas and Beachy, 1998). The embedded samples were placed in microscope slides with approximately 200 microlitres of liquid MS medium that generated air bubbles within the liquid layer. Altogether, the system provided the aerobic environment and nutrients necessary for the survival of the tissues over the time course. Samples were maintained under LL conditions at 60-100 µmol $m^{-2}s^{-1}$. Fluorescent signals from the shoot apex, leaf vascular and leaf mesophyll cells were imaged once every 30 min with an argon laser (transmissivity: 40%; excitation: 515 nm; emission range: 530-630 nm) in a FV-1000 confocal microscope (Olympus, Tokyo, Japan) with a 40x/1.3 oil immersion objective. About 15-20 serial optical sections (z stacks) were scanned using the scanned mode "XYZT" with image sizes of 640 x 640 (0.497 µm/pixel) and sampling speed of 4 µs/pixel. Sections of 2.0-3.0 µm step sizes perpendicular to the z-axis (microscope optical axis) were imaged using the filter mode Kalman line (set at 2). Fluorescence intensity quantification in the nuclei was analyzed using ImageJ software using Mean Gray Value option. The results are representative of at least three biological replicates for shoot apex and leaf vascular cells and two biological replicates for leaf mesophyll cells. About 30-40 different nuclei were examined per experiment with each of the three different reporters (CCA1, PRR7 and ELF3). Signals from individual nuclei that moved or got out of focus were excluded from the analysis.

Gene expression analysis by RT-QPCR

RNA was isolated using the Maxwell 16 LEV simply RNA Tissue kit (Promega). Single strand cDNA was synthesized using iScript™ Reverse Transcription Supermix for RT-qPCR (BioRad) following manufacturer recommendations. For QPCR analysis, cDNAs were diluted 10-fold with nuclease-free water and QPCR was performed with the iTaq Universal SYBR Green Supermix (BioRad) in a 96-well CFX96 Touch Real-Time PCR Detection System (BioRad). The protein phosphatase 2A subunit A3 (At1g13320) was used as control (Kaufmann et al., 2010).

SUPPLEMENTAL REFERENCES

Aryee, M., Gutierrez-Pabello, J., Kramnik, I., Maiti, T., and Quackenbush, J. (2009). An improved empirical bayes approach to estimating differential gene expression in microarray time-course data: BETR (Bayesian Estimation of Temporal Regulation). BMC Bioinformatics *10*, 409.

Ding, Z., Doyle, M.R., Amasino, R.M., and Davis, S.J. (2007). A complex genetic interaction between *Arabidopsis thaliana* TOC1 and CCA1/LHY in driving the circadian clock and in output regulation. Genetics *176*, 1501-1510.

Dixon, L.E., Knox, K., Kozma-Bognar, L., Southern, M.M., Pokhilko, A., and Millar, A.J. (2011). Temporal Repression of Core Circadian Genes Is Mediated through EARLY FLOWERING 3 in Arabidopsis. Curr Biol *21*, 120-125.

Hazen, S.P., Schultz, T.F., Pruneda-Paz, J.L., Borevitz, J.O., Ecker, J.R., and Kay, S.A. (2005). LUX ARRHYTHMO encodes a Myb domain protein essential for circadian rhythms. Proc Natl Acad Sci USA *102*, 10387-10392.

Hicks, K.A., Millar, A.J., Carré, I.A., Somers, D.E., Straume, M.D., Meeks-Wagner, R., and Kay, S.A. (1996). Conditional circadian dysfunction of the *Arabidopsis early-flowering 3* mutant. Science *274*, 790-792.

Hirata, Y., Shiro, M., Takahashi, N., Aihara, K., Suzuki, H., and Mas, P. (2015). Approximating high-dimensional dynamics by barycentric coordinates with linear programming. Chaos: An Interdisciplinary Journal of Nonlinear Science *25*, 013114.

Hughes, M.E., Hogenesch, J.B., and Kornacker, K. (2010). JTK_CYCLE: An Efficient Nonparametric Algorithm for Detecting Rhythmic Components in Genome-Scale Data Sets. Journal of Biological Rhythms *25*, 372-380.

Katari, M.S., Nowicki, S.D., Aceituno, F.F., Nero, D., Kelfer, J., Thompson, L.P., Cabello, J.M., Davidson, R.S., Goldberg, A.P., Shasha, D.E., *et al.* (2010). VirtualPlant: A Software Platform to Support Systems Biology Research. Plant Physiology *152*, 500-515.

Kaufmann, K., Wellmer, F., Muiño, J.M., Ferrier, T., Wuest, S.E., Kumar, V., Serrano-Mislata, A., Madueño, F., Krajewski, P., Meyerowitz, E.M., *et al.* (2010). Orchestration of Floral Initiation by APETALA1. Science *328*, 85-89.

Kim, D., Pertea, G., Trapnell, C., Pimentel, H., Kelley, R., and Salzberg, S. (2013). TopHat2: accurate alignment of transcriptomes in the presence of insertions, deletions and gene fusions. Genome Biology *14*, R36.

Kuramoto, Y. (1975). Self-entrainment of a population of coupled nonlinear oscillators. Lect N Phys *39*, 420-422.

Lindgreen, S. (2012). AdapterRemoval: easy cleaning of next-generation sequencing reads. BMC Research Notes *5*, 337.

Malapeira, J., Khaitova, L.C., and Mas, P. (2012). Ordered changes in histone modifications at the core of the Arabidopsis circadian clock. Proc Natl Acad Sci USA *109*, 21540-21545.

Más, P., Alabadí, D., Yanovsky, M.J., Oyama, T., and Kay, S.A. (2003). Dual role of TOC1 in the control of circadian and photomorphogenic responses in Arabidopsis. The Plant cell *15*, 223-236.

Mas, P., and Beachy, R.N. (1998). Distribution of TMV movement protein in single living protoplasts immobilized in agarose. The Plant Journal *15*, 835–842.

Michael, T.P., Mockler, T.C., Breton, G., McEntee, C., Byer, A., Trout, J.D., Hazen, S.P., Shen, R., Priest, H.D., Sullivan, C.M., *et al.* (2008). Network discovery pipeline elucidates conserved time-of-day-specific cis-regulatory modules. PLoS Genet *4*, e14.

Millar, A.J., Carre, I.A., Strayer, C.A., Chua, N.H., and Kay, S.A. (1995). Circadian clock mutants in *Arabidopsis* identified by luciferase imaging. Science *267*, 1161-1163.

Mizoguchi, T., Wheatley, K., Hanzawa, Y., Wright, L., Mizoguchi, M., Song, H.R., Carre, I.A., and Coupland, G. (2002). *LHY* and *CCA1* are partially redundant genes required to maintain circadian rhythms in Arabidopsis. Dev Cell *2*, 629-641.

Mockler, T., Michael, T., Priest, H., Shen, R., Sullivan, C., Givan, S., McEntee, C., Kay, S., and Chory, J. (2007). The DIURNAL project: DIURNAL and circadian expression profiling, model-based pattern matching, and promoter analysis. Cold Spring Harb Symp Quant Biol *72*, 353-363.

Nakamichi, N., Kiba, T., Henriques, R., Mizuno, T., Chua, N.-H., and Sakakibara, H. (2010). PSEUDO-RESPONSE REGULATORS 9, 7, and 5 Are Transcriptional Repressors in the Arabidopsis Circadian Clock. The Plant cell *22*, 594-605.

Perales, M., and Más, P. (2007). A functional link between rhythmic changes in chromatin structure and the Arabidopsis biological clock. The Plant cell *19*, 2111-2123.

Plautz, J.D., Straume, M., Stanewsky, R., Jamison, C.F., Brandes, C., Dowse, H., Hall, J.C., and Kay, S.A. (1997). Quantitative analysis of Drosophila period gene transcription in living animals. J Biol Rhythms *12*, 204-217.

Robinson, J.T., Thorvaldsdottir, H., Winckler, W., Guttman, M., Lander, E.S., Getz, G., and Mesirov, J.P. (2011). Integrative genomics viewer. Nat Biotech *29*, 24-26.

Salomé, P.A., and McClung, C.R. (2005). PSEUDO-RESPONSE REGULATOR 7 and 9 are partially redundant genes essential for the temperature responsiveness of the *Arabidopsis* circadian clock. The Plant cell *17*, 791-803.

Strayer, C.A., Oyama, T., Schultz, T.F., Raman, R., Somers, D.E., Más, P., Panda, S., Kreps, J.A., and Kay, S.A. (2000). Cloning of the Arabidopsis clock gene *TOC1*, an autoregulatory response regulator homolog. Science *289*, 768-771.

Thorvaldsdóttir, H., Robinson, J.T., and Mesirov, J.P. (2013). Integrative Genomics Viewer (IGV): high-performance genomics data visualization and exploration. Briefings in Bioinformatics *14*, 178-192.

Trapnell, C., Williams, B.A., Pertea, G., Mortazavi, A., Kwan, G., van Baren, M.J., Salzberg, S.L., Wold, B.J., and Pachter, L. (2010). Transcript assembly and quantification by RNA-Seq reveals unannotated transcripts and isoform switching during cell differentiation. Nat Biotech *28*, 511-515.

Vatén, A., Dettmer, J., Wu, S., Stierhof, Y.-D., Miyashima, S., Yadav, Shri R., Roberts, Christina J., Campilho, A., Bulone, V., Lichtenberger, R., *et al.* (2011). Callose Biosynthesis Regulates Symplastic Trafficking during Root Development. Developmental Cell *21*, 1144-1155.

Yakir, E., Hilman, D., Kron, I., Hassidim, M., Melamed-Book, N., and Green, R.M. (2009). Posttranslational Regulation of CIRCADIAN CLOCK ASSOCIATED1 in the Circadian Oscillator of Arabidopsis. Plant Physiology *150*, 844-857.

Yoo, S.-D., Cho, Y.-H., and Sheen, J. (2007). Arabidopsis mesophyll protoplasts: a versatile cell system for transient gene expression analysis. Nat Protocols *2*, 1565-1572.

Annex III:

Approximating high-dimensional dynamics by barycentric coordinates with linear programming

Yoshito Hirata , Masanori Shiro, Nozomu Takahashi, Kazuyuki Aihara, Hideyuki Suzuki, and Paloma Mas

Citation: Chaos **25**, 013114 (2015); doi: 10.1063/1.4906746
View online: http://dx.doi.org/10.1063/1.4906746
View Table of Contents: http://aip.scitation.org/toc/cha/25/1
Published by the American Institute of Physics

PHYSICS TODAY
Welcome to a
Smarter Search
with the redesigned
Physics Today Buyer's Guide
Find the tools you're looking for today!

CHAOS 25, 013114 (2015)

Approximating high-dimensional dynamics by barycentric coordinates with linear programming

Yoshito Hirata,[1,2,3,a)] Masanori Shiro,[2,4] Nozomu Takahashi,[5] Kazuyuki Aihara,[1,2,3]
Hideyuki Suzuki,[1,2,3] and Paloma Mas[5]
[1]*Institute of Industrial Science, The University of Tokyo, 4-6-1 Komaba, Meguro-ku, Tokyo 153-8505, Japan*
[2]*Department of Mathematical Informatics, The University of Tokyo, Bunkyo-ku, Tokyo 113-8656, Japan*
[3]*CREST, JST, 4-1-8 Honcho, Kawaguchi, Saitama 332-0012, Japan*
[4]*Mathematical Neuroinformatics Group, Advanced Industrial Science and Technology, Tsukuba, Ibaraki 305-8568, Japan*
[5]*Center for Research in Agricultural Genomics (CRAG), Consorci CSIC-IRTA-UAB-UB, Barcelona 08193, Spain*

(Received 23 October 2014; accepted 15 January 2015; published online 22 January 2015)

The increasing development of novel methods and techniques facilitates the measurement of high-dimensional time series but challenges our ability for accurate modeling and predictions. The use of a general mathematical model requires the inclusion of many parameters, which are difficult to be fitted for relatively short high-dimensional time series observed. Here, we propose a novel method to accurately model a high-dimensional time series. Our method extends the barycentric coordinates to high-dimensional phase space by employing linear programming, and allowing the approximation errors explicitly. The extension helps to produce free-running time-series predictions that preserve typical topological, dynamical, and/or geometric characteristics of the underlying attractors more accurately than the radial basis function model that is widely used. The method can be broadly applied, from helping to improve weather forecasting, to creating electronic instruments that sound more natural, and to comprehensively understanding complex biological data. © *2015 AIP Publishing LLC.* [http://dx.doi.org/10.1063/1.4906746]

Modeling and predicting a high-dimensional time series is still a challenge because common methods such as neural networks[1–5] and radial basis functions[6–11] have many parameters to be fitted compared with the length of the time series. This challenge is often called as the *curse of dimensionality*.[12] Here, we propose to model a high-dimensional time series with barycentric coordinates[13] by using linear programming.[14] Mees[13] demonstrated that barycentric coordinates obtained by tessellations are effective to reproduce typical behavior of the two-dimensional Hénon map and the three-dimensional Rössler model, while the tessellations are difficult to be applied to high-dimensional phase space. We overcome this difficulty by formulating the problem for obtaining barycentric coordinates, employing linear programming and expressing the approximation error directly. Toy and real-world examples show the wide applicability of the proposed method.

I. INTRODUCTION

Although the recent advances in measurement techniques have highly facilitated the acquisition of high-dimensional time series, it is still difficult to model such data. About 25 years ago, the theory of neural networks[1–5] and radial basis functions[6–11] was intensively studied to prove that they can approximate any continuous function arbitrarily well if there are enough neurons or basis functions, respectively. However, this approach needs many parameters to be fitted,[12] and hence data of a long time series for modeling. Recently, sparse modeling[15] has been aiming at extracting a small number of fundamental variables and providing interpretable models for target systems by paying the costs of modeling accuracy in the dynamics. Therefore, such sparse modeling has the trade-off between the interpretability and the modeling accuracy, which is governed by the number of variables used for explanations. If the sparse modeling is restricted to be linear, the modeling errors may be acceptable. However, modeling a nonlinear system that may be chaotic might lead to model errors that are often at unacceptable levels.

Modeling accurately a low-dimensional nonlinear dynamics was advanced in 1991, when Mees[13] proposed to use the barycentric coordinates for this sake. In the barycentric coordinates, the current point in phase space is approximated by a linear combination of neighboring points where each coefficient for the linear combination is between 0 and 1 and their total is 1 exactly. Then, one predicts the next point in time for the current point by using the linear combination of the next points in time for the neighboring points, weighting them by using the same corresponding coefficients (see Fig. 1). Mees[13] modeled the Hénon map, a two-dimensional toy model of deterministic chaos by using its time series of only 50 time points, and reproduced the typical characteristics of the Hénon map. It was also shown mathematically in Ref. 13 that the original barycentric coordinate is the first order approximation, continuous, and converges to the true dynamics when the number of points increases. However, it

---

[a)]Electronic mail: yoshito@sat.t.u-tokyo.ac.jp

© 2015 AIP Publishing LLC

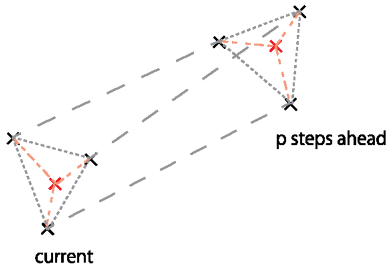

FIG. 1. Schematic image for barycentric coordinate modeling of a dynamical system.

was difficult to apply the method to high-dimensional dynamics because the method uses tessellations,[13] a geometrical method that is most effective computationally in two-dimensional space rather than high-dimensional space, although there were some free-run prediction examples of Lorenz'63 (Ref. 16) and Rossler models.[13] The barycentric coordinates were also applied for finding unstable periodic orbits[17] and modeling noisy data.[18]

Here, we extend the barycentric coordinates to high-dimensional space by employing linear programming,[14] and expressing the approximation errors directly. This extension enables us to easily model high-dimensional dynamics and reproduce relatively better long-term behavior given a multivariate time series generated from a target system. In addition, whether our modeling becomes the first order or not because there were few similar events in the past can be evaluated simultaneously without additional computational costs. In Ref. 19, the first author proposed an index to identify when the prediction goes wrong because there were few similar events in the past.

II. BARYCENTRIC COORDINATES BY LINEAR PROGRAMMING

The problem for constructing the barycentric coordinates by linear programming can be mathematically formulated as follows: Let $\vec{v}_i = (\, v_{i,1}\ v_{i,2} \cdots v_{i,J}\,)$ $(i = 1, 2, \ldots, I)$ be the i th point of J-dimensional time series located in phase space; here we may use delay coordinates[20,21] to reconstruct phase space for the underlying dynamics. For each time t, we find K nearest neighbors for the current point $\vec{v} = (\, v_1\ v_2 \cdots v_J\,)$ and denote a set of their indexes by I_t. We often encounter the situation with $K \leq J$. Then, we may approximate $\vec{v}$ by

$$\vec{v} \approx \sum_{i \in I_t} \lambda_i \vec{v}_i, \tag{1}$$

$$\sum_{i \in I_t} \lambda_i = 1, \tag{2}$$

$$0 \leq \lambda_i \leq 1. \tag{3}$$

Let us evaluate the approximation error by the maximum norm

$$\max_j \left| v_j - \sum_{i \in I_t} \lambda_i v_{i,j} \right|. \tag{4}$$

Then, the problem of the optimal approximation can be written as follows:

$$\min_{\{\lambda_i\}} \varepsilon \tag{5}$$

such that

$$\begin{aligned}
&\varepsilon \geq 0,\\
&-\varepsilon \leq v_j - \sum_{i \in I_t} \lambda_i v_{i,j} \leq \varepsilon \quad \text{for} \quad j = 1, 2, \ldots, J,\\
&\sum_{i \in I_t} \lambda_i = 1, \text{ and}\\
&0 \leq \lambda_i \leq 1,
\end{aligned}$$

where Eq. (5) gives the approximation error. This problem is linear programming and thus we can use varieties of software to solve it. After we construct this approximation, a direct p steps ahead prediction for the underlying dynamics defined by map f satisfying $\vec{v}_{t+1} = f(\vec{v}_t)$ can be obtained by

$$f^p(\vec{v}) \approx \hat{f}^p(\vec{v}) = \sum_{i \in I_t} \lambda_i \vec{v}_{i+p}. \tag{6}$$

We call it as the direct prediction.

When the approximation of one step prediction is in good accuracy, we may use the one step prediction p times iteratively to produce a free-run prediction at p steps ahead. We call it as the iterative prediction. Mathematically, the iterative prediction can be written as

$$\hat{f}^p(\vec{v}) = \sum_{i \in I_{t+p-1}(\hat{f}^{p-1}(\vec{v}))} \lambda_i(\hat{f}^{p-1}(\vec{v}))\vec{v}_{i+1}, \tag{7}$$

$$\hat{f}^0(\vec{v}) = \vec{v}. \tag{8}$$

In the Appendix, we show analytical results that the proposed method approximates the underlying dynamics and provides the bounded prediction.

We used MATLAB and its optimization toolbox to solve the linear programming formulated above by the interior point method if not mentioned. In the toolbox, the interior point method is implemented based on Ref. 22, which is a variant of primal-dual interior point method.[23] When the toolbox of MATLAB did not provide an appropriate optimal solution, then we set $\lambda_i = 1/K$.

III. EXAMPLES

A. Toy models: Low-dimensional chaos

First, we tested the performance for the proposed method using toy models of low-dimensional chaos such as the Rössler model[24] and the Lorenz'63 model.[25] The Rössler model[24] used in this manuscript is given as follows:

$$\begin{aligned}&\dot{x} = -(y+z),\\&\dot{y} = x + ay,\\&\dot{z} = b + z(x-c),\\&a = 0.36, b = 0.4, \text{ and } c = 4.5.\end{aligned} \tag{9}$$

We sampled x every 0.5 unit time to generate a time series of length 300. We used 10-dimensional delay coordinates[20,21] to predict the following 400 points. The Lorenz'63 model[25] is given as follows:

$$\begin{aligned}&\dot{x} = -s(x-y),\\&\dot{y} = -xz + gx - y,\\&\dot{z} = xy - bz,\\&s = 10, g = 28, \text{ and } b = \frac{8}{3}.\end{aligned} \tag{10}$$

We sampled x every 0.05 unit time to generate a time series of length 300. The rest is same as the Rössler model. For both systems, we used five nearest neighbors in the Euclidean distance to obtain the barycentric coordinates. These results demonstrate that 300 time points were sufficient to produce accurate free-run predictions at least up to 20 time steps for the time series generated from these three-dimensional models (Figs. 2(c) and 2(f)). Especially, the rough shapes of the corresponding attractors were reproduced well (compare Figs. 2(a) and 2(d) with Figs. 2(b) and 2(e), respectively).

B. Toy models: High-dimensional dynamics

Second, we also evaluate the proposed prediction method with time series generated from high-dimensional dynamics such as the coupled map lattice[26] and the Lorenz'96 I model.[27] The coupled map lattice[26] used here is defined as follows:

$$\begin{aligned}x_j(i+1) = {}&(1-2\beta)\{\alpha x_j(i)[1-x_j(i)]\}\\&+(\beta-\gamma)\{\alpha x_{j+1}(i)[1-x_{j+1}(i)]\}\\&+(\beta+\gamma)\{\alpha x_{j-1}(i)[1-x_{j-1}(i)]\},\\x_{j+J}(i) = {}&x_j(i),\end{aligned} \tag{11}$$

where we set $J = 10, \alpha = 3.8, \beta = 0.05$, and $\gamma = 0.01$. We generated 100 time series of dimension 10 containing 2010 points by using different initial conditions. We used the first 2000 points to model the dynamics and predict the following 10 points. An example of predicted time series is shown in Fig. 3. The free-run prediction for the radial basis function model obtained by the method of Ref. 10 looked more constant in x_1, x_2, and x_3 than the proposed method. We used the

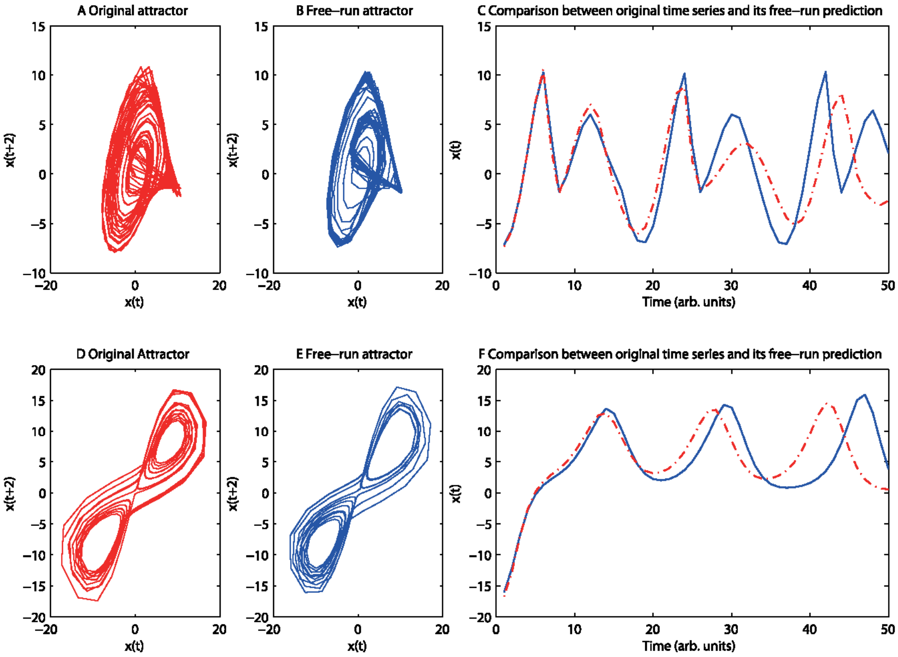

FIG. 2. Attractors of original time series and free-run prediction. (a)–(c) Correspond to the Rössler model, and (d)–(f) correspond to the Lorenz'63 model. (a) and (d) The original attractors, (b) and (e) the attractors obtained from the free-run prediction, and (c) and (f) the free-run prediction (blue solid lines) and the truth (red dashed lines).

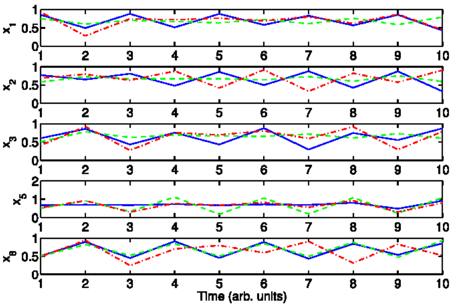

FIG. 3. Example of free-run prediction for coupled map lattice. In each panel, the blue solid line, the green dashed line, and the red dash-dotted line correspond to the results of the proposed method, those of radial basis function model, and the truth, respectively.

mean correlation coefficients over 100 realizations of time series to evaluate the accuracy of prediction as done in Ref. 28 (Fig. 4). We found a property that the proposed method tended to achieve the higher correlation coefficient than the radial basis function model.

To further characterize their free-run predictions for the coupled map lattice topologically, dynamically, and geometrically, we used the joint topological entropy, joint metric entropy,[29] and transitivity dimension,[30,31] respectively. We define the joint topological entropy by first defining symbolic dynamics for each logistic map j using its critical point 0.5 as commonly done,[32] assigning 0 for $s_j(i)$ if the value $x_j(i) < 0.5$ and 1 for $s_j(i)$ otherwise. Second, we defined a combined symbol $s(i) = \sum_{j-1}^{10} s_j(i)2^{10-j}$. Third, we counted the number of unique combined symbols appearing: $\# = |\{s(i)|i = 2001, \ldots, 3000\}|$. Then, we defined the joint topological entropy as $\log_2\#$. For free-run predictions, we predicted up to 1000 steps ahead using their iterative predictions and obtained their joint topological entropies by replacing $x_j(i)$ with $\tilde{x}_j(i)$, applying the following calculations similarly.

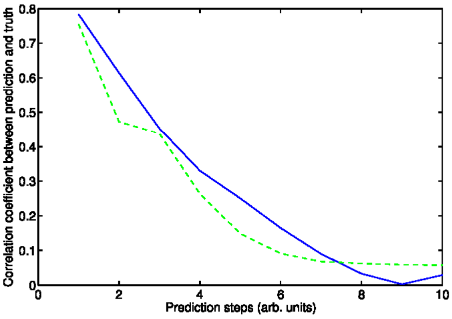

FIG. 4. Evaluation of prediction for coupled map lattice. The figure shows the mean correlation coefficients between the predicted time series (proposed method (blue solid line) and radial basis function model (green dashed line)) and the truth given a prediction step over 100 realizations of time series.

To characterize the reconstructed dynamics dynamically, we defined the joint metric entropy as the joint entropy[29] of $\{s(i)|i = 2001, \ldots, 3000\}$. Here, we call it as joint metric entropy to distinguish it with the joint topological entropy. Namely, denoting $q(l) = |\{i = 2001, ..., 3000|s(i) = l\}|/1000$, our joint metric entropy is defined as $\sum_{l-0}^{2^{10}-1} -q(l)\log_2 q(l)$.

We used the transitivity dimension[30,31] to evaluate the reconstructed dynamics geometrically. We first define a recurrence plot[33] R over 10-dimensional space with the threshold ξ such that 20% of places have points plotted except for the central diagonal line. Mathematically, the recurrence plot can be defined as

$$R(i,k) = \begin{cases} 1, & \text{if} \sqrt{\sum_{j-1}^{10}(x_j(i) - x_j(k))^2} \leq \xi \\ 0, & \text{otherwise.} \end{cases} \tag{12}$$

Next, we define the adjacency matrix for its recurrence network as $E(i,k) = R(i,k) - \delta_{i,k}$, where $\delta_{i,k}$ is Kronecker's delta: $\delta_{i,k} = 1$, if $i = k$ and $\delta_{i,k} = 0$ otherwise. Then, the transitivity dimension[30,31] D is defined as

$$T = \frac{\sum_{i,k,m} E(i,k)E(k,m)E(m,i)}{\sum_{i,k,m} E(i,k)E(i,m)}, \tag{13}$$

and

$$D = \frac{\log T}{\log(3/4)}. \tag{14}$$

The results are summarized in Fig. 5. We can see that the values obtained over 100 simulations for the proposed barycentric coordinates are distributed more similar to the ones for the original dynamics than those for the radial basis function model. When we quantified their distances using the Kantorovich metric,[34] the distances between the original dynamics and the free-run by the barycentric coordinates were 0.4696, 0.5692, and 0.4801 in the joint topological entropy, joint metric entropy, and transitivity dimension, respectively; while the distances between the original dynamics and the free-run by the radial basis function model were 4.1727, 5.3126, and 2.1174, respectively. Therefore, the free-run by the proposed barycentric coordinates is more consistent with the original dynamics than that by the radial basis function model.

The Lorenz'96 I (Ref. 27) model used here is defined as follows:

$$\begin{aligned} \dot{x}_j &= -x_{j-2}x_{j-1} + x_{j-1}x_{j+1} - x_j + F, \\ x_{j+J} &= x_j, \end{aligned} \tag{15}$$

where we used $J = 10$ and $F = 8$. We sampled all x_j ($j = 1, 2, \ldots, 10$) every 0.05 unit time to generate 100 time series of 2050 time points in 10 dimensional space. Then, we use the first 2000 points to predict the following 50 time points. An example of free-run prediction is shown in Fig. 6. We can see the property that the free-run prediction by the

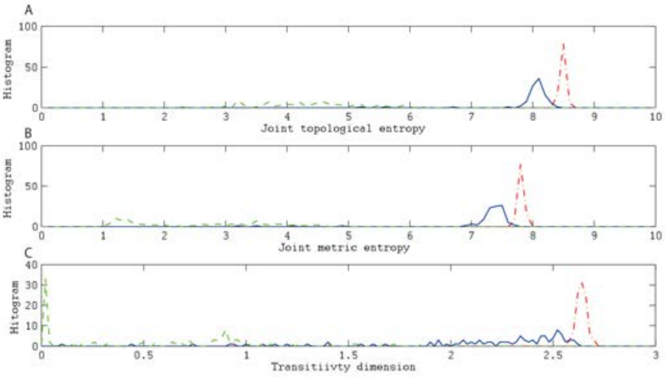

FIG. 5. Topological, dynamical, and geometric comparisons between the barycentric coordinates and the radial basis function model in their free-run predictions for the coupled map lattice. The interior point method was used in this figure. Panels (a), (b), and (c) correspond to distributions of the joint topological entropy, joint metric entropy, and transitivity dimension obtained by 100 different simulations. In each panel, the red dash-dotted line, the blue solid line, and the green dashed line correspond to the original dynamics, the free-run by the barycentric coordinates, and the free-run by the radial basis function model, respectively.

proposed method tended to follow the truth more closely than the radial basis function model constructed by Ref. 10. The mean correlation coefficients over 100 realizations of time series also showed that the free-run prediction by the proposed method agreed better with the truth than the radial basis function model up to 30 steps ahead prediction (Fig. 7).

We also compared the free-run by the barycentric coordinates with that by the radial basis function model using the joint topological entropy, joint metric entropy, and transitivity dimension. But, this time, symbolic dynamics used to obtain the joint topological entropy and joint metric entropy was permutations[35,36] of length 2. Namely, we assign 0 for $s_j(i)$ if the value $x_j(i) < x_j(i+1)$ and 1 otherwise. It is known that the topological[37] and metric[38] entropies obtained by permutations agree with the conventional topological and metric entropies, respectively, when the length of permutations is sufficiently large. The joint permutations[39,40] and joint metric permutation entropy[39,41,42] were considered previously, but the joint topological permutation entropy is used for the first time in this paper as far as we noticed.

We found that the free-run by the barycentric coordinates is closer to the original dynamics than the free-run by the radial basis function model topologically, dynamically, and geometrically, because the distributions for the joint topological permutation entropy, the joint metric permutation entropy, and the transitivity dimension obtained from 100 free-run prediction obtained by the barycentric coordinates are much more similar to those of the original dynamics compared with those obtained by 100 free-run predictions obtained by the radial basis function model (Fig. 8). The distances obtained by the Kantorovich metric[34] between the original time series and the free-run predictions by the barycentric coordinates for the joint topological permutation entropy, the joint metric permutation entropy, and the transitivity dimension were 0.6499, 0.6820, and 0.2819, respectively; while the distances between the original time series and the free-run predictions by the radial basis function model were 1.5706, 2.1863, and 0.8541, respectively.

Altogether, we conclude that the proposed method works fairly well topologically, dynamically, and geometrically even though the underlying dynamics is high-dimensional.

C. Violin sounds

Third, we produced free-run prediction for violin sounds to demonstrate the performance on a real high-dimensional

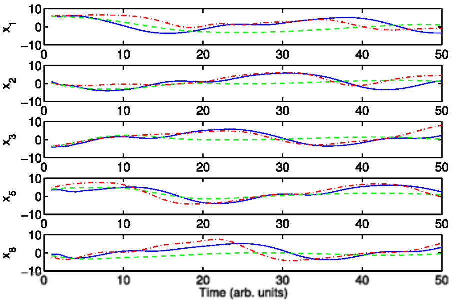

FIG. 6. Example for free-run prediction for Lorenz'96 I model. See the caption of Fig. 3 to interpret the results.

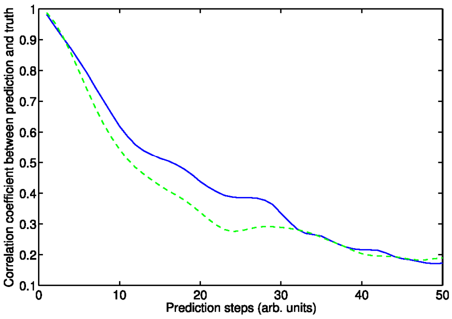

FIG. 7. Evaluation of prediction accuracy for Lorenz'96 I model. The figure shows the mean correlation coefficients for the proposed method (blue solid line) and the radial basis function model (green dashed line) with the truth given a prediction step over 100 time series.

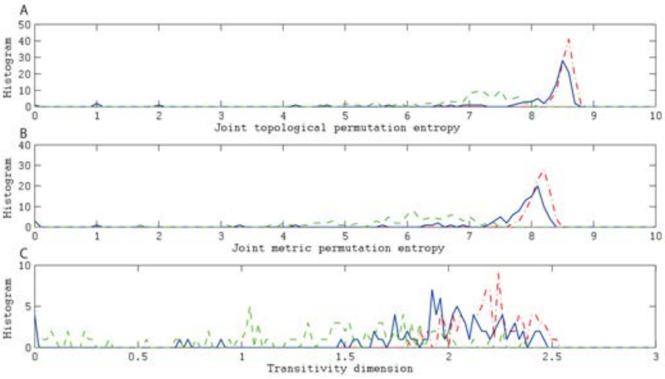

FIG. 8. Topological, dynamical, and geometric comparisons between the barycentric coordinates and the radial basis function model in their free-run predictions for Lorenz'96 I model using the interior point method. See the caption of Fig. 5 to interpret the results.

system. The violin data were taken from the third violin of RWC Music Database.[43] Because the sampling frequency was 44.1 kHz and the sound corresponds to the sound of the note *A* (440 Hz), the sound wave of violin has periodicity of period 100. The sound of the note *A* is normally used for an orchestra to tune the tones of its various musical instruments. We used the first 20 000 points to predict the following points. We used 20 nearest neighbors to yield the prediction. In addition, we employed 20 and 50-dimensional delay coordinates to compare the performance. The results presented in Fig. 9, which were obtained with the 50-dimensoinal delay coordinates, show that the attractor and hence the sounds of violin were modeled quite well; listen the supplementary Sound Files 1 and 2 in the supplementary material[44] to compare the two sounds. Particularly, the free-run prediction matched the sound wave almost exactly up to 1000 steps ahead (see Fig. 9(a)). In addition, the attractor reproduced by the free-run prediction looks quite similar to that of the original violin sounds (Figs. 9(a) and 9(c)). However, when we used 20-dimensional delay coordinates, the prediction, especially, its long-term behavior did not look great (Fig. 10). Therefore, the high-dimensional reconstruction was essential for the results in Fig. 9.

D. Solar irradiation

Fourth, we predicted time series for solar irradiation. The solar irradiation data were provided by the Japan Meteorological Agency. We chose 48 weather stations in Japan that have valid solar irradiation measurements during most of time between years 2010 and 2012. The original measurements were every 10 min. We took 1 h moving average. We used the delay coordinates of length 2 days and 10 neighbors for the prediction. In addition, we provided hourly predictions from 0 am, March 1, 2012 up to 7 days ahead by direct predictions based on the datasets of years 2010 and 2011. We obtained the density predictions by dressing the predictions obtained by the neighbors with the coefficients of the barycentric coordinates and the Gaussian kernels[10] of mean 0 and standard deviation that is the same as the root mean squared errors for January and February, 2012. Mathematically, suppose that neighbors $\{\vec{v}_i | i \in I_t\}$ and their coefficients $\{\lambda_i | i \in I_t\}$ are given. In addition, we assume that the prediction error of the one-step prediction for the *j* th variable between January and February 2012 was given by their standard deviation σ_j. Then, the prediction density for the *j* th variable $u_{p,j}$ for *p* steps ahead is defined as

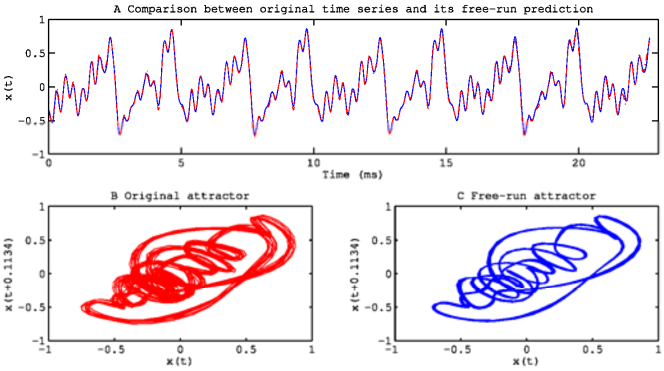

FIG. 9. Free-run prediction for violin sounds with 50-diemensional delay coordinates. (a) Comparison of free-run prediction (blue solid line) and actual data (red dash-dotted line). (b) Attractor of original time series. (c) Attractor of the free-run prediction.

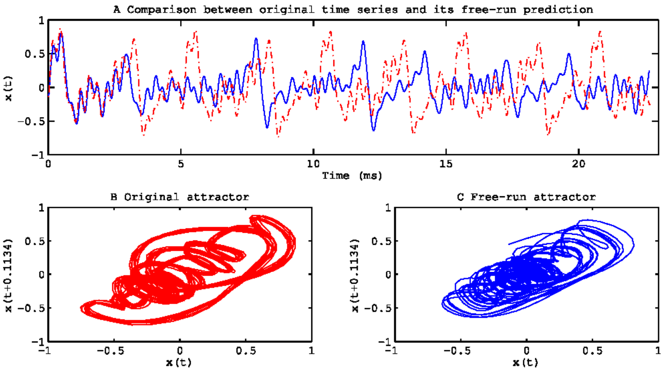

FIG. 10. Free-run prediction for violin sounds with 20-dimensional delay coordinates. See the caption of Fig. 9 to interpret the results.

$$\rho(i,p,j,u_{p,j}) = \sum_{i\in I_t} \frac{\lambda_i}{\sqrt{2\pi}\sigma_j} \exp\left[-\frac{(u_{p,j}-v_{i+p,j})^2}{2\sigma_j{}^2}\right]. \quad (16)$$

We showed the 95% confidence interval by cutting at 2.5% and 97.5% points for the j th variable for each prediction step p.

The result of barycentric coordinates is presented in Fig. 11, while the result obtained by direct predictions of the radial basis function model[6–11] was shown in Fig. 12. The result presented in Fig. 11 shows that the low values for the solar irradiation were captured by the 95% confidence intervals by the proposed barycentric coordinates for the daytime of the fourth day, while the 95% confidence intervals constructed by the radial basis function model missed the low values (Fig. 12). In Fig. 13, we compared the two predictions by the ignorance score.[45,46] When we provide the probabilistic forecast by $\rho(i,p,j,u_{p,j})$ and the actual value observed is $\breve{u}_{p,j}$, the ignorance score is given by $-\log(\rho(i,p,j,\breve{u}_{p,j}))$. When we used this ignorance score, we found that the predictions obtained by the proposed barycentric coordinates were relatively better than those obtained by the radial basis function model when the prediction steps were up to 4 days.

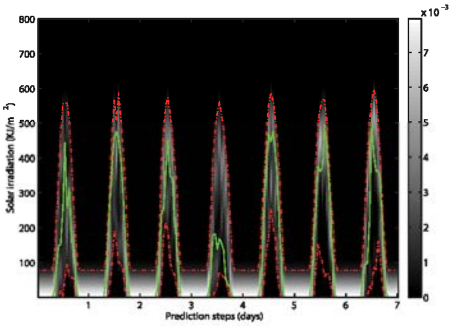

FIG. 11. A weekly prediction for solar irradiation at Chichi Island, Japan, by the proposed barycentric coordinates. The gray scale shows the predicted density for solar irradiation, the red-dash-dotted lines show the 95% confidence intervals, and the green solid line shows the actual value.

Because we assumed that the prediction errors are constant in time, we have the wide 95% confidence intervals especially at the night times. But, if we consider the prediction errors that depend on the time of day, we can improve our predictions better from this standpoint.

IV. IDENTIFYING COUPLING STRENGTH

A. Modified method

The proposed algorithm can be also used as an efficient tool to explore complex aspects of biological data, for instance, the degree of circadian coupling among plant cells. To that end, we used the weighted delay coordinates to identify the coupling strength by minimizing the prediction errors according to the weights. Mathematically, given a multivariate time series of $\vec{v}_t$, we obtain the weighted time series $\vec{w}_t(k,\eta)$ for the prediction of node k as follows:

$$w_{t,j}(k,\eta) = \begin{cases} v_{t,j} & \text{if } j = k, \\ \eta v_{t,j} & \text{otherwise,} \end{cases} \quad (17)$$

where η $(0 \le \eta \le 1)$ is the coupling strength. Next, we employ the proposed algorithm (Eq. (5)) and approximate $\vec{w}_t(k,\eta)$ by a linear combination of neighboring points

$$\vec{w}_t(k,\eta) \approx \sum_{i\in I_{t,k}} \lambda_i(k,\eta)\vec{w}_i(k,\eta), \quad (18)$$

$$\sum_{i\in I_t} \lambda_i(k,\eta) = 1, \quad (19)$$

$$0 \le \lambda_i(k,\eta) \le 1. \quad (20)$$

Then we can calculate a one-step prediction as follows:

$$w_{t+1,k}(k,\eta) = f_k(\vec{w}_t(k,\eta)) \approx \sum_{i\in I_t(k,\varepsilon)} \lambda_i(k,\eta) w_{i+1,k}(k,\eta). \quad (21)$$

Finally, we minimize, over η, the one-step prediction error for the underlying dynamics f_k of the k th variable

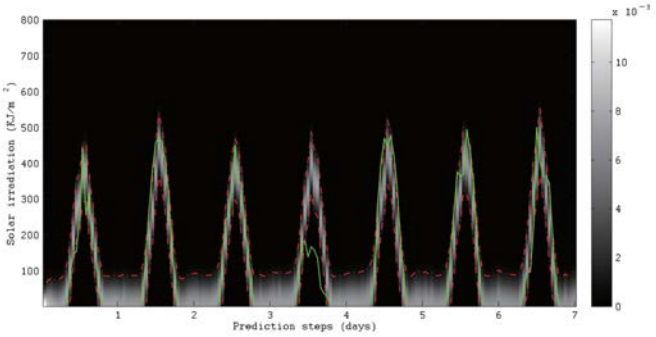

FIG. 12. A weekly prediction for solar irradiation at Chichi Island, Japan, by the radial basis function model. See the caption of Fig. 11 to interpret the results.

approximated by the barycentric coordinates to obtain the optimal "coupling strength" $\hat{\eta}(k)$ for each node k as follows:

$$\hat{\eta}(k) = \underset{\eta\in\{0.01,\ldots,1\}}{\arg\min} \sum_{t} \Bigg| w_{t+1,k}(k,\eta) - \sum_{i\in I_t(k,\varepsilon)} \lambda_i(k,\eta) w_{i+1,k}(k,\eta) \Bigg|. \tag{22}$$

Namely, we consider the weights η for the other variables which are the integer multiples of 0.01 up to 1. In this section, we use 3 nearest neighbors to obtain the barycentric coordinates for all the examples.

B. Toy examples

First, we tested the modified method with two toy models. The coupled Rössler models[24] used in this paper are given as follows:

$$\begin{aligned}
\dot{x}_i &= -\varpi_i y_i - z_i + \kappa((x_{i+1} - x_i) + (x_{i-1} - x_i)),\\
\dot{y}_i &= \varpi_i x_i + a y_i,\\
\dot{z}_i &= b + z_i(x_i - c),\\
x_{i+10} &= x_i, y_{i+10} = y_i, z_{i+10} = z_i,\\
\varpi_1 &= 1.05, \varpi_2 = 1.04, \varpi_3 = 1.03, \varpi_4 = 1.02, \varpi_5 = 1.01,\\
\varpi_6 &= 1.00, \varpi_7 = 0.99, \varpi_8 = 0.98, \varpi_9 = 0.97, \varpi_{10} = 0.96,\\
a &= 0.15, b = 0.2, \text{ and } c = 10.
\end{aligned} \tag{23}$$

We chose the initial conditions $(x(0), y(0), z(0))$ randomly so that each component follows the Gaussian distribution with mean 0 and standard deviation 1. We sampled $x_i (i = 1, \ldots, 10)$ every 0.5 unit time to have a time series of length 50. We used the delay coordinates of maximum delay 8 to reconstruct the dynamics, and estimated the coupling strength $\hat{\eta}(k)$. We repeated this process 100 times by choosing κ randomly between 0.001 and 0.01 for the weak coupling condition and its 100 times for the strong coupling condition.

The Kuramoto model[47] used in this manuscript is given as follows:

$$\begin{aligned}
\dot{x}_i &= \omega_i + \kappa(\sin(x_{i+1} - x_i) + \sin(x_{i-1} - x_i)),\\
x_{i+5} &= x_i,\\
\omega_1 &= 1.5, \omega_2 = 1.4, \omega_3 = 1.3, \omega_4 = 1.2, \text{ and } \omega_5 = 1.1.
\end{aligned} \tag{24}$$

We chose $x(0)$ so that each component follows the Gaussian distribution with mean 0 and standard deviation 1. We sampled $\sin(x_i)(i = 1, \ldots, 5)$ every 0.5 unit time to generate a 5-dimensional time series of length 50. We used delay coordinates of maximum delay 8 to reconstruct the dynamics, and estimated the coupling strength $\hat{\eta}(k)$. We repeated this procedure 100 times for the weak coupling condition and the strong coupling condition. In each weak coupling

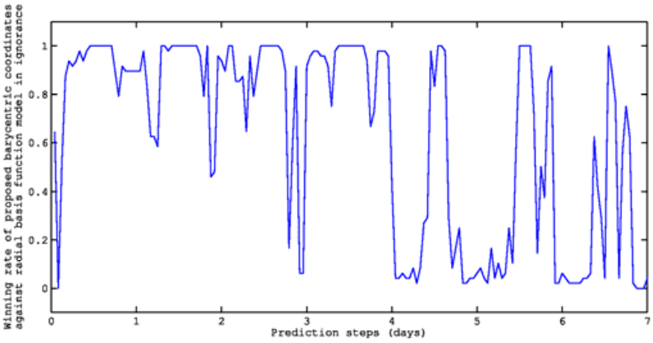

FIG. 13. Comparison between the weekly predictions by the proposed barycentric coordinates and that by the radial basis function model in the ignorance score. We compared which ignorance score was smaller at each of 48 weather stations and obtained the winning rates by taking statistics over the 48 weather stations for each prediction step.

condition, κ was randomly chosen between 0.01 and 0.1. In each of the strong coupling conditions, κ was chosen as 100 times the coupling strength for the corresponding weak coupling condition.

The results are presented in Fig. 14. The toy examples of the coupled Rössler models[24] and the Kuramoto model[47] show that $\hat{\eta}(k)$ is larger when the actual coupling strength is larger. When we used the rank sum test, the differences were statistically significant; the p-values for the two sided test were both less than 0.001.

C. Circadian rhythms

We next performed a time course analysis of circadian rhythmicity in single cells by *in vivo* confocal microscopy as described in Ref. 48. Briefly, leaves were excised from *Arabidopsis thaliana* plants expressing the clock component PRR7 under its own promoter (PRR7:FLAG-PRR7-GFP).[49] Tissues were then embedded in low-melting-point agarose (LM-agarose, National Diagnostic) dissolved in Murashige and Skoog (MS) medium following a protocol previously described.[50] Samples were rapidly placed in microscope slides with 200 μl of liquid MS medium. Agarose-embedded tissues were imaged once every 30 min using an FV-1000 confocal microscope (Olympus). GFP signals were detected with the argon laser (excitation: 488 nm, emission: 510 nm). Samples were maintained under LL conditions at 60–100 μmol m^{-2} s^{-1}. Fluorescence quantification in the nuclei was analyzed using ImageJ software. We used the delay coordinates of maximum delay 8 to identify the coupling strength for each observation. In each tissue, we used the first 18 points to predict the following 3 time points. The dimension for the used time series was 18.

Considering the two toy examples, the *in vivo* analysis of circadian rhythms in single PRR7:FLAG-PRR7-GFP cells was interpreted as if the coupling strength in leaves is only moderate (see Fig. 14). This conclusion is fully consistent with the results of previous experimental analyses.[51] Full details of the circadian methods and the experimental setup are provided in Ref. 48.

V. DISCUSSIONS

The longer a given time series is, the better the prediction accuracy is. See Fig. 15 for the results of free-run predictions when we assumed to have 2000 time points. In these cases, the free-run predictions for both the Rössler model and the Lorenz'63 model almost shadowed the original time series even when the prediction steps were 35 and 50 steps, respectively. More formal comparisons between the length of time series and the prediction accuracy are presented in Figs. 16 and 17, which show that the prediction accuracy for the barycentric coordinates tends to become higher when the time series gets longer in the tested prediction steps, and that the prediction accuracy for the barycentric coordinates tends to be higher than that for the radial basis function model except for the cases where the prediction steps are small and the time series is short. In the examples of circadian rhythms, the numbers of time points was comparable with the dimensions of time series. Thus, the barycentric coordinates extended in this paper can deal with various situations where high-dimensional time series data are observed.

We cannot evaluate the performance of Mees[13] in 10 or higher dimensional space because the tessellations for MATLAB do not support such a high-dimensional space due to their computational complexity; MATLAB only supports the tessellations for two- or three-dimensional space. Therefore, the proposed method qualitatively improved the performance of Mees.[13]

The number of neighbors necessary to construct barycentric coordinates is possibly related to the local dimension of the underlying dynamics, and seems to be important for the proposed method to work appropriately (see Fig. 18). If the number of neighbors is small, then the generated time

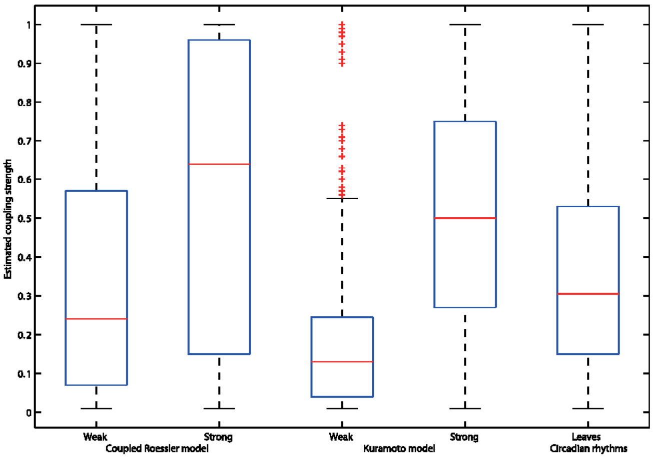

FIG. 14. Estimation of coupling strength. In the coupled Rössler models (left) and the Kuramoto model (center), we show the estimated coupling strength by the box plots for weak coupling and strong coupling cases. The estimated coupling strength among leaf cells is shown by the box plot on the right-hand side. In each box plot, the box shows the 25%–75% range, and the red horizontal middle line shows the median.

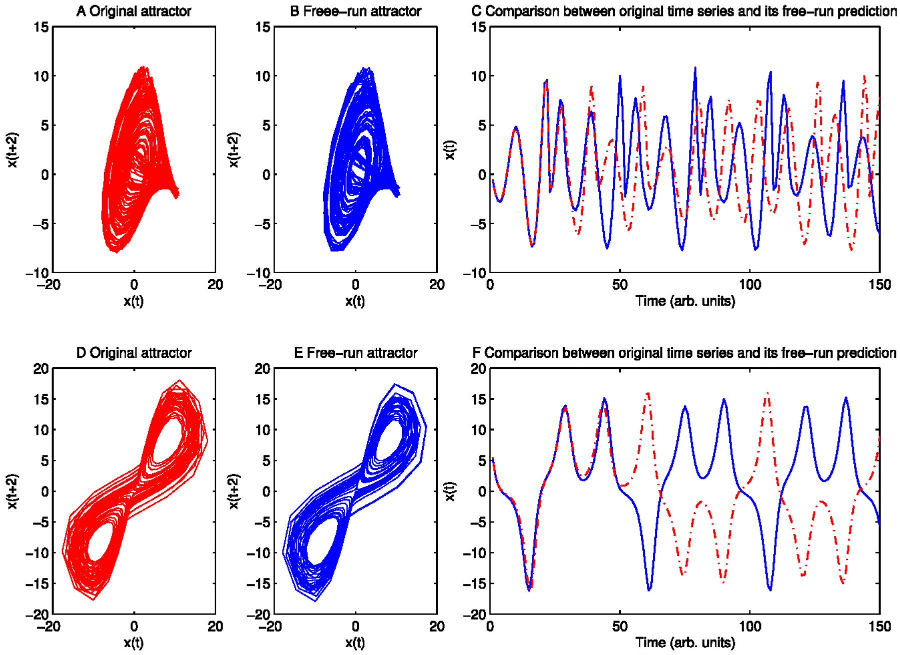

FIG. 15. Free-run prediction for time series with length 2000. See the caption of Fig. 2 to interpret the results.

series tends to become periodic. For instance, in the examples shown in Figs. 18(b) and 18(c), we obtained periodic orbits of periods 247 and 595 for $K = 2$ and $K = 5$ for the Rössler models, while in Figs. 18(g) and 18(h), we obtained periodic orbits of periods 1465 and 687 for $K = 2$ and $K = 5$ for the Lorenz'63 model, respectively. If the number of neighbors is large, the reconstructed attractors look nice and smooth, and are different from a periodic orbit of period

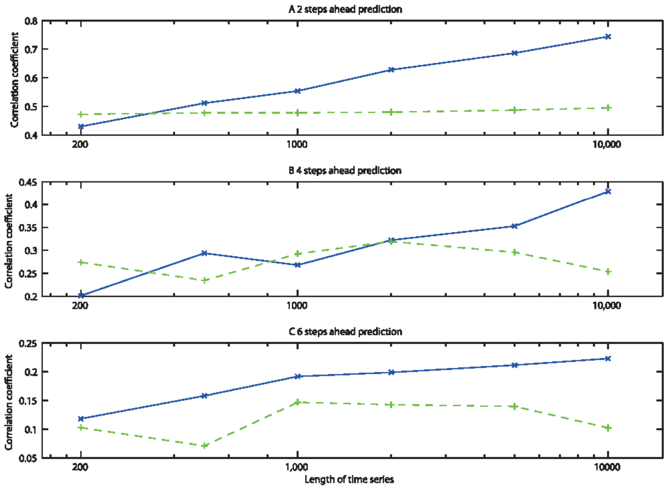

FIG. 16. Length of time series versus correlation coefficients showing the accuracy of prediction for the example of coupled map lattice. Panels (a), (b), and (c) correspond to 2, 4, and 6 steps ahead predictions, respectively. In each panel, the blue solid line corresponds to the proposed barycentric coordinates and the green dashed line corresponds to the radial basis function model.

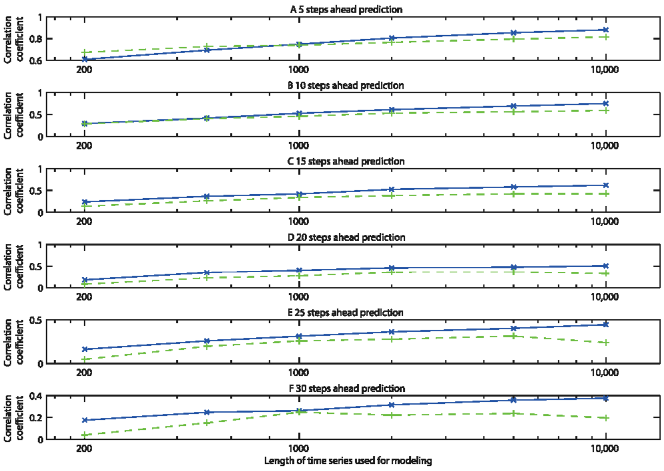

FIG. 17. Length of time series versus correlation coefficients showing the prediction accuracy in the example of Lorenz'96 I model. Panels (a), (b), (c), (d), (e), and (f) correspond to 5, 10, 15, 20, 25, and 30 steps ahead predictions, respectively. In each panel, the blue solid line and the green dashed line correspond to the barycentric coordinates and the radial basis function model, respectively.

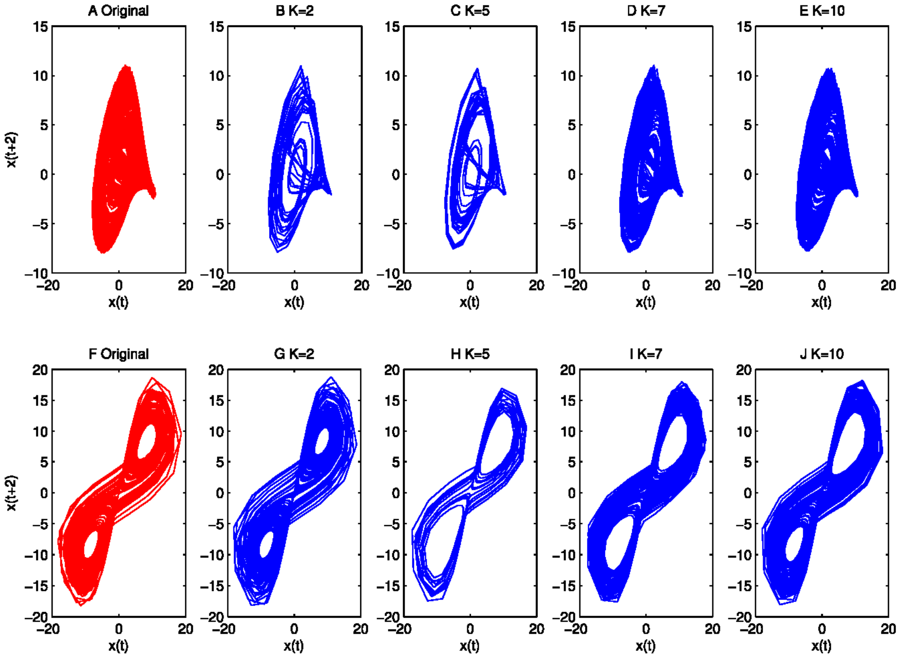

FIG. 18. Dependence on the number of neighbors used for obtaining free-run prediction by using the interior point method. In each panel, the corresponding attractor is shown. (a)–(e) correspond to the cases of the Rössler model and (f)–(j) correspond to the cases of the Lorenz'63 model. (a) and (f) The original attractors. (b) and (g), (c) and (h), and (d) and (i), and (e) and (j) correspond to the cases of $K = 2$, 5, 7, and 10, respectively. The length of original time series was set to 2000.

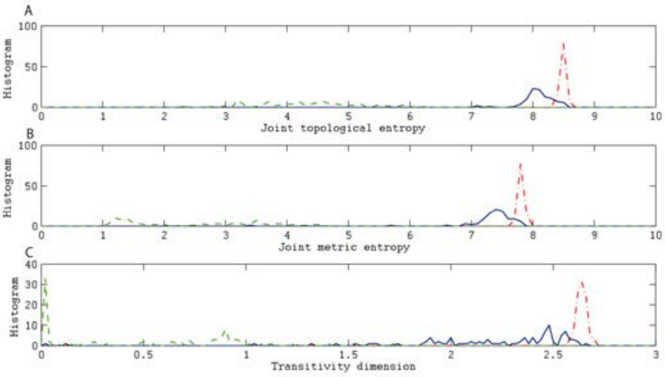

FIG. 19. Topological, dynamical, and geometric characterizations of the free-run prediction for the coupled map lattice by the simplex method. See the caption of Fig. 5 to interpret the results. The Kantorovich metrics between the distributions obtained from the original time series and those from the barycentric coordinates were 0.3887, 0.4513, and 0.4266 for the joint topological entropy, joint metric entropy, and transitivity dimension, respectively.

10 000 or smaller (Figs. 18(d), 18(e), 18(i), and 18(j)). If the number of neighbors is large enough, then the solutions do not seem to fall into periodic orbits with small periods. Thus, how to choose the number of neighbors properly is a problem similar to choosing the embedding dimension for delay coordinates appropriately.[52–54] This is an important challenge to be solved in the future.

Choosing the interior point method might not be so important in successful modelings by barycentric coordinates. We compared the performance of the interior point method with the simplex method, which evaluates the boundary of the feasible solutions to reach an optimal solution. Here, we used the simplex method implemented in MATLAB. The results of the simplex method are shown in Figs. 19–21. We skip here the comparisons in correlation coefficients as ones in Figs. 3 and 6 because there are no visible differences between the solutions by the interior point method and the simplex method. When we evaluated the topological, dynamical, and geometric aspects of free-run predictions, there were no significant differences between them (see Figs. 19 and 20). When we drew the figure corresponding Fig. 18 but using the simplex method, we obtained Fig. 21. When we used the simplex method, the reconstructed attractors looked more similar to the original attractors than when we used the interior point method (compare Fig. 18 with Fig. 21). But, the free-run predictions by the simplex method tended to fall into periodic orbits with short periods. When the numbers of used neighbors were 2, 5, 7, and 10, the free-runs fell into the periodic orbits with periods 247, 1465, 608, and 1335 for the Rössler model and those with periods 1154, 1839, 445, and 1058, for the Lorenz'63 model. Predicting up to 1000 steps ahead for one of 100 simulations in Figs. 8 and 21 took 231 and 168 s for the interior point method and the simplex method, respectively. We used a computer with CPU of two 2.66 GHz 6-Core Intel Xenon and 64GB memory. Therefore, there are the advantage and disadvantage for using the interior point method compared with using the simplex method.

The proposed method is tolerant for observational noise to some extent because it showed the good prediction performance in the real data (see Figs. 9 and 11). For extra tests, we added 5% Gaussian observational noise to the datasets of the Rössler model and the Lorenz'63 model, and redrew Fig. 2 (see Fig. 22). Although the accuracy decayed more quickly when we increased the prediction steps (Figs. 22(c) and 22(f)), the shapes of the attractors for the free-run

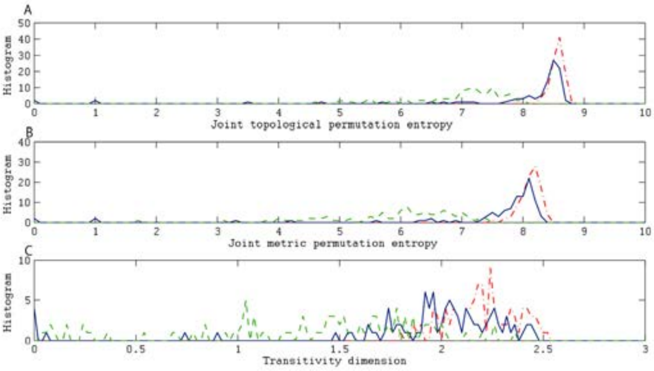

FIG. 20. Topological, dynamical, and geometric characterizations of the free-run prediction for the Lorenz'96 I model by the simplex method. See the caption of Fig. 8 to interpret the results. The Kantorovich metrics between the distributions for the original time series and those for the barycentric coordinates were 0.6779, 0.6730, and 0.2894 for the joint topological permutation entropy, joint metric permutation entropy, and transitivity dimension, respectively.

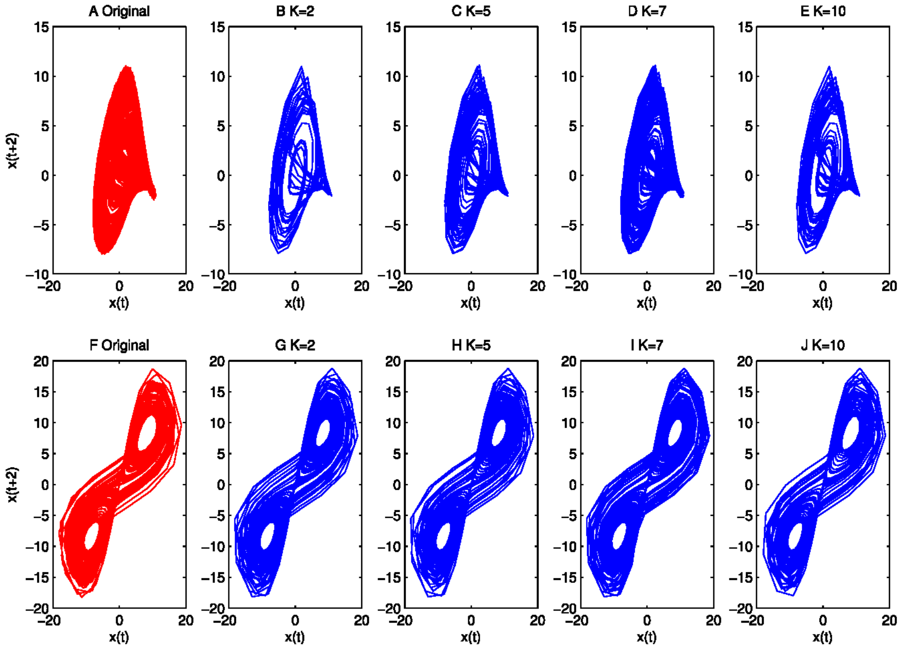

FIG. 21. The same figure as Fig. 18 except that the simplex method was used to obtain the barycentric coordinates. See the caption of Fig. 18 to interpret the results.

predictions were almost preserved (Figs. 22(a), 22(b), 22(d), and 22(e)).

In Fig. 13, the radial basis function model might have had the better score when the prediction steps were more than 4 days because the actual solar irradiation fell into its narrower confidence intervals by chance. Thus, we will investigate more closely when the barycentric coordinates provide good prediction in our future communication.

In its current stage, the proposed method cannot be used to predict transient dynamics such as climate change. Addressing this and other particular topics related to climate change could be an interesting area of development for the current method. Together with the global circulation models, the current state-of-the-art method for predicting weather conditions, the proposed method may help to introduce more renewable energy and reduce CO_2 emissions by assisting to estimate and schedule operations of backup power plants.

The proposed barycentric coordinates can be obtained quickly. It only took 23.5 s to produce Fig. 2, even if we include integrating the two sets of equations, predicting both of them and plotting the figure; we used the computer we used previously, and the code was written in MATLAB. Given the prediction errors for obtaining the confidence intervals, it took about 7.7 min to obtain the predictions of the solar irradiations, a part of which is shown in Fig. 11, up to 7 days ahead in the time resolution of 1 h at 48 weather stations in Japan. Judging from the required computational time and the accuracy, an empirical model such as the proposed method may potentially improve the operational weather forecasting as discussed in Ref. 55.

Our results in Fig. 9 show that the dominant part of violin sounds can be modeled as a high-dimensional deterministic model. We will discuss whether or not violin sounds are chaotic in our future communication.

The proposed method is different from the method of Ref. 19 because the proposed method constructs barycentric coordinates for high-dimensional dynamics, while the method of Ref. 19 proposes when the prediction may go wrong because few similar events happened in the past, while Eq. (5) may be used as an alternative for the index of Ref. 19. This research needs further verification.

Modeling a noisy time series is the next target. By following the work of Allie *et al.*,[18] we are thinking of combining the proposed method with minimum description length.[10]

Our extension of the barycentric coordinates thus offers enough accuracy and versatility to reproduce the behavior of target dynamical systems. It naturally solves the problem of under-fitting often observed when dynamical systems are modeled.[56] Furthermore, our extension partially solved the curse of dimensionality[12] in a simple way because the number of parameters does not increase even if the dimension of phase space increases. Therefore, the proposed method will

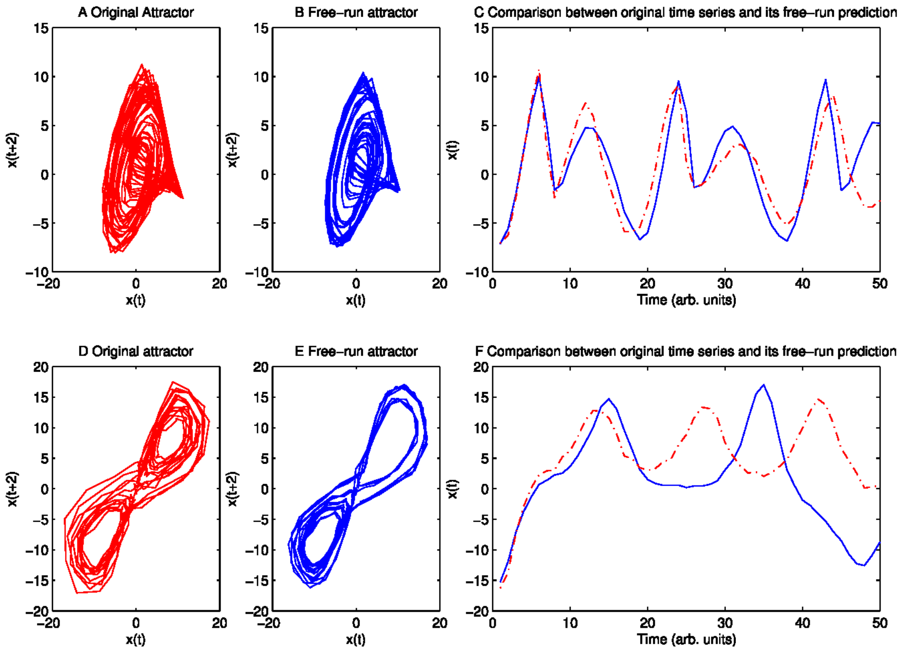

FIG. 22. Free-run prediction for time series contaminated by 5% observational noise. See the caption of Fig. 2 to interpret the results. The length of original time series is 300 for both cases.

open a new area of modeling and predictions for high-dimensional dynamical systems.

ACKNOWLEDGMENTS

We appreciate the Real World Computing (RWC) Music Database and the Japan Meteorological Agency, respectively, for providing the violin data and the solar irradiation data used in this study. We are also grateful to Professor N. Nakamichi for providing the PRR7:FLAG-PRR7-GFP seeds. In addition, we got benefits through the discussions with Dr. Tomoya Takeuchi. This research was supported by Core Research for Evolutional Science and Technology (CREST), Japan Science and Technology Agency (JST), and Platform for Dynamic Approaches to Living System from the Ministry of Education, Culture, Sports, Science and Technology, Japan. Research in P.M. Laboratory was supported by a research grant from the Spanish Ministry of Economy and Competitiveness (MINECO). N.T. was supported by a CRAG fellowship.

APPENDIX: TECHNICAL DETAILS

Lemma 1. *If the original dynamics $f(\vec{v})$ is Lipschitz continuous and differentiable, then*

$$\hat{f}(\vec{v}) = f(\vec{v}) + f'(\vec{v})\left(\sum_i \vec{v}_i\lambda_i - \vec{v}\right) + O(\delta^2), \tag{A1}$$

where δ is the size of neighborhood defined by K nearest neighbors.

Proof. If we apply the Taylor expansion, we have

$$f(\vec{v}_i) = f(\vec{v}) + f'(\vec{v})(\vec{v}_i - \vec{v}) + O(\delta^2). \tag{A2}$$

By multiplying λ_i for both sides and taking the sum over i, we have

$$\begin{aligned}\hat{f}(\vec{v}) &= \sum_i \lambda_i f(\vec{v}_i)\\ &= \sum_i \lambda_i f(\vec{v}) + \sum_i f'(\vec{v})\vec{v}_i\lambda_i - \sum_i f'(\vec{v})\vec{v}\lambda_i + O(\delta^2)\\ &= f(\vec{v}) + f'(\vec{v})\sum_i \vec{v}_i\lambda_i - f'(\vec{v})\vec{v} + O(\delta^2)\\ &= f(\vec{v}) + f'(\vec{v})\left(\sum_i \vec{v}_i\lambda_i - \vec{v}\right) + O(\delta^2).\end{aligned} \tag{A3}$$

By using $\varepsilon = \max_j |\sum_i v_{i,j}\lambda_i - v_j|$, we can show that the second term for the right hand side of Eq. (A1) is in the order of $O(\varepsilon)$, which shows the "modeling error," namely, how badly the neighboring points represent the current point $\vec{v}$ in the space which the neighboring points do not span. When we use the Lipschitz constant U for $f(\vec{v})$, the norm for the second term is bounded by $U\varepsilon$. When we approximate the low-dimensional chaos, ε often becomes zero and the second term of the right hand side of Eq. (A1) vanishes, meaning that our approximation becomes the first order ($\hat{f}(\vec{v}) = f(v) + O(\delta^2)$) in terms of the neighborhood size δ as similarly to the work of Mees.[13]

Lemma 2. *The prediction by the proposed method is bounded.*

Proof. Because $0 \leq \lambda_i \leq 1$ and $\sum_i \lambda_i = 1$, the j th variable for p steps ahead direct prediction is upper-bounded as

$$\hat{f}_j^{\,p}(\vec{v}) = \sum_i v_{i+p,j}\lambda_i \leq \max_i v_{i+p,j} \leq \max_i v_{i,j}. \tag{A4}$$

Similarly, we have

$$\hat{f}_j^{\,p}(\vec{v}) = \sum_i v_{i+p,j}\lambda_i \geq \min_i v_{i+p,j} \geq \min_i v_{i,j}. \tag{A5}$$

Therefore, the solution is bounded for all the variables.

[1] W. S. Mc Culloch and W. Pitts, Bull. Math. Biophys. **5**, 115 (1943).
[2] K.-I. Funahashi, Neural Networks **2**, 183 (1989).
[3] G. Cybenko, Math. Control Signals Syst. **2**, 303 (1989).
[4] K. Hornik, M. Stinchcombe, and H. White, Neural Networks **2**, 359 (1989).
[5] M. Small and C. K. Tse, Phys. Rev. E **66**, 066701 (2002).
[6] R. P. Lippman, IEEE Commun. Mag. **27**, 47 (1989).
[7] J. Park and I. W. Sandberg, Neural Comput. **3**, 246 (1991).
[8] J. A. Leonard and M. A. Kramer, IEEE Control Syst. **11**, 31 (1991).
[9] S. Chen, C. E. N. Cowan, and P. M. Grant, IEEE Trans. Neural Networks **2**, 302 (1991).
[10] K. Judd and A. Mees, Phys. D **82**, 426 (1995).
[11] B. Pilgram, K. Judd, and A. Mees, Phys. D **170**, 103 (2002).
[12] N. Gershenfeld, *Nature of Mathematical Modeling* (Cambridge University Press, Cambridge, 1998).
[13] A. Mees, Int. J. Bifurcation Chaos **1**, 777 (1991).
[14] J. Matoušek and B. Gärtner, *Understanding and Using Linear Programming* (Springer-Verlag, Berlin, 2007).
[15] T. Hastie, R. Tibshirani, and J. Friedman, *The Elements of Statistical Learning: Data Mining, Inference, and Prediction* (Springer, New York, NY, 2009).
[16] A. Mees, *Dynamics of Complex Interconnected Biological Systems* (Birkhäuser, Boston, MA, 1990), p. 104.
[17] S. Allie and A. Mees, Phys. Rev. E **56**, 346 (1997).
[18] S. Allie, A. Mees, K. Judd, and D. Watson, Phys. Rev. E **55**, 87 (1997).
[19] Y. Hirata, Phys. Rev. E **89**, 052916 (2014).
[20] F. Takens, Lect. Notes Math. **898**, 366 (1981).
[21] T. Sauer, J. A. Yorke, and M. Casdagli, J. Stat. Phys. **65**, 579 (1991).
[22] Y. Zhang, Solving Large-Scale Linear Programs by Interior-Point Methods under the MATLAB Environment, Department of Mathematics and Statistics, University of Maryland, Baltimore County, Baltimore, MD, Technical Report TR96-01, 1996.
[23] S. Mehrotra, SIAM J. Optim. **2**, 575 (1992).
[24] O. E. Rössler, Phys. Lett. A **57**, 397 (1976).
[25] E. N. Lorenz, J. Atmos. Sci. **20**, 130 (1963).
[26] K. Kaneko, Prog. Theor. Phys. **72**, 480 (1984).
[27] E. N. Lorenz, in *Proceedings of the Seminar on Predictability* (ECMWF, Reading, 1996), Vol. 1, p. 1.
[28] G. Sugihara and R. M. May, Nature **344**, 734 (1990).
[29] T. M. Cover and J. A. Thomas, *Elements of Information Theory* (Wiley-Interscience, New York, NY, 1991).
[30] R. V. Donner, J. Heitzig, J. F. Donges, Y. Zou, N. Marwan, and J. Kurths, Eur. Phys. J. B **84**, 653 (2011).
[31] J. H. Feldhoff, R. V. Donner, J. F. Donges, N. Marwan, and J. Kurths, Europhys. Lett. **102**, 30007 (2013).
[32] B.-L. Hao and W.-M. Zheng, *Applied Symbolic Dynamics and Chaos* (World Scientific, Singapore, 1998).
[33] N. Marwan, M. C. Romano, M. Thiel, and J. Kurths, Phys. Rep. **438**, 237 (2007).
[34] A. Baba and T. Komatsuzaki, Proc. Natl. Acad. Sci. U. S. A. **104**, 19297 (2007).
[35] C. Bandt and B. Pompe, Phys. Rev. Lett. **88**, 174102 (2002).
[36] C. Bandt, G. Keller, and B. Pompe, Nonlinearity **15**, 1595 (2002).
[37] J. M. Amigó and M. B. Kennel, Phys. D **231**, 137 (2007).
[38] J. M. Amigó, M. B. Kennel, and L. Kocarev, Phys. D **210**, 77 (2005).
[39] J. M. Amigó, R. Monetti, T. Aschenbrenner, and W. Bunk, Chaos **22**, 013105 (2012).
[40] E. P. Bravo, K. Aihara, and Y. Hirata, Chaos **23**, 043104 (2013).
[41] D. Arroyo, P. Chamorro, J. M. Amigó, F. B. Rodríguez, and P. Varona, Eur. Phys. J. Spec. Top. **222**, 457 (2013).
[42] S. Oya, K. Aihara, and Y. Hirata, New J. Phys. **16**, 115015 (2014).
[43] M. Goto, "Development of the RWC music database," in *Proceedings of 18th International Congress on Acoustics (ICA 2004)* (2004), pp. 553–556.
[44] See supplementary material at http://dx.doi.org/10.1063/1.4906746 for the original violin sounds (supplementary Sound File 1) and the violin sounds generated by using the proposed barycentric coordinates (supplementary Sound File 2).
[45] I. J. Good, J. R. Stat. Soc. B **14**, 107 (1952).
[46] H. Du and L. A. Smith, J. Atmos. Sci. **71**, 469 (2014).
[47] Y. Kuramoto, Lect. Notes Phys. **39**, 420 (1975).
[48] N. Takahashi, Y. Hirata, K. Aihara, and P. Mas, "A hierarchical multi-oscillator network orchestrates the Arabidopsis circadian system," (submitted).
[49] N. Nakamichi *et al.*, Plant Cell **22**, 594 (2010).
[50] P. Mas and R. N. Beachy, Plant J. **15**, 835 (1998).
[51] B. Wenden, D. L. Toner, S. K. Hodge, R. Grima, and A. J. Millar, Proc. Natl. Acad. Sci. U. S. A. **109**, 6757 (2012).
[52] H. D. I. Abarbanel, *Analysis of Observed Chaotic Data* (Springer-Verlag, New York, NY, 1996).
[53] H. Kantz and T. Schreiber, *Nonlinear Time Series Analysis* (Cambridge University Press, Cambridge, 1997).
[54] M. Small, *Applied Nonlinear Time Series Analysis: Applications in Physics, Physiology and Finance* (World Sciencitfic, Singapore, 2005).
[55] E. B. Suckling and L. A. Smith, J. Clim. **26**, 9334 (2013).
[56] D. Kilminster, "Modelling dynamical systems via behaviour criteria," Ph.D. dissertation (School of Mathematics and Statistics, University of Western Australia, 2003).

ACKNOWLEDGEMENTS

Acknowledgements

This PhD thesis could not have been completed without the huge support that I have received from so many people. First I really would like to thank Dr. Paloma Mas for giving me the opportunity to develop this fantastic project. I am also really grateful to her tremendous support, guidance, and enormous enthusiasm throughout years. Every suggestion she gave me at every discussion helped not just the project but also me growing as a researcher.

Thanks to all the past and present lab members for supporting my study and being great bench mates. I also thank cheerful conversations and positive atmosphere created by them.

Thanks to all CRAG staff for helping my experiments and paperwork possible. Especially I would like to thank Montse Amenós for supporting microscopy experiments.

Thanks to our collaborators, Dr. Yoshito Hirata and Dr. Kazuyuki Aihara for their assistance in the mathematical analysis of circadian coupling.

Thanks to my PhD program coordinator Dr. Charlotte Poschenrieder, without her kind help, I would not have been able to continue the program.

Thanks to my PhD committee members Dr. Josep Allué, Dr. Mercè Llugany and Dr. David Caparrós for valuable suggestions at meetings.

Thanks to all the scientists who shared research materials with us, and scientists in researches I referred in my PhD thesis. I truly recognized that I am standing on the shoulders of giants.

Thanks to TAKA-ST for the fascinating artwork representing our study.

Thanks to all the musicians who created songs I was listening in the lab. Those tunes definitely helped my experiments.

Thanks to the beautiful city of Barcelona. I am really fortunate to be in the place where outside of the lab is also wonderful.

Thanks to Dr. Motonori Hoshi for his support and advice from Japan.

Last but not the least, I really would like to thank my family and friends for inspiring, supporting and encouraging me, in particular, my mother Mariko Takahashi, and my late father Susumu Takahashi, and my brother Yu Takahashi for making my accomplishments possible.

REFERENCES

References

Abe M, Herzog ED, Yamazaki S, Straume M, Tei H, Sakaki Y, Menaker M, Block GD (2002) Circadian rhythms in isolated brain regions. J Neurosci **22**: 350–356

Abraham U, Granada AE, Westermark PO, Heine M, Kramer A, Herzel H (2010) Coupling governs entrainment range of circadian clocks. Mol Syst Biol **6**: 438

Alabadí D, Yanovsky MJ, Más P, Harmer SL, Kay SA (2002) Critical role for CCA1 and LHY in maintaining circadian rhythmicity in Arabidopsis. Curr Biol **12**: 757–761

Amasino RM, Michaels SD (2010) The Timing of Flowering. Plant Physiol **154**: 516–520

Aryee MJ, Gutiérrez-Pabello JA, Kramnik I, Maiti T, Quackenbush J (2009) An improved empirical bayes approach to estimating differential gene expression in microarray time-course data: BETR (Bayesian Estimation of Temporal Regulation). BMC Bioinformatics **10**: 409

Bainbridge K, Bennett T, Crisp P, Leyser O, Turnbull C (2014) Grafting in Arabidopsis. Methods Mol Biol **1062**: 155–63

Balsalobre A, Brown SA, Marcacci L, Tronche F, Kellendonk C, Reichardt HM, Schütz G, Schibler U, Dunlap JC, Brown SA, et al (2000) Resetting of circadian time in peripheral tissues by glucocorticoid signaling. Science **289**: 2344–7

Baudry A, Ito S, Song YH, Strait AA, Kiba T, Lu S, Henriques R, Pruneda-Paz JL, Chua N-H, Tobin EM, et al (2010) F-box proteins FKF1 and LKP2 act in concert with ZEITLUPE to control Arabidopsis clock progression. Plant Cell **22**: 606–22

Bishopp A, Lehesranta S, Vatén A, Help H, El-Showk S, Scheres B, Helariutta K, Mähönen AP, Sakakibara H, Helariutta Y (2011) Phloem-transported cytokinin regulates polar auxin transport and maintains vascular pattern in the root meristem. Curr Biol **21**: 927–932

Bordage S, Sullivan S, Laird J, Millar AJ, Nimmo HG (2016) Organ specificity in the plant circadian system is explained by different light inputs to the shoot and root clocks. New Phytol **212**: 136–149

Bretzl H (1903) Botanische Forschungen des Alexanderzuges. Leipzig: B.G. Teubner

Chen M, Chory J, Fankhauser C (2004) Light signal transduction in higher plants. Annu Rev Genet **38**: 87–117

Corbesier L, Vincent C, Jang S, Fornara F, Fan Q, Searle I, Giakountis A, Farrona S, Gissot L, Turnbull C, et al (2007) FT Protein Movement Contributes to Long-Distance Signaling in Floral Induction of Arabidopsis. Science (80-) **316**: 1030–1033

Covington MF, Harmer SL (2007) The circadian clock regulates auxin signaling and responses in Arabidopsis. PLoS Biol **5**: 1773–1784

Covington MF, Maloof JN, Straume M, Kay SA, Harmer SL (2008) Global transcriptome analysis reveals circadian regulation of key pathways in plant growth and development. Genome Biol **9**: R130

Damiola F, Le Minh N, Preitner N, Kornmann B, Fleury-Olela F, Schibler U (2000) Restricted feeding uncouples circadian oscillators in peripheral tissues from the central pacemaker in the suprachiasmatic nucleus. Genes Dev **14**: 2950–61

Devlin PF, Kay SA (2000) Cryptochromes are required for phytochrome signaling to the circadian clock but not for rhythmicity. Plant Cell **12**: 2499–2510

Devlin PF, Kay SA (2001) Circadian photoperception. Annu Rev Physiol **63**: 677–94

Ding Z, Doyle MR, Amasino RM, Davis SJ (2007) A complex genetic interaction between Arabidopsis thaliana TOC1 and CCA1/LHY in driving the circadian clock and in output regulation. Genetics **176**: 1501–10

Dixon LE, Knox K, Kozma-Bognar L, Southern MM, Pokhilko A, Millar AJ (2011) Temporal repression of core circadian genes is mediated through EARLY FLOWERING 3 in Arabidopsis. Curr Biol **21**: 120–125

Dodd AN, Salathia N, Hall A, Kévei E, Tóth R, Nagy F, Hibberd JM, Millar AJ, Webb A a R (2005) Plant circadian clocks increase photosynthesis, growth, survival, and competitive advantage. Science **309**: 630–633

Dowson-Day MJ, Millar AJ (1999) Circadian dysfunction causes aberrant hypocotyl elongation patterns in Arabidopsis. Plant J **17**: 63–71

Doyle MR, Davis SJ, Bastow RM, McWatters HG, Kozma-Bognár L, Nagy F, Millar AJ, Amasino RM (2002) The ELF4 gene controls circadian rhythms and flowering time in Arabidopsis thaliana. Nature **419**: 74–77

Duhamel du Monceau HL (1758) La physique des arbres. Vol.2. H.L. Guerin and L.F. Delatour

Eckel-Mahan K, Sassone-Corsi P (2013) Metabolism and the Circadian Clock Converge. Am Physiol Soc **93**: 107–135

Endo M, Shimizu H, Nohales MA, Araki T, Kay SA (2014) Tissue-specific clocks in Arabidopsis show asymmetric coupling. Nature **515**: 419–422

Evans JA, Pan H, Liu AC, Welsh DK (2012) *Cry1* $^{-/-}$ Circadian Rhythmicity Depends on SCN Intercellular Coupling. J Biol Rhythms **27**: 443–452

Farré EM, Harmer SL, Harmon FG, Yanovsky MJ, Kay SA (2005) Overlapping and Distinct Roles of PRR7 and PRR9 in the Arabidopsis Circadian Clock. Curr Biol **15**: 47–54

Fukuda H, Nakamichi N, Hisatsune M, Murase H, Mizuno T (2007) Synchronization of plant circadian oscillators with a phase delay effect of the vein network. Phys Rev Lett **99**: 1–4

Fukuda H, Ukai K, Oyama T (2012) Self-arrangement of cellular circadian rhythms through phase-resetting in plant roots. Phys Rev E - Stat Nonlinear, Soft Matter Phys **86**: 1–5

Gardner MJ, Hubbard KE, Hotta CT, Dodd AN, Webb AAR (2006) How plants tell the time. Biochem J **397**: 15–24

Gendron JM, Pruneda-Paz JL, Doherty CJ, Gross AM, Kang SE, Kay SA (2012) Arabidopsis circadian clock protein, TOC1, is a DNA-binding transcription factor. Proc Natl Acad Sci **109**: 3167–3172

Golombek D a, Rosenstein RE (2010) Physiology of Circadian Entrainment. Physiol Rev **90**: 1063–1102

Green RM, Tingay S, Wang ZY, Tobin EM (2002) Circadian rhythms confer a higher level of fitness to Arabidopsis plants. Plant Physiol **129**: 576–584

Green RM, Tobin EM (1999) Loss of the circadian clock-associated protein 1 in Arabidopsis results in altered clock-regulated gene expression. Proc Natl Acad Sci **96**: 4176–4179

Guo Z, Wang F, Xiang X, Ahammed GJ, Wang M, Onac E, Zhou J, Xia X, Shi K, Yin X, et al (2016) Systemic induction of photosynthesis via illumination of the shoot apex is mediated by phytochrome B. Plant Physiol **172**: pp.01202.2016

Habte E, Müller LM, Shtaya M, Davis SJ, Von Korff M (2014) Osmotic stress at the barley root affects expression of circadian clock genes in the shoot. Plant, Cell Environ **37**: 1321–1337

Hanano S, Domagalska MA, Nagy F, Davis SJ (2006) Multiple phytohormones influence distinct parameters of the plant circadian clock. Genes to Cells **11**:

1381–1392

Harmer SL (2009) The circadian system in higher plants. Annu Rev Plant Biol **60**: 357–77

Harrington M (2010) Location, location, location: Important for jet-lagged circadian loops. J Clin Invest **120**: 2265–2267

Haydon MJ, Mielczarek O, Robertson FC, Hubbard KE, Webb AAR (2013) Photosynthetic entrainment of the Arabidopsis thaliana circadian clock. Nature **502**: 689–692

Hazen SP, Naef F, Quisel T, Gendron JM, Chen H, Ecker JR, Borevitz JO, Kay SA (2009) Exploring the transcriptional landscape of plant circadian rhythms using genome tiling arrays. Genome Biol **10**: R17

Hazen SP, Schultz TF, Pruneda-Paz JL, Borevitz JO, Ecker JR, Kay SA (2005) LUX ARRHYTHMO encodes a Myb domain protein essential for circadian rhythms. Proc Natl Acad Sci U S A **102**: 10387–92

Herrero E, Kolmos E, Bujdoso N, Yuan Y, Wang M, Berns MC, Uhlworm H, Coupland G, Saini R, Jaskolski M, et al (2012) EARLY FLOWERING4 recruitment of EARLY FLOWERING3 in the nucleus sustains the Arabidopsis circadian clock. Plant Cell **24**: 428–43

Hicks KA, Albertson TM, Wagner DR (2001) EARLY FLOWERING3 encodes a novel protein that regulates circadian clock function and flowering in Arabidopsis. Plant Cell **13**: 1281–92

Hicks K a, Millar a J, Carré I a, Somers DE, Straume M, Meeks-Wagner DR, Kay SA (1996) Conditional circadian dysfunction of the Arabidopsis early-flowering 3 mutant. Science **274**: 790–792

Hill J (1757) The sleep of plants, and cause of motion in the sensitive plant, explained.

Hirata Y, Shiro M, Takahashi N, Aihara K, Suzuki H, Más P (2015) Approximating high-dimensional dynamics by barycentric coordinates with linear programming. Chaos. doi: 10.1063/1.4906746

Holbrook NM (2002) Stomatal control in tomato with ABA-deficient roots: response of grafted plants to soil drying. J Exp Bot **53**: 1503–1514

Hsu PY, Harmer SL (2014) Wheels within wheels: The plant circadian system. Trends Plant Sci **19**: 240–249

Huang W, Perez-Garcia P, Pokhilko A, Millar AJ, Antoshechkin I, Riechmann JL, Mas P (2012) Mapping the Core of the Arabidopsis Circadian Clock Defines the Network Structure of the Oscillator. Science

(80-) **336**: 75–79

Hughes ME, Hogenesch JB, Kornacker K (2010) JTK_CYCLE: An Efficient Nonparametric Algorithm for Detecting Rhythmic Components in Genome-Scale Data Sets. J Biol Rhythms **25**: 372–380

Inoue K, Araki T, Endo M (2017) Integration of Input Signals into the Gene Network in the Plant Circadian Clock. Plant Cell Physiol **0**: 1–6

Ishida N, Kaneko M, Allada R (1999) Biological clocks. Proc Natl Acad Sci **96**: 8819–8820

James AB, Monreal JA, Nimmo GA, Kelly CL, Herzyk P, Jenkins GI, Nimmo HG (2008) The Circadian Clock in Arabidopsis Roots Is a Simplified Slave Version of the Clock in Shoots. Science (80-) **322**: 1832–1835

James AB, Syed NH, Bordage S, Marshall J, Nimmo GA, Jenkins GI, Herzyk P, Brown JWS, Nimmo HG (2012) Alternative Splicing Mediates Responses of the Arabidopsis Circadian Clock to Temperature Changes. Plant Cell **24**: 961–981

Johnson CH (1999) Forty years of PRCs--what have we learned? Chronobiol Int **16**: 711–43

Johnson CH, Kyriacou CP (2007) Clock Evolution and Adaptation: Whence and Whither? Endog Plant Rhythm 237–260

Jones MA (2009) Entrainment of the Arabidopsis circadian clock. J Plant Biol **52**: 202–209

Kamioka M, Takao S, Suzuki T, Taki K, Higashiyama T, Kinoshita T, Nakamichi N (2016) Direct repression of evening genes by CIRCADIAN CLOCK-ASSOCIATED 1 in Arabidopsis circadian clock. Plant Cell **28**: 696–711

Karlsson PM, Herdean A, Adolfsson L, Beebo A, Nziengui H, Irigoyen S, Ünnep R, Zsiros O, Nagy G, Garab G, et al (2015) The Arabidopsis thylakoid transporter PHT4;1 influences phosphate availability for ATP synthesis and plant growth. Plant J **84**: 99–110

Katari MS, Nowicki SD, Aceituno FF, Nero D, Kelfer J, Thompson LP, Cabello JM, Davidson RS, Goldberg AP, Shasha DE, et al (2010) VirtualPlant: A Software Platform to Support Systems Biology Research. Plant Physiol **152**: 500–515

Kaufmann K, Wellmer F, Muino JM, Ferrier T, Wuest SE, Kumar V, Serrano-Mislata A, Madueno F, Krajewski P, Meyerowitz EM, et al (2010) Orchestration of Floral Initiation by APETALA1. Science (80-) **328**:

85–89

Kiba T, Henriques R, Sakakibara H, Chua N-H (2007) Targeted degradation of PSEUDO-RESPONSE REGULATOR5 by an SCFZTL complex regulates clock function and photomorphogenesis in Arabidopsis thaliana. Plant Cell **19**: 2516–30

Kim D, Pertea G, Trapnell C, Pimentel H, Kelley R, Salzberg SL (2013) TopHat2: accurate alignment of transcriptomes in the presence of insertions, deletions and gene fusions. Genome Biol **14**: R36

Kim J, Somers DE (2010) Rapid assessment of gene function in the circadian clock using artificial microRNA in Arabidopsis mesophyll protoplasts. Plant Physiol **154**: 611–621

Kobayashi Y (1999) A Pair of Related Genes with Antagonistic Roles in Mediating Flowering Signals. Science (80-) **286**: 1960–1962

Kobayashi Y, Weigel D (2007) Move on up, it’s time for change - Mobile signals controlling photoperiod-dependent flowering. Genes Dev **21**: 2371–2384

Kornfeld J-W, Brüning JC (2014) Regulation of metabolism by long, non-coding RNAs. Front Genet **5**: 1–8

Kuramoto Y (1975) Self-entrainment of a population of coupled non-linear oscillators. Lect. Notes Phys. Springer-Verlag, Berlin/Heidelberg, pp 420–422

Lai AG, Doherty CJ, Mueller-Roeber B, Kay SA, Schippers JHM, Dijkwel PP (2012) CIRCADIAN CLOCK-ASSOCIATED 1 regulates ROS homeostasis and oxidative stress responses. Proc Natl Acad Sci **109**: 17129–17134

Legnaioli T, Cuevas J, Mas P (2009) TOC1 functions as a molecular switch connecting the circadian clock with plant responses to drought. EMBO J **28**: 3745–3757

Li G, Siddiqui H, Teng Y, Lin R, Wan X, Li J, Lau O-S, Ouyang X, Dai M, Wan J, et al (2011) Coordinated transcriptional regulation underlying the circadian clock in Arabidopsis. Nat Cell Biol **13**: 616–622

Lindgreen S (2012) AdapterRemoval: easy cleaning of next-generation sequencing reads. BMC Res Notes **5**: 337

Liu AC, Welsh DK, Ko CH, Tran HG, Zhang EE, Priest AA, Buhr ED, Singer O, Meeker K, Verma IM, et al (2007) Intercellular Coupling Confers Robustness against Mutations in the SCN Circadian Clock Network. Cell **129**: 605–616

de Mairan J (1729) Observation Botanique. Hist L’Academie R Des Sci 35

Makino S, Matsushika A, Kojima M, Yamashino T, Mizuno T (2002) The APRR1/TOC1 quintet implicated in circadian rhythms of Arabidopsis thaliana: II. Characterization with CCA1-overexpressing plants. Plant Cell Physiol **43**: 118–122

Mandoli DF, Briggs WR (1984) Fiber-optic plant-tissues: spectral dependence in dark-grown and green tissues. Photochem Photobiol **39**: 419–424

Marcheva B, Ramsey KM, Peek CB, Affinati A, Maury E, Bass J (2013) Circadian Clocks and Metabolism. Curr. Biol. pp 127–155

Marshall CM, Tartaglio V, Duarte M, Harmon FG (2016) The Arabidopsis *sickle* Mutant Exhibits Altered Circadian Clock Responses to Cool Temperatures and Temperature-Dependent Alternative Splicing. Plant Cell **28**: 2560–2575

Más P (2008) Circadian clock function in Arabidopsis thaliana: time beyond transcription. Trends Cell Biol **18**: 273–281

Más P, Alabadí D, Yanovsky MJ, Oyama T, Kay SA (2003a) Dual role of TOC1 in the control of circadian and photomorphogenic responses in Arabidopsis. Plant Cell **15**: 223–36

Más P, Beachy RN (1998) Distribution of TMV movement protein in single living protoplasts immobilized in agarose. Plant J **15**: 835–842

Más P, Kim W-Y, Somers DE, Kay SA (2003b) Targeted degradation of TOC1 by ZTL modulates circadian function in Arabidopsis thaliana. Nature **426**: 567–70

McClung CR (2006) Plant Circadian Rhythms. Plant Cell **18**: 792–803

Michael TP, Mockler TC, Breton G, McEntee C, Byer A, Trout JD, Hazen SP, Shen R, Priest HD, Sullivan CM, et al (2008) Network discovery pipeline elucidates conserved time-of-day-specific cis-regulatory modules. PLoS Genet **4**: e14

Michael TP, Salome PA, Yu HJ, Spencer TR, Sharp EL, McPeek MA, Alonso JM, Ecker JR, McClung CR (2003) Enhanced Fitness Conferred by Naturally Occurring Variation in the Circadian Clock. Science (80-) **302**: 1049–1053

Millar a J, Straume M, Chory J, Chua NH, Kay SA (1995) The regulation of circadian period by phototransduction pathways in Arabidopsis. Science **267**: 1163–1166

Mizoguchi T, Wheatley K, Hanzawa Y, Wright L, Mizoguchi M, Song HR, Carré IA, Coupland G (2002) LHY and CCA1 are partially redundant genes required to maintain circadian rhythms in Arabidopsis. Dev Cell **2**: 629–641

Mizuno T, Nomoto Y, Oka H, Kitayama M, Takeuchi A, Tsubouchi M, Yamashino T (2014) Ambient temperature signal feeds into the circadian clock transcriptional circuitry through the EC night-time repressor in arabidopsis thaliana. Plant Cell Physiol **55**: 958–976

Mockler TC, Michael TP, Priest HD, Shen R, Sullivan CM, Givan SA, McEntee C, Kay SA, Chory J (2007) The DIURNAL project: DIURNAL and circadian expression profiling, model-based pattern matching, and promoter analysis. Cold Spring Harb Symp Quant Biol **72**: 353–63

Mohawk JA, Green CB, Takahashi JS (2013) Central and peripheral circadian clocks in mammal. 445–462

Moore RY, Eichler VB (1972) Loss of a circadian adrenal corticosterone rhythm following suprachiasmatic lesions in the rat. Brain Res **42**: 201–206

Mormann F, Lehnertz K, Daivd P, Elger CE (2000) Mean phase coherence as a measure for phase synchronization and its application to the EEG of epilepsy patients. Phys D **144**: 358–369

Morse D, Sassone-Corsi P (2002) Time after time: Inputs to and outputs from the mammalian circadian oscillators. Trends Neurosci **25**: 632–637

Muranaka T, Kubota S, Oyama T (2013) A single-cell bioluminescence imaging system for monitoring cellular gene expression in a plant body. Plant Cell Physiol **54**: 2085–2093

Nakamichi N, Kiba T, Henriques R, Mizuno T, Chua N-H, Sakakibara H (2010) PSEUDO-RESPONSE REGULATORS 9, 7, and 5 are transcriptional repressors in the Arabidopsis circadian clock. Plant Cell **22**: 594–605

Nakamichi N, Matsushika A, Yamashino T, Mizuno T (2003) Cell autonomous circadian waves of the APRR1/TOC1 quintet in an established cell line of Arabidopsis thaliana. Plant Cell Physiol **44**: 360–365

Nohales MA, Kay SA (2016) Molecular mechanisms at the core of the plant circadian oscillator. Nat Struct Mol Biol **23**: 1061–1069

Nusinow DA, Helfer A, Hamilton EE, King JJ, Imaizumi T, Schultz TF, Farré EM, Kay SA (2011) The ELF4-ELF3-LUX complex links the circadian clock to diurnal control of hypocotyl growth. Nature **475**: 398–402

Oishi K, Sakamoto K, Okada T, Nagase T, Ishida N (1998) Antiphase circadian expression between BMAL1 and period homologue mRNA in the suprachiasmatic nucleus and peripheral tissues of rats. Biochem Biophys

Res Commun **253**: 199–203

Pando MP, Morse D, Cermakian N, Sassone-Corsi P (2002) Phenotypic rescue of a peripheral clock genetic defect via SCN hierarchical dominance. Cell **110**: 107–117

Pant BD, Buhtz A, Kehr J, Scheible WR (2008) MicroRNA399 is a long-distance signal for the regulation of plant phosphate homeostasis. Plant J **53**: 731–738

Para A, Farré EM, Imaizumi T, Pruneda-Paz JL, Harmon FG, Kay SA (2007) PRR3 Is a vascular regulator of TOC1 stability in the Arabidopsis circadian clock. Plant Cell **19**: 3462–73

Penfield S, Hall A (2009) A role for multiple circadian clock genes in the response to signals that break seed dormancy in Arabidopsis. Plant Cell **21**: 1722–32

Perales M, Más P (2007) A functional link between rhythmic changes in chromatin structure and the Arabidopsis biological clock. Plant Cell **19**: 2111–23

Pokhilko A, Fernández AP, Edwards KD, Southern MM, Halliday KJ, Millar AJ (2012) The clock gene circuit in Arabidopsis includes a repressilator with additional feedback loops. Mol Syst Biol **8**: 574

Portolés S, Más P (2010) The functional interplay between protein kinase CK2 and cca1 transcriptional activity is essential for clock temperature compensation in Arabidopsis. PLoS Genet. doi: 10.1371/journal.pgen.1001201

Putterill J, Robson F, Lee K, Simon R, Coupland G (1995) The CONSTANS gene of arabidopsis promotes flowering and encodes a protein showing similarities to zinc finger transcription factors. Cell **80**: 847–857

Rascher U, Hütt M-T, Siebke K, Osmond B, Beck F, Lüttge U (2001) Spatiotemporal variation of metabolism in a plant circadian rhythm: the biological clock as an assembly of coupled individual oscillators. Proc Natl Acad Sci U S A **98**: 11801–11805

Robinson JT, Thorvaldsdóttir H, Winckler W, Guttman M, Lander ES, Getz G, Mesirov JP (2011) Integrative genomics viewer. Nat Biotechnol **29**: 24–6

Rössler OE (1976) An equation for continuous chaos. Phys Lett A **57**: 397–398

Ruts T, Matsubara S, Wiese-Klinkenberg A, Walter A (2012) Aberrant temporal growth pattern and morphology of root and shoot caused by a defective circadian clock in Arabidopsis thaliana. Plant J **72**: 154–161

Salomé PA, McClung CR (2005) PSEUDO-RESPONSE REGULATOR 7 and 9 are partially redundant genes essential for the temperature responsiveness of the Arabidopsis circadian clock. Plant Cell **17**: 791–803

Salomé PA, To JPC, Kieber JJ, McClung CR (2006) Arabidopsis response regulators ARR3 and ARR4 play cytokinin-independent roles in the control of circadian period. Plant Cell **18**: 55–69

Salome PA, Weigel D, McClung CR (2010) The Role of the Arabidopsis Morning Loop Components CCA1, LHY, PRR7, and PRR9 in Temperature Compensation. Plant Cell Online **22**: 3650–3661

Salomé P, Michael T (2002) The out of phase 1 mutant defines a role for PHYB in circadian phase control in Arabidopsis. Plant … **129**: 1674–1685

Schaffer R, Ramsay N, Samach A, Corden S, Putterill J, Carré IA, Coupland G (1998) The late elongated hypocotyl mutation of Arabidopsis disrupts circadian rhythms and the photoperiodic control of flowering. Cell **93**: 1219–1229

Seo PJ, Park M-J, Lim M-H, Kim S-G, Lee M, Baldwin IT, Park C-M (2012) A Self-Regulatory Circuit of CIRCADIAN CLOCK-ASSOCIATED1 Underlies the Circadian Clock Regulation of Temperature Responses in *Arabidopsis*. Plant Cell **24**: 2427–2442

Somers DE, Devlin PF, Kay SA (1998a) Phytochromes and cryptochromes in the entrainment of the Arabidopsis circadian clock. Science **282**: 1488–1490

Somers DE, Webb AA, Pearson M, Kay SA (1998b) The short-period mutant, toc1-1, alters circadian clock regulation of multiple outputs throughout development in Arabidopsis thaliana. Development **125**: 485–94

Stephan FK, Zucker I (1972) Circadian rhythms in drinking behavior and locomotor activity of rats are eliminated by hypothalamic lesions. Proc Natl Acad Sci U S A **69**: 1583–6

Stokkan K, Yamazaki S, Tei H, Sakaki Y, Menaker M (2001) Entrainment of the Circadian Clock in the Liver by Feeding. Science (80-) **291**: 490–493

Strayer C, Oyama T, Schultz TF, Raman R, Somers DE, Más P, Panda S, Kreps JA, Kay SA (2000) Cloning of the Arabidopsis clock gene TOC1, an autoregulatory response regulator homolog. Science **289**: 768–71

Takahashi N, Hirata Y, Aihara K, Más P (2015) A hierarchical multi-oscillator network orchestrates the Arabidopsis circadian system. Cell **163**: 148–59

Tester M, Morris C (1987) The penetration of light through soil. Plant Cell

Environ **10**: 281–286

Thines B, Harmon FG (2010) Ambient temperature response establishes ELF3 as a required component of the core Arabidopsis circadian clock. Proc Natl Acad Sci **107**: 3257–3262

Thorvaldsdóttir H, Robinson JT, Mesirov JP (2013) Integrative Genomics Viewer (IGV): high-performance genomics data visualization and exploration. Brief Bioinform **14**: 178–92

Trapnell C, Williams BA, Pertea G, Mortazavi A, Kwan G, van Baren MJ, Salzberg SL, Wold BJ, Pachter L (2010) Transcript assembly and quantification by RNA-Seq reveals unannotated transcripts and isoform switching during cell differentiation. Nat Biotechnol **28**: 511–5

Turnbull CGN, Booker JP, Leyser HMO (2002) Micrografting techniques for testing long-distance signalling in Arabidopsis. Plant J **32**: 255–262

Valverde F (2004) Photoreceptor Regulation of CONSTANS Protein in Photoperiodic Flowering. Science (80-) **303**: 1003–1006

Vatén A, Dettmer J, Wu S, Stierhof YD, Miyashima S, Yadav SR, Roberts CJ, Campilho A, Bulone V, Lichtenberger R, et al (2011) Callose Biosynthesis Regulates Symplastic Trafficking during Root Development. Dev Cell **21**: 1144–1155

Vollmers C, Schmitz RJ, Nathanson J, Yeo G, Ecker JR, Panda S (2012) Circadian oscillations of protein-coding and regulatory RNAs in a highly dynamic mammalian liver epigenome. Cell Metab **16**: 833–45

Voß U, Wilson MH, Kenobi K, Gould PD, Robertson FC, Peer W a., Lucas M, Swarup K, Casimiro I, Holman TJ, et al (2015) The circadian clock rephases during lateral root organ initiation in Arabidopsis thaliana. Nat Commun **6**: 7641

Wang W, Barnaby JY, Tada Y, Li H, Tör M, Caldelari D, Lee D, Fu X-D, Dong X (2011) Timing of plant immune responses by a central circadian regulator. Nature **470**: 110–4

Wang ZY, Tobin EM (1998) Constitutive expression of the CIRCADIAN CLOCK ASSOCIATED 1 (CCA1) gene disrupts circadian rhythms and suppresses its own expression. Cell **93**: 1207–1217

Welsh DK, Logothetis DE, Meister M, Reppert SM (1995) Individual neurons dissociated from rat suprachiasmatic nucleus express independently phased circadian firing rhythms. Neuron **14**: 697–706

Wenden B, Toner DLK, Hodge SK, Grima R, Millar AJ (2012) Spontaneous spatiotemporal waves of gene expression from biological clocks in the leaf. Proc Natl Acad Sci **109**: 6757–6762

Yakir E, Hassidim M, Melamed-Book N, Hilman D, Kron I, Green RM (2011) Cell autonomous and cell-type specific circadian rhythms in Arabidopsis. Plant J **68**: 520–531

Yakir E, Hilman D, Kron I, Hassidim M, Melamed-Book N, Green RM (2009) Posttranslational Regulation of CIRCADIAN CLOCK ASSOCIATED1 in the Circadian Oscillator of Arabidopsis. Plant Physiol **150**: 844–857

Yamazaki S (2000) Resetting Central and Peripheral Circadian Oscillators in Transgenic Rats. Science (80-) **288**: 682–685

Yao Z, Shafer OT (2014) The Drosophila circadian clock is a variably coupled network of multiple peptidergic units. Science **343**: 1516–20

Yeom M, Kim H, Lim J, Shin AY, Hong S, Kim J Il, Nam HG (2014) How do phytochromes transmit the light quality information to the circadian clock in arabidopsis? Mol Plant **7**: 1701–1704

Yoo S-D, Cho Y-H, Sheen J (2007) Arabidopsis mesophyll protoplasts: a versatile cell system for transient gene expression analysis. Nat Protoc **2**: 1565–1572

Yoo S-H, Yamazaki S, Lowrey PL, Shimomura K, Ko CH, Buhr ED, Siepka SM, Hong H-K, Oh WJ, Yoo OJ, et al (2004) PERIOD2::LUCIFERASE real-time reporting of circadian dynamics reveals persistent circadian oscillations in mouse peripheral tissues. Proc Natl Acad Sci U S A **101**: 5339–46

Young MW, Kay SA (2001) Time zones: a comparative genetics of circadian clocks. Nat Rev Genet **2**: 702–715

Zinn JG (1759) Von dem Schlafe der Pflanzen. Hambg. Mag. Vol.22. pp 40–50